FEDERAL UNIVERSITY OF SANTA CATARINA
SCHOOL OF TECHNOLOGY
MATERIALS SCIENCE AND ENGINEERING GRADUATE PROGRAM

Lucas Bories Fachin

Green synthesis of TiO_2 nanoparticles by laser ablation in water

Florianopolis
2020

Lucas Bories Fachin

Green synthesis of TiO_2 nanoparticles by laser ablation in water

Thesis presented to the Materials Science and Engineering Graduate Program of the Federal University of Santa Catarina to obtain the Master of Science degree in Materials Science and Engineering.

Supervisor: Dachamir Hotza, Prof. Dr.-Ing.
Co-supervisor: Edson Costa Santos, PhD

Florianópolis
2020

Ficha de identificação da obra elaborada pelo autor,
através do Programa de Geração Automática da Biblioteca Universitária da UFSC.

Fachin, Lucas Bories
Green synthesis of TiO2 nanoparticles by laser ablation in water / Lucas Bories Fachin ; orientador, Dachamir Hotza, coorientador, Edson Costa Santos, 2020.
108 p.

Dissertação (mestrado) - Universidade Federal de Santa Catarina, Centro Tecnológico, Programa de Pós-Graduação em Ciência e Engenharia de Materiais, Florianópolis, 2020.

Inclui referências.

1. Ciência e Engenharia de Materiais. 2. Nanotecnologia. 3. Nanopartículas. 4. Ablação a laser. 5. Dióxido de titânio. I. Hotza, Dachamir. II. Costa Santos, Edson. III. Universidade Federal de Santa Catarina. Programa de Pós-Graduação em Ciência e Engenharia de Materiais. IV. Título.

Lucas Bories Fachin

Green synthesis of TiO_2 nanoparticles by laser ablation in water

This Master's Degree thesis was evaluated and approved by the examining board, here composed of:

Prof. Dr. Dachamir Hotza
EQA/UFSC (president)

Prof. Dr. Carlos Cesar Bof Bufon
LNNANO/CNPEM (external member)

Prof. Dr. Claudio Abilio da Silveira
DAMM/IFSC (external member)

We certify that this is the **original and final version** of this thesis, which was deemed adequate for the obtaining of the degree of Master of Science in Materials Science and Engineering.

Prof. Dr. Guilherme Barra
PGMAT/UFSC (coordinator)

Prof. Dr.-Ing. Dachamir Hotza
PGMAT/UFSC (supervisor)

Florianopolis, June 2020.

Dedicated to Mom, Dad and Sis. Not only for the support and love, but for giving me the means to pursue this academic and entrepreneur dream (for that is what this is) while so many do not get that kind of chance.

ACKNOWLEDGMENTS

My first and utmost thanks goes to my family, who above all have always been there for me and on whom I can rely completely.

Big shout out to Edson Costa Santos and Moisés Felipe Teixeira, partners in Nanogreen and who got me into this crazy ride that has been the last couple of years.

To professor Dachamir Hotza, for agreeing to be my supervisor and supporting not only this academic and Master's endeavor, but also the grants and projects we have been envisioning.

To Letícia Silva de Bortoli, who bought our idea and has been helping us develop our idea and concept, and that has been handling our changes of directions, heart and strategy like a champion.

To FAPESC, that through the Sinapse da Inovação grant and scholarship has funded most of this project.

To UFSC and its many laboratories, professionals and students that somehow have a part in this work, to name a few:

- PROCER: Gilberto, Camila, Marcela, Bernardo, Gabriela, Ricardo and all the others that eventually shared the lab with me;
- LINDEN: Steferson, Aline, Thiago with the help with DLS, XRD
- LABMASSA: Alexsandra, Wagner, and others who have helped with questions and analyses;
- LCP: Daniela, Karina and the team for their contributions;
- LTBR: Adri, Alison, Maikon and all of whom I've annoyed in order to use the scientific balance;
- CERMAT: Prof. Fredel and Prof. Luciana, Roberta, Douglas for the use of the polisher, SEM and other conversations;
- LABMAT: Prof. Binder, Marcel, Daniel, Bruno, Beiço, Patrícia, and the others for all the analyses I've used their space for;
- MAGMA: Valmir for the help with deposition and sputtering;
- LCME: Américo and crew for the TEM images.

To Welle Laser, Gabriel and Rafael Bottós, João and Felipe for the partnership and help with the use of the laser machine.

To all friends and colleagues who have heard me excitedly talk about this (or sometimes rant about it) and gave feedback, opinions or even threw some cold water on the most ludicrous ideas we have had.

“This isn’t right. This isn’t even wrong!” (PAULI, Wolfgang)

“Don’t panic.” (ADAMS, Douglas)

RESUMO

A ablação a laser pulsado em líquidos é uma rota verde para a produção de nanopartículas que se baseia em reduzir o tamanho de um alvo sólido até a escala nanométrica através do uso de um pulso concentrado de laser. Este trabalho abriu uma nova linha de pesquisa para o grupo e universidade ao testar a produção de nanopartículas de dióxido de titânio em água deionizada a partir de um alvo de titânio comercialmente puro de grau 2. Há grande interesse comercial na nanotitânia, que é encontrada em produtos como tintas, revestimentos, tecidos, cosméticos, placas solares e catalisadores. Os alvos de titânio foram fotografados com microscopia ótica para avaliar a interação do laser com a superfície dos mesmos. As nanopartículas foram caracterizadas através de técnicas de DLS, MET, Raman, DRX e UV-Vis, e uma aplicação inicial foi testada com a degradação do corante RR141. Imagens de MET apontam para duas populações de nanopartículas, uma esférica (com tamanhos entre 8 e 13 nm) e uma com o formato de rocas (com o eixo maior variando entre 17 e 35 nm), e estudos de composição com DRX e Raman apontam para a formação de anatase, rutilo e titânia amorfa. A coloração da solução produzida se mostrou azulada, o que pode indicar a presença de defeitos de superfície que estendem a banda de absorção de luz para a faixa do visível. No entanto, enquanto os experimentos de catálise apresentaram bons resultados para o espectro UV, não foram obtidos resultados positivos no visível, e os *band gaps* calculados ficaram próximos ao da anatase, por volta de 3,2 eV. O trabalho foi desenvolvido em parceria com a *startup* Nanogreen, de Joinville, através do edital Sinapse da Inovação da FAPESC.

Palavras-chave: Ablação a laser em água. Nanotecnologia verde. Nanopartículas de dióxido de titânio. Água deionizada.

RESUMO EXPANDIDO

Introdução

O crescimento do uso de nanotecnologia e nanopartículas em diversas frentes da indústria tem sido acompanhado nos últimos anos de um maior interesse também no desenvolvimento de métodos menos agressivos ao meio ambiente, principalmente através do uso de reagentes e materiais menos tóxicos ou de fontes naturais. Um dos métodos que vem sendo estudado na última década é o de ablação a laser pulsado em líquidos. Resumidamente, neste processo um feixe de laser pulsado com duração de pulso na casa de nano, pico ou femtosegundos (10-9, 10-12 ou 10-15 segundos, respectivamente) é irradiado sobre um alvo sólido do material do qual se deseja produzir nanopartículas, este alvo estando imerso em um meio líquido de acordo com características desejadas do produto final. Este trabalho é apoiado pela startup Nanogreen através pro programa Sinapse da Inovação, da FAPESC, e está bem alinhado à tendência nacional de investimento e pesquisa na área de nanotecnologia.

O processo de ablação a laser em meio líquido é considerado um processo *top-down* de produção de nanopartículas, ou seja, utiliza um método físico para a redução do tamanho de um material alvo até a escala nanométrica. Embora tenha uma configuração inicial bastante simples, sendo necessário apenas o meio líquido de escolha, o alvo sólido do material e a fonte de laser para a produção de nanopartículas, a quantidade de variáveis que influenciam o processo é considerável, englobando parâmetros do laser (potência, frequência, duração de pulso, comprimento de onda, velocidade de escaneamento), do material (densidade, condutividade térmica, absortividade), do meio líquido (composição, temperatura, pH) e da configuração em si (altura de filme do líquido, agitação ou fluxo de líquido, tempo de ablação, entre outros).

Para este trabalho, alvos de titânio comercialmente puro grau 2 (TiBrasil) foram usados em água deionizada e irradiados com um laser comercial pulsado em nanosegundo (Welle Laser) para a produção de dióxido de titânio (TiO2). Experimentos foram realizados alterando frequência, duração do pulso, velocidade de escaneamento e tempo de ablação para avaliar a influência dessas variações na produtividade e nas características das nanopartículas produzidas. O material foi então caracterizado por DLS, TEM, Raman e DRX para análise das partículas em si, e testado em um experimento de fotocatálise para avaliação dessa propriedade.

Objetivo

O principal objetivo deste trabalho foi a validação do método de ablação a laser para a produção de nanopartículas de titânia. Considerando as vantagens ambientais do processo, é do interesse da Universidade e da startup envolvida conseguir desenvolver a produção por essa metodologia para aplicações de mercado. Dessa maneira, decidiu-se variar parâmetros básicos do equipamento (frequência, duração de pulso, velocidade de escaneamento) e o tempo de processo para permitir um entendimento básico dos fenômenos envolvidos e caracterizar os produtos obtidos.

Metodologia

Para o processo de ablação, foi utilizada uma máquina Welle Laser L2000 (potência: 20 W; comprimento de onda: 1064 nm; M^2: <1,6; distância focal da lente: 100 mm; diâmetro nominal do feixe: 27 μm) e placas de titânio comercialmente puro grau 2 (TiBrasil) de área 25 x 25 mm^2 e espessura 5 mm, preparadas previamente através de polimento. Para cada amostra, foram utilizados 30 mL água deionizada em um béquer de 250 mL, de maneira que o filme de líquido acima do alvo de titânio seja de 4 mm. O sistema foi agitado com agitador magnético a 500 rpm

de maneira a homogeneizar a solução irradiada pelo laser. Para esta dissertação, foram utilizados os formatos de onda 0 (frequência: 20 kHz; energia de pulso: 1,00 mJ; duração de pulso em FWHM: 40 ns; duração de pulso em 10% de potência: 241 ns; potência de pico: 14 kW) e 10 (frequência: 41 kHz; energia de pulso: 0,49 mJ; duração de pulso em FWHM: 26 ns; duração de pulso em 10% de potência: 100 ns; potência de pico: 14 kW), duas velocidades de escaneamento (270 mm/s e 1350 mm/s) e três tempos de ablação (5 min, 15 min e 30 min) para a comparação de resultados de produtividade e das nanopartículas produzidas.
Depois da produção, a massa de material removido dos alvos foi medida e esse valor foi tomado como produtividade. A superfície de cada alvo ablacionado foi analisada através de microscopia óptica (Leica DM4000) para uma análise visual dos efeitos da ablação e para a medida do diâmetro efetivo do feixe de laser na superfície do alvo e as partículas produzidas foram visualizadas por TEM (JEM-1011 Jeol) para definição da morfologia e medida de tamanho de partícula. Ambas as medidas foram feitas através da distribuição Fiji do software ImageJ.
Outras caracterizações realizadas foram difração de raios-x (DRX, Rigaku MiniFlex600), espectroscopia UV-Vis (Hitachi U-1900 NIR), espectroscopia Raman (Renishaw inVia micro-Raman) e espalhamento dinâmico de luz (DLS, Malvern Zetasizer Nano ZS). Por último, foi realizado um teste de fotocatálise do corante RR141 tanto no espectro visível quanto no ultravioleta. As partículas produzidas neste trabalho foram comparadas a nanopartículas de TiO_2-WO_3 comerciais (NanoAmor) de acordo com a degradação do corante mencionado.

Resultados e discussão

O primeiro resultado foram as soluções azuladas de nanopartículas obtidas. De maneira geral, partículas de titânia azuladas são indicativas de defeitos de superfície ou dopagem com outros materiais. As soluções produzidas inicialmente se mostram bem dispersas, mas sofrem aglomeração ao longo de algumas horas. Após cerca de dois dias acontece a sedimentação do material. No entanto, as nanopartículas são facilmente redispersas usando um banho ou ponteira de ultrassom, como pode ser visto nas imagens de TEM, que foram tiradas não imediatamente após a produção, mas sim depois de alguns dias, e depois desse processo de sedimentação e redispersão. O potencial zeta medido através do DLS também indica uma boa carga superficial, com todas as amostras tendo resultados menores que -30 mV e um pH próximo de 7, o que indica suspensões estáveis do ponto de vista elétrico e isso leva a acreditar que a agregação se dá por causa de concentração ou morfologia das partículas.
A superfície dos alvos após ablação mostra que o processo foi efetivo e houve remoção de material dos alvos, portanto a fluência utilizada foi suficiente. Aumentos no tempo de ablação e velocidade de escaneamento indicam uma maior remoção de material conforme o esperado, considerando que estas duas variáveis aumentam o número de vezes que o feixe de laser passará sobre o alvo. Esses mesmos aumentos também demonstram uma maior área afetada no alvo em si, possivelmente tanto pelo aumento do número de passes quanto pela concentração de nanopartículas na solução, que interagem com os próximos feixes de laser difratando-os e retirando-os do foco, aumentando a área irradiada. Usando as amostras irradiadas por 5 min foi possível medir um diâmetro efetivo de ablação, que para as nossas amostras foi de em média 150 μm. Com base neste diâmetro, a fluência calculada foi de em média 6,4 J/cm^2 para o formato de onda 0 e 2,7 J/cm^2 para o formato de onda 10. Considerando os resultados de produtividade, tivemos que a maior remoção de material aconteceu no regime de formato de onda 10, com maior velocidade e maior tempo de ablação. Ainda assim, a maior produtividade obtida foi de 20,8 mg/h, o que significa que seriam necessárias cerca de 48 h para a produção de 1 g desse material, quantidade muito pequena considerando a maior parte das aplicações da nanotitânia.
Inicialmente, medidas de DLS foram realizadas para obter o tamanho das partículas produzidas. Os resultados indicaram tamanhos entre 30 nm e 60 nm, consideravelmente grandes perto do

esperado e encontrado na literatura. Além disso, os gráficos obtidos de distribuição de tamanho se mostraram, na maior parte das vezes, bimodais e com picos largos, o que pode significar que as partículas em questão não obedecem a algumas hipóteses que esta técnica requer para uma correta medida, como serem esféricas, homogêneas e com propriedades ópticas conhecidas. Para verificar na prática a morfologia e o tamanho das partículas, imagens de TEM foram obtidas e tratadas.

Imediatamente percebe-se que não temos apenas partículas esféricas, mas sim uma mistura de esferas e rocas, o que explica os resultados do DLS. De posse das imagens consegue-se medir os tamanhos dos dois formatos separadamente. O tamanho das esferas medidas fica entre 8 nm e 13 nm, e as rocas têm seu eixo maior com tamanho entre 18 nm e 36 nm, o que se aproxima mais dos números da literatura e do esperado. Entretanto, pelas imagens consegue-se perceber partículas de 1 nm até 60 nm, o que representa uma grande distribuição de tamanho, e isso não é o ideal considerando principalmente aplicações mais nobres da nanotecnologia.

Quanto ao formato, encontram-se relatos da produção de nanopartículas de titânia no formato de rocas na literatura, mas essa produção normalmente depende do uso de estabilizantes ou dopantes, por exemplo, enquanto o método de ablação a laser produziu essas estruturas sem influência externa. Um ponto em comum entre todos os trabalhos encontrados é que a fase cristalina dessas rocas em todos os trabalhos era anatase. Nos experimentos aqui realizados, percebeu-se que um aumento no tempo de ablação e/ou na velocidade de escaneamento (ambos relacionados ao número de passes sobre o alvo) causou uma diminuição no número de rocas e um aumento do tamanho médio das partículas esféricas.

Uma hipótese foi formulada para explicar o comportamento tanto do formato dar partículas quanto da alta distribuição de tamanho das mesmas. Por causa da configuração em batelada utilizada, há a concentração de nanopartículas no meio líquido ao longo do processo. Isso quer dizer que durante o último minuto de ablação, por exemplo, existirão partículas que foram formadas nos primeiros pulsos, e que estão circulando no líquido desde então, e partículas recém geradas, pelos últimos pulsos. A chance de que as primeiras partículas tenham sido novamente irradiadas pelo laser durante o tempo de processo é bem grande, e essa pós-irradiação pode ter causado uma mudança de formato e até mesmo de fase. Uma das possibilidades é que as partículas recém formadas sejam condensadas como rocas ou partículas ultra pequenas de anatase (fase que é mais estável quanto menor o tamanho das esferas, e também que é mais comum na formação de rocas), e durante o processo, com a pós-irradiação, energia suficiente é transferida para essas partículas de maneira que haja uma agregação e mudança de fase das mesmas, o que ocasionaria o aparecimento de esferas maiores e de fase rutilo. Para uma confirmação, novos experimentos devem ser realizados em uma configuração com fluxo, garantindo que não haja pós-irradiação, ou sem a geração de novas partículas de maneira a garantir uma pós-irradiação completa.

Análises de Raman e de DRX foram realizadas para a identificação da fase das partículas. Após algumas alterações no procedimento padrão de maneira a permitir a análise da pequena quantidade de material obtida, os resultados foram semelhantes para ambas as técnicas. Os estudos indicaram a presença de titânia amorfa, rutilo e anatase, o que corrobora a hipótese levantada sobre o formato e distribuição de tamanho. Infelizmente esses métodos realizam uma análise da solução como um todo, não sendo possível obter a fase de partículas individuais.

Finalmente, os testes de fotocatálise para a degradação de RR141 demonstraram um bom resultado da titânia azul produzida por ablação a laser no espectro ultravioleta, como esperado de nanopartículas de titânia e comparável com o resultado da titânia dopada com tungstênia. No visível, no entanto, a titânia produzida neste trabalho não apresentou fotocatálise enquanto as partículas comerciais obtiveram bons resultados. Para estudar este efeito mais a fundo, espectroscopia no UV-Vis foi realizada nas amostras para o cálculo do *band gap* através do

gráfico de Tauc. O resultado apontou que não houve expansão da faixa de absorção para o visível, como era o esperado, e o valor do *band gap* ficou em torno de 3,25 eV, maior do que o normalmente encontrado para anatase (3,2 eV) e rutilo (3,0 eV).

Considerações finais

As nanopartículas propostas foram produzidas através do método proposto, e caracterizadas com as técnicas esperadas. A primeira observação realizada foi a de que as soluções produzidas apresentavam um tom azulado, indicativo de defeitos na superfície e uma possível atividade catalítica no espectro visível, fato que não foi comprovado nos testes de fotocatálise.

O formato das nanopartículas foi o segundo resultado importante. Populações de esferas e rocas foram encontradas nas imagens de TEM, com tamanhos dentro do esperado (10 nm para esferas e 25 nm para o eixo maior das rocas). No entanto, a distribuição de tamanho das partículas ficou consideravelmente largo, com partículas encontradas entre 1 nm e 60 nm. Análises de Raman e XRD indicam a presença de fases amorfa, anatase e rutilo nas dispersões.

De maneira a entender e controlar melhor o processo, alguns passos são sugeridos. Inicialmente a homogeneizar a população de partículas produzidas, seja através da inclusão de um sistema de fluxo, que garanta que as partículas produzidas não sejam irradiadas novamente, ou através de um sistema de batelada que remova o alvo após o tempo final e mantenha alguns min de pós-irradiação para garantir que todas as partículas sejam tratadas. Com essa homogeneização, fica mais fácil caracterizar fases e quantidades presentes, através de Raman, XRD e até mesmo XPS e HR-TEM com SAED.

Observando aspectos de produtividade e mercado para as nanopartículas de titânia, chega-se à conclusão de que o processo aqui desenvolvido, embora interessante em aspectos técnicos, não atende à demanda atual de nanopartículas desse material. Com isso em mente, procurou-se mercados de maior valor agregado e menor volume utilizado, onde a ablação a laser possa ser aplicado e no qual as partículas altamente puras sejam um diferencial, e hoje a startup está focando no desenvolvimento de nanopartículas de ouro para aplicações biomédicas e biossensores, incluindo aí diagnósticos até mesmo contra a COVID-19, que no momento assola o mundo.

Palavras-chave: Ablação a laser em água. Nanotecnologia verde. Nanopartículas de dióxido de titânio. Água deionizada.

ABSTRACT

Pulsed laser ablation in liquids is a green route to produce nanoparticles that is based on reducing the size of a solid target to the nanoscale using a concentrated laser pulse. This work opened a new line of research for the group and university by testing the production of titanium dioxide nanoparticles in deionized water from a grade 2 commercially pure titanium target. There is great commercial interest in nano titania, which can be found in products including paints, coatings, textiles, cosmetics, solar panels and catalysts. The titanium targets were photographed with optical microscopy to assess the interaction of the laser with their surface. The nanoparticles were characterized using DLS, TEM, Raman, XRD and UV-Vis techniques, and an initial application was tested with the degradation of the dye RR141. TEM images point to two populations of nanoparticles, one spherical (with sizes between 8 and 13 nm) and one spindle-like (with the major axis ranging between 17 and 35 nm), and composition studies with XRD and Raman point out to the formation of anatase, rutile and amorphous titania. The color of the solution produced was bluish, which may indicate the presence of surface defects that extend the light absorption band to the visible range. However, while the catalysis experiments showed good results for the UV spectrum, no result was obtained in the visible range, and the calculated bandgaps were close to that of anatase, around 3.2 eV. The work was developed in partnership with the startup Nanogreen, from Joinville, through FAPESC's Sinapse da Inovação grant.

Keywords: Pulsed Laser Ablation in Water. Green nanotechnology. Titanium dioxide nanoparticles. Deionized water.

LIST OF FIGURES

LIST OF TABLES

LIST OF ABBREVIATIONS AND ACRONYMS

ART - Anatase-Rutile Transformation

CERTI - Center of Reference in Innovative Technologies

CTAB - Cetyltrimethylammonium Bromide

CV - Coefficient of Variation

DI – Deionized

DDI – Distilled and Deionized

DLS - Dynamic Light Scattering

FAPESC - Foundation for the Support of Research and Innovation of the State of Santa Catarina

FFF - Field Flow Fractionation

FWHM - Full Width Half Maximum

GE - General Electric

HRTEM - High Resolution Transmission Electron Microscopy

ICSD - Inorganic Crystal Structure Database

INB - Brazilian Nanotechnology Initiative

KET - Key Enabling Technologies

LABMAT - Materials Laboratory

LCM - Microstructural Characterization Laboratory

LCME - Electronic Microscopy Central Laboratory

LINDEN - Interdisciplinary Laboratory for the Development of Nanostructures

LINDEN-metro - Linden's nanometrology laboratory

MCTIC - Ministry of Science, Technology, Innovation and Communications

NANoREG - Common European approach to regulatory testing of nanomaterials

NM - Nanomaterial

NP - Nanoparticles

OM - Optical Microscopy

PLAL - Pulsed Laser Ablation in Liquids

PROCER - Ceramic Processing Laboratory

RR141 - Reactive Red 141

SAED - Selected Area Electron Diffraction

SC - Santa Catarina

SD - Standard Deviation

SENAI - National Service for Industrial Training

SibratecNANO - Brazilian Technology System – Nanotechnology

SisNANO - National Laboratory System in Nanotechnology

TEM - Transmission Electron Microscopy

UFSC - Federal University of Santa Catarina

UV-vis - Ultraviolet-visible

VdW - Van der Waals

LIST OF SYMBOLS AND UNITS

pulses – Number of pulses

d_b – Beam diameter [μm]

d_p – Average particle diameter [nm]

E_p – Pulse energy [mJ]

F – Fluence [J/cm^2]

F – Frequency [kHz]

PO – Pulse Overlap [%]

P_p – Peak power [W]

S_s – Spot size [μm]

t – Time [min]

v_s – Scan speed [mm/s]

ζ – Zeta potential [mV]

λ – Wavelength [nm]

τ – Pulse width [ns]

$\tau_{\_10\%}$ [ns] – Pulse width at 10% E_p

$\tau_{\_FWHM}$ [ns] – Pulse width at Full Width Half Maximum E_p

SUMMARY

1 INTRODUCTION

"The story so far: In the beginning the Universe was created.
This has made a lot of people very angry and been widely regarded as a bad move."
(ADAMS, Douglas)

Nanoparticles are considerably widespread amongst different sectors and industries, and can find applications in the most diverse settings. From antimicrobial and antiviral paints, coatings, textiles and plastics, which are produced in a very high volume and relatively low product value, to highly specific electronic components (smartphones' touchscreens), diagnostics (biosensors), aerospace technology (special alloys) and energy applications that appear in lower volume but in high value-added products. Nanotechnology is considered multidisciplinary, combining technology and knowledge from physics, chemistry, biology, engineering, medicine and other subjects into a single platform technology, hence this huge number of applications.

While nanoparticles are being increasingly used in many sectors of the economy, there is growing interest in the environmental safety of their production. The main methods for nanoparticles production are chemical and physical approaches that are often costly and potentially harmful to the environment, due to the intense use of solvents and other chemicals that need proper disposal. There is also an increasing interest in the customization of nanoparticles for specific applications, where size distribution, shape and composition play an important role. Nowadays, the primary nanoparticles suppliers overall tend to work with pre-defined products and sizes, due to the nature of the synthesis method.

This proposal is devoted to kickstart the development and production of nanoparticles using laser ablation in liquids in the Federal University of Santa Catarina (UFSC) and the PROCER (Processing of Ceramics) research group, since this significantly reduces the needed solvents and chemicals while maintaining a highly versatile and adaptable process.

Shortly, the laser ablation in liquids technology uses a pulsed laser beam to remove material from the surface of a solid target dipped in a specific liquid (usually deionized water). While this method is usually applied for the processing of the surface itself by texturization, and in that sense the results are evaluated mostly on the surface, this work focuses instead on the removed material, which condensates in the liquid media as nanoparticles. Further explanation of the process and phenomena involved is given in the following sections.

1.1 MOTIVATION

This work is mainly motivated by the opportunity to develop a green route for nanoparticles production within this research group, university and in Santa Catarina state as a whole, while also having a direct relationship with the market and opportunities with the startup Nanogreen. Brazil has been developing several initiatives for the application of nanotechnology in our industry lately, with this technology being considered one of the "Convergent and Enabling Technologies" (also known as "Key Enabling Technologies", KET) by the Ministry of Science, Technology, Innovation and Communication (MCTIC). These are considered technologies that have the capability to drastically change humankind, culture and industry, and as such have received increasing attention from many countries and industries. Programs such as the INB (Brazilian Nanotechnology Initiative), SibratecNANO (Brazilian Technology System – Nanotechnology), SisNANO (National Laboratory System in Nanotechnology), the National Nanosafety Program, which is being developed in collaboration with NANoREG (the common European approach to the regulatory testing of nanomaterials), and several other grants, calls for projects and contract developments have been released in the recent years in order to support the advance and application of nanotechnology in our country.

The state of Santa Catarina in Brazil has a successful program called "Sinapse da Inovação" which provides grant money for innovative startups to start developing their product or service. In 2018, the startup Nanogreen approved a project focusing on the validation of laser ablation in liquids to produce nanoparticles of different materials and with different parameters. This approval, and the approval of other projects developed since, represent the interest not only of the academia but also of companies and industries in the results of this work, both in the environmental aspect and also due to the customization inherent to this method.

This work is derived from the Sinapse da Inovação grant and seeks to test the method and one of the materials that are most used as nanoparticles: titanium dioxide, also called titania (TiO_2). This material was chosen by its numerous applications in the industry, ranging from food to construction, and for the interest that companies have already shown in applying titania nanoparticles (TiO_2NPs) in their products. Besides developing and validating the TiO_2NPs by laser ablation in water, this work will also open up the possibilities of producing nanoparticles of many materials for other applications through this method and may enhance the capacity of this research group and university to develop new materials and meet the market's demands.

1.2 GOALS

In order to correctly guide and define this work's results, a main goal is described here, along with specific goals to be achieved during this master's research program.

1.2.1 Main goal

The main goal is to validate the feasibility and the characteristics of titania nanoparticles produced by laser ablation in water. By producing such nanoparticles from a pre-defined target, testing different laser parameters (waveform and scan speed) and ablation time for that production and characterizing the results, we hope to achieve the production of nanoparticles (< 100 nm) with an acceptable size distribution, thus opening the door to further research in this area, such as the production of new materials through this method.

Considering the economical and practical aspects of the project, this work will focus on working with low-cost materials and machines, in order to keep the overall price of the products as low as possible.

1.2.2 Specific goals

In order to achieve the main goal, the following specific goals were defined:

a) synthesize titania nanoparticles (<100 nm) using a ns-pulsed laser ablation in water setup;
b) characterize the ablated targets and produced nanoparticles through physical and chemical methods such as OM, TEM, DLS, XRD, UV-vis, Raman spectroscopy and photocatalysis experiments;
c) study the effects of ablation time, scan speed and waveform (laser parameters to be defined further in this work) on the nanoparticles produced.

2 LITERATURE REVIEW

"- Just believe everything I tell you, and it will all be very, very simple.
- Ah, well, I'm not sure I believe that."
(ADAMS, Douglas)

For this first part, a literature review was prepared to introduce critical aspects of nanoparticles, laser technology and of the chosen material, titanium dioxide. This is not an exhaustive list of all the parameters, details and specificities inherent to this project, but should provide the reader with a basic understanding of the process in order to perceive the results and conclusions of this work.

2.1 GENERAL CONSIDERATIONS ON NANOPARTICLES AND THEIR SYNTHESIS

Nanoparticles are a subject that has gotten more and more attention in recent years. Their application in many industries and products has grown, and their unique properties have found markets in all areas of our lives. Though they are most commonly defined as particles with at least one dimension in the range of 1-100 nm (ASTM, 2006), many different definitions can be found in the literature, ranging from discussions on the lower and upper boundaries to discussions on whether there should be a boundary at all (BOHOLM; ARVIDSSON, 2016).

Figure 1: Increasing total surface area by particle size reduction

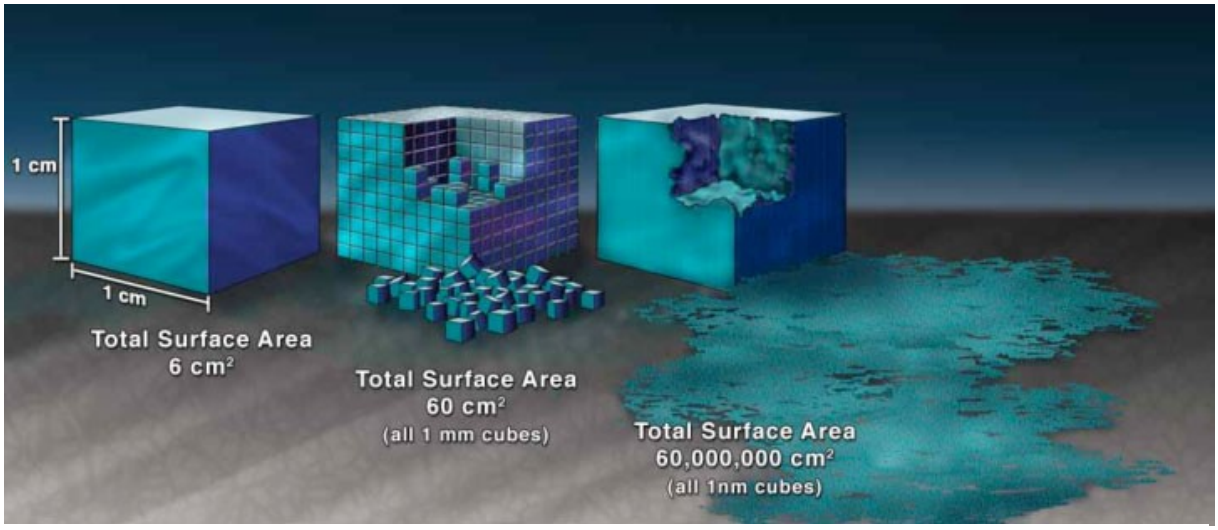

Source: (NNI, 2020)

It is common sense, though, that nanoparticles exhibit properties and qualities that do not show or that are too weakly present in bulk materials. Properties such as higher reactivity,

color change, stability, absorptivity, reflectance, and magnetism, among others, may change as we scale down to the nano level (ANU MARY EALIA; SARAVANAKUMAR, 2017; FANG et al., 2013; KHAN; SAEED; KHAN, 2017). This is mainly due to the increase in surface area as we reduce the size of the particles, as shown in Figure 1. This leads to weaker bonds in the surface, and thus more reactive and available surface atoms. Besides that, quantum effects have higher representativeness as the size of the particles goes down, leading to phenomena that are too weak to be observed in bulk materials (PELLARIN et al., 2018; PILLAI et al., 2007).

Many methods exist to produce nanoparticles, divided into "bottom-up" and "top-down" processes (Figure 2). The bottom-up approach involves the "construction" of the nanoparticles atom by atom, cluster by cluster. This means using precursors such as salts and other chemicals and through the right conditions, inducing their reaction and/or organization into the desired nanoparticles (BEHARI, 2010). Examples of such methods are sol-gel, spinning, chemical vapor deposition (CVD), pyrolysis (ANU MARY EALIA; SARAVANAKUMAR, 2017) and even biosynthesis, where plants and plant extracts are used in the production (MAKAROV et al., 2014). These methods are known for producing highly homogeneous nanoparticles with little defects and have a considerable size and size distribution controllability and yield (BEHARI, 2010). However, due to the nature of some of them, there may be by-products or residues on the nanoparticles' surface after the process, or the stabilizers needed to ensure the stability of the nanoparticles may not be biocompatible, which can prevent the use of those nanoparticles in some very specific and controlled areas such as medicine, health and food applications (KABASHIN et al., 2010).

Figure 2: Nanoparticles synthesis methods.

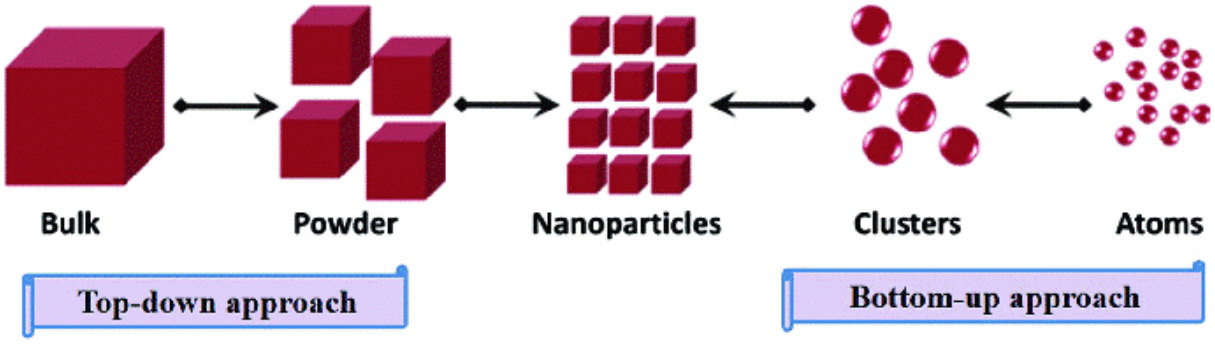

Source: (PAREEK et al., 2017)

The top-down methods, on the other hand, are considered destructive since they start with the bulk material and reduce its size to the nanometric scale. Grinding, milling, physical

vapor deposition (PVD), nanolithography, thermal decomposition and laser ablation are examples of such methods (ANU MARY EALIA; SARAVANAKUMAR, 2017; KHAN; SAEED; KHAN, 2017). These methods tend to produce nanoparticles with a higher amount of surface defects, which may interfere in the final application of the material. Besides, in some of the cases, such as grinding and milling, there may be impurities in the nanoparticle due to the medium used, and it is hard to control the size and size distribution (BEHARI, 2010).

Amongst the top-down methods, laser ablation is one that has been studied in the last decade, but it is not too widely known or commercially used, mainly due to its low productivity and very specific requirements such as the laser machine. However, new developments and applications are gaining attention and companies using this technique can be found worldwide. By focusing a high-intensity pulsed laser beam on the surface of a solid target of the desired material, it is possible to ablate, i.e. to remove by melting or evaporation, pieces of the surface, which are quenched by air, liquid or vacuum, and solidify them into nanoparticles. Further explanation will be given in the following sections.

2.2 PULSED LASER ABLATION

Laser ablation can be performed in gas/vacuum or in a liquid environment, and both are used for the preparation of nanoseconds structures. As aforementioned, these are options that allow for a clean and straightforward synthesis of nanoparticles, consisting “only” of the desired material’s target, a laser machine and the medium where the ablation will take place. This simple setup makes sure that the produced nanoparticles are as pure as the target and medium, without by-products or contamination from stabilizers, reducing agents or other chemicals that may need to be used in other routes (TSUJI, 2012). This also makes the surface free from impurities and leaves the active sites available for functionalization or even for catalytic activity (SINGH et al., 2012a, 2012b).

Figure 3: Laser ablation in vacuum (left) and laser ablation in liquid (right).

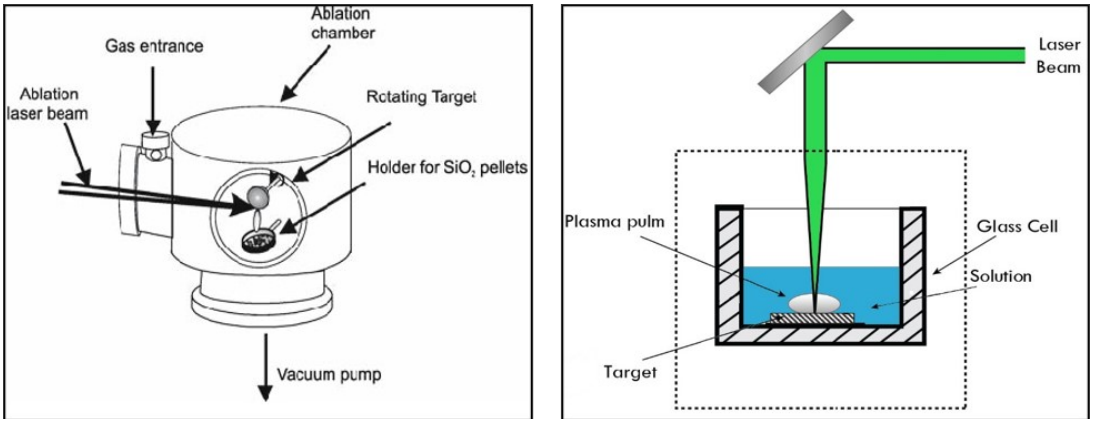

Source: left - (SAVASTENKO et al., 2008); right - (SAHEHCO, [s.d.])

Both laser ablation routes are complex to describe due to the number of parameters that influence the results. Table 1 presents some of the variables that need to be taken into account to fully comprehend the ablation process (BARCIKOWSKI et al., 2007; ZHU et al., 2001; LEWIS; PEREZ, 2012).

Table 1: Main parameters that influence the laser ablation process.

Laser Parameters	Fluence [J/cm^2]
	Frequency [Hz, kHz]
	Wavelength [nm]
	Pulse duration [ns, ps, fs]
	Scan speed [mm/s]
Material Properties	Thermal conductivity [$Wm^{-1}K^{-1}$]
	Density [g/cm^3]
	Absorptivity
Medium type	Vacuum
	Air
	Deionized water
	Organic solvents
Medium properties	Volume [mL]
	Pressure [Pa]
	Film height [mm]
Process setup	Ablation time [min]
	Fluid flow rate [mL/min]
	Agitation [rpm]

Source: Author (2020)

When deciding between Pulsed Laser Ablation in Liquid (PLAL) and Pulsed Laser Ablation in Gas (PLAG), there are a couple of differences to consider. Starting with the experimental and production setup itself, it is overall simpler to work with PLAL (Figure 3). This is due to the need of either a vacuum chamber or a controlled atmosphere for the environment in PLAG, and the necessity of some sort of gas removal and filtering mechanism, to collect and store the produced nanoparticles, which may then be subject to some thermal treatment, depending on the case (KIM et al., 2017). As for PLAL, while there are more complex setups, including vertical targets and flow chambers (CHEN; ZHANG, 2012; KOHSAKOWSKI et al., 2017; STREUBEL; BARCIKOWSKI; GÖKCE, 2016), it is quite quick and straightforward to obtain nanoparticles using "just" the laser, the target material and the solvent (e.g. distilled water), and it is also easier to fine-tune the size, shape and properties of the nanoparticles by changing process parameters. The production in a dispersion, and not as a dry powder, increase occupational safety and handling security (SINGH et al., 2012a).

Besides the setup, differences continue into the physical and chemical interaction between the laser, the target and the medium, which affect the nanoparticles produced. When the laser beam hits the surface of the target, a plasma plume is created due to the high energy transferred to the material (the nature of this interaction will depend on the material's properties and the laser parameters). This plume behaves very differently, whether in a liquid or gas/vacuum environment, as expected. Gas/vacuum environments tend to allow for a faster and more linear plume expansion, and less aggregation of the produced nanoparticles, which can be deposited in the form of an atomic layer. In contrast, while liquid environments confine the plasma, increasing the temperature, pressure and density to a thermodynamic state where particular reactions can take place between the plasma produced by the target material and the liquid molecules, allowing for the production of metastable structures and particles with varying compositions (SINGH et al., 2012a). Overall, ablation in liquids tends to render a higher ablation rate and nanoparticle formation and lower the ablation threshold (i.e. the minimum fluence needed to remove material of a substrate) of some materials (HAMAD; KHASHAN; HADI, 2016; KIM; LEE, 2001; PATEL; SINGH; THAREJA, 2014; ZHU et al., 2001). Fluence (F), mentioned above, is defined as energy per area, usually J/cm^2 in the case of lasers. In this work, and considering what has been seen in the literature, it will be regarded as pulse energy (E_p) divided by the area irradiated by the laser beam as presented in Equation (1), where S_s is the spot size.

$$F = E_p / (\pi*(S_s/2)^2) \quad (1)$$

The nanoparticles formed can be quite different too, with the ones created in liquid being more spherical and eventually aggregating in the dispersion, while the ones in air or gas can have a less defined morphology, looking more amalgamated when deposited on the ablating surface (KUMAR; THAREJA, 2013).

2.3 PLAL PROCESS AND SETUP

For the PLAL method, the interaction between the laser and the solid-liquid interface produces two events: the generation of a localized plasma plume and the creation of a cavitation bubble, which will expand and collapse in a matter of microseconds (GRIGOROPOULOS; MAO, 2012). It is shown that the nanoparticles are created during the plasma phase, when they are ejected from the material, and grow and are released to the dispersion during the cavitation bubble collapse (DELL'AGLIO et al., 2015) (Figure 4).

Figure 4: Schematic of laser ablation in liquids events occurring during and after the irradiation. This is typically for a short (ps) or ultra-short (fs) pulse, since there is no interaction of the pulse with the cavitation bubble.

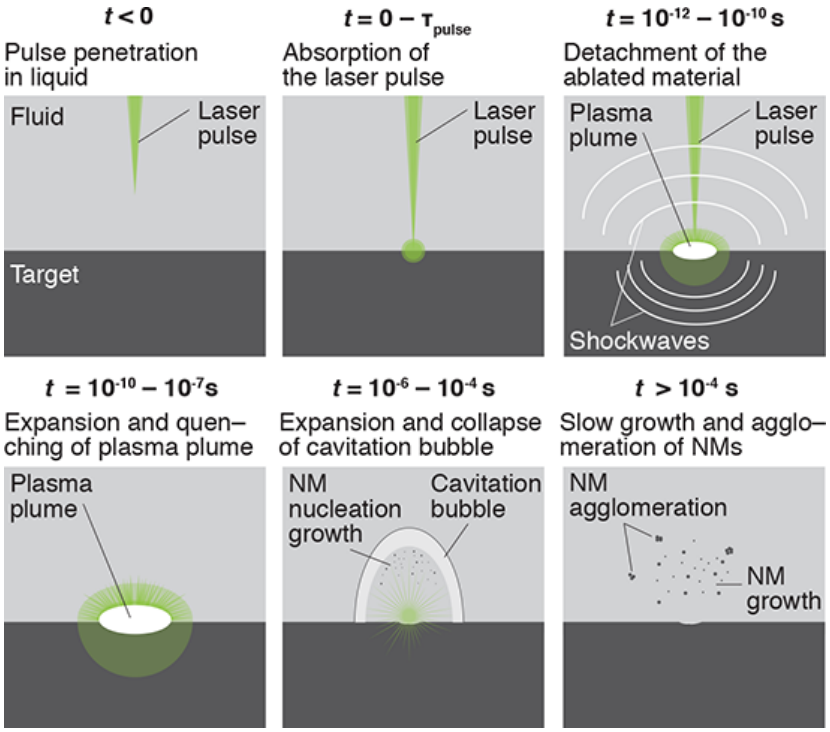

Source: (STAUSS et al., 2016)

The dynamics of such interaction is quite complex, mainly because the system reaches very high temperatures, pressures and densities during the plasma phase for very short periods, due to the high energy involved, which increase the non-linearity of the process. The pressure inside the plasma can reach 5 to 10 GPa (BERTHE et al., 1997; FABBRO et al., 1990) and temperatures get to 2000-10000 K (DE GIACOMO et al., 2013; GRIGOROPOULOS; MAO, 2012; SEMALTIANOS et al., 2010). These conditions allow for the formation of metastable phases in the nanoparticles, which are not thermodynamically achievable in most of the usual synthesis methods. A clear example is the synthesis of crystalline diamond nanoparticles from a graphite target using PLAL(GUO-WEI; JIN-BIN; QUI-XIANG, 1998; WANG; YANG, 1999). Because of the thermodynamics of the carbon-diamond phase equilibrium, high temperature and high pressure are needed for the synthesis of this material, and the equipment for such process is costly and cumbersome. With PLAL, and due to the specifics of the laser-matter interaction, one can simplify this synthesis.

One of the main parameters that influences the kind of interaction between laser and solid that will take place, as well as the creation and propagation of the plasma plume and the cavitation bubble is the pulse width. For laser ablation processes, three main regimes are currently considered: long pulse (in nanoseconds, ns), short pulse (in picoseconds, ps), and ultra-short pulse (in femtoseconds, fs), in contrast to other laser processes such as welding, which consider millisecond regimes as short. In long pulse durations (ns), there is considerable heating of the lattice due to electron-phonon and phonon-phonon interaction (coupling time), causing melting and vaporization of a large area and the production of the nanoparticles from this evaporation (SEMALTIANOS, 2010; TSUJI, 2012). In addition, because of the timescale of the events happening at the solid-liquid interface, the rear end of the long pulse interacts with the plasma plume and cavitation bubble created by its front (HAMAD, 2016; SINGH et al., 2012a), which in turn heats the system even more through inverse bremsstrahlung effect (DE GIACOMO et al., 2013; TOMKO et al., 2017). All of this interaction causes this regime to show a sizeable heat-affected zone, surface debris and an overall deformed look to the crater created (SEMALTIANOS, 2010) (Figure 5).

Figure 5: Interaction of long and short pulses (ultra-short pulses behave similarly to the short pules) with the target material.

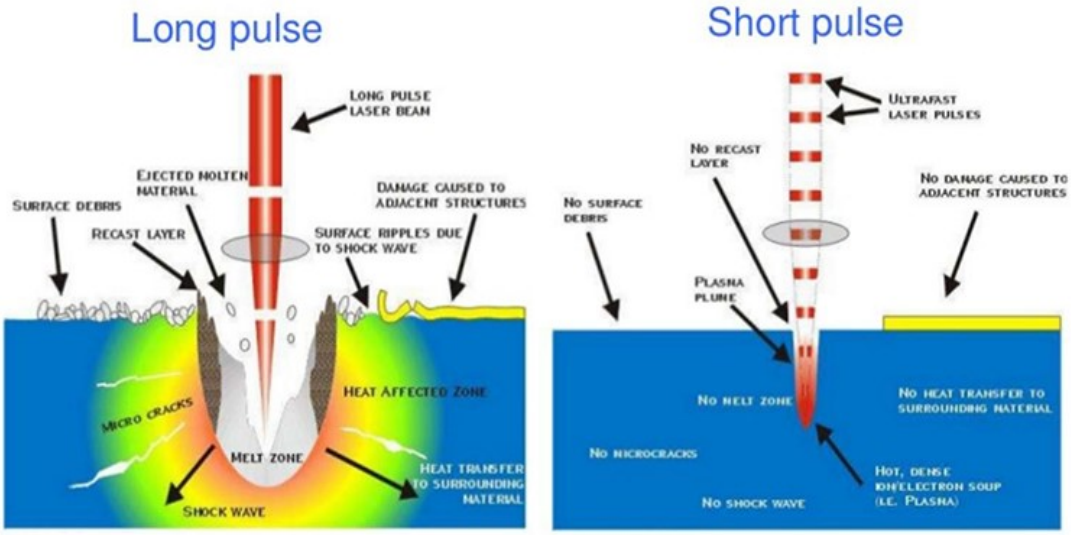

Source: (HAMAD, 2016)

As we move to short and ultra-short regimes, there is no heating of the lattice, since the pulse exists for a time shorter than the electron-phonon coupling time (KABASHIN et al., 2010; KABASHIN; MEUNIER, 2003; SINGH et al., 2012a). This way, all the energy from the laser beam is transferred to the material before there is appreciable heating of the surface through bremsstrahlung effect (radiation emitted by the deceleration of a charged particle by the interaction with another charged particle) through free electrons present in the lattice (TSUJI, 2012). Because of the accumulated energy, the material may suffer sublimation, going straight from the solid to the vapor phase and generating the nanoparticles (SEMALTIANOS, 2010). Another possible route is the fast ejection of the particles from the lattice by fragmentation due to photomechanical effects (photodissociation) and coulombic explosions (HAMAD, 2016; SEMALTIANOS, 2010). The absence of melting effects makes the heat-affected zone very small or even inexistent, and the structure of craters is very clean when compared to long pulse ablation (HAMAD, 2016; KABASHIN et al., 2010). Besides, because of the short pulse duration, there is no interaction between the pulse itself and the plasma, which is generated after the pulse duration is over. This leads to a shorter lifetime of the plasma and is expected to lower the time for particle growth, which may help to control the size of the ablated particles (LIU et al., 2012) (Figure 5).

Figure 6 illustrates the difference between the nano and femtosecond regimes in the ablation of a solid target, with a clear difference in the aspect of the process. While debris and melted zones can be seen in the nanosecond regime, the ultra-short pulse shows a very clean

cut. There has been evidence of heat-affected zones and surface debris in ultra-short laser ablation, but it is attributed to a secondary ablation done by the plasma itself, during its microsecond existence. This is shown in ablations performed at very high fluences and give rise to a second size distribution in the created nanoparticles. Experiments have shown that femtosecond lasers used at a fluence close to the ablation threshold of the material produce small and very narrowly distributed nanoparticles, and examination of the craters show the characteristic clean cuts and small heat-affected zones. However, as the fluence increases, so does the temperature and pressure of the created plasma and cavitation bubble, which perform the mentioned secondary ablation and generate larger nanoparticles with a broader size distribution, while also affecting the craters and material surface (KABASHIN; MEUNIER, 2003).

Figure 6: Surface images of materials ablated with nanosecond (left) and femtosecond (right) lasers.

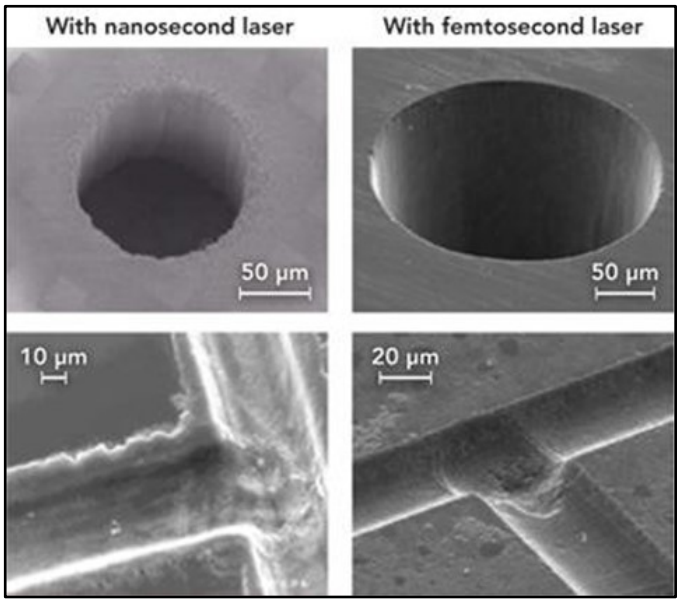

Source: (HAMAD, 2016)

In addition to the interaction between laser beam and solid due to the chosen pulse width, the operating frequency and scan speed of the system are also to be chosen taking into consideration the pulse width, mainly because of the cavitation bubble dynamics. It is important to remember that while the plasma phase happens in the nanoseconds scale, the cavitation bubble phase goes on much longer, to around 300 microseconds or more (DELL'AGLIO et al., 2015; HAMAD; LI; LIU, 2015), and that it can reach diameters of around 100 µm (JIMENEZ et al., 2015). This long lifetime can interfere with the next laser pulse in the sequence if it hits the same position during the bubble's lifetime (or if the scan speed is not enough to displace

the next pulse enough to avoid the original spot while the bubble is still expanding). In any of these cases, the energy that actually gets to the surface will be considerably smaller than the desired, since the cavitation bubble can effectively scatter the incoming radiation, while the nanoparticles contained in that bubble may reflect or absorb it, and this has a significant effect on the ablation rate of the material (HAMAD; LI; LIU, 2015; SAJTI et al., 2010a). However, the efficiency of the ablation, especially in the nanoseconds pulse width regime, increases with the irradiated area's temperature and possible surface defects (e.g. if that spot has been affected by a laser pulse before) (WANG et al., 2008). This leads to competing effects and a possible maximum of productivity to be achieved by optimizing the frequency and scan speed of the process (SAJTI et al., 2010a) (Figure 7).

Figure 7: Productivity of nanoparticles as a function of interpulse distance and scan speed (left). PO (pulse overlap) is calculated as percentage of pulse area overlap between two subsequent pulses. Scheme demonstrating the impact of cavitation bubble and heat affected zone on subsequent pulses (right).

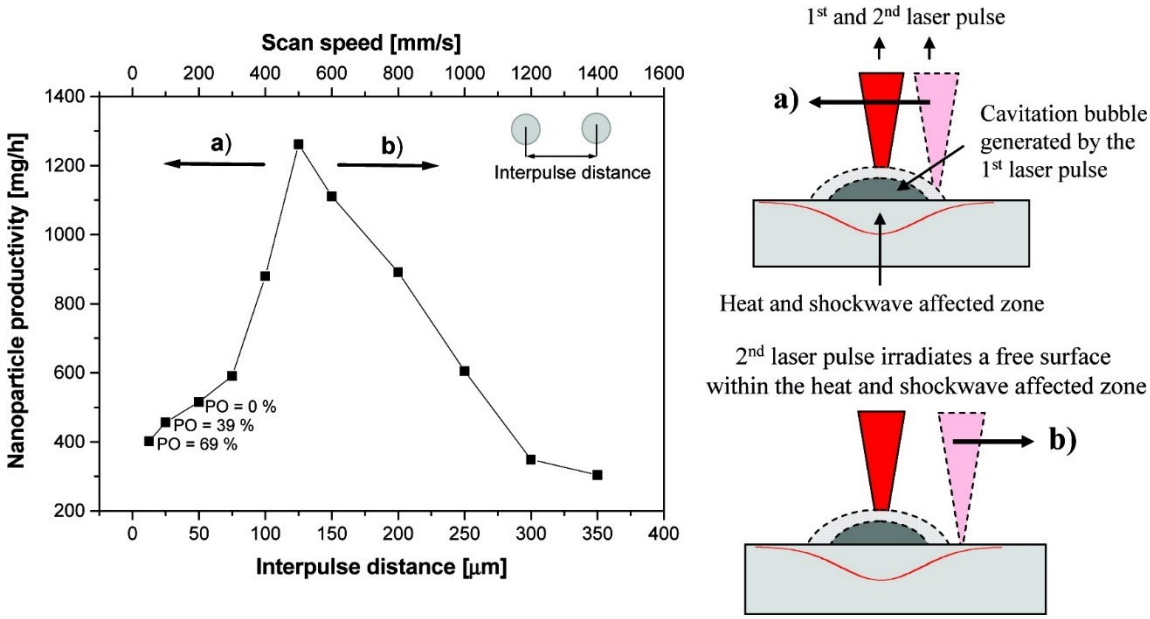

Source: (SAJTI et al., 2010b)

Fluence, calculated as the pulse's energy divided by the area of irradiation, is yet another important parameter when designing the laser ablation process. As mentioned before, ablation will only occur in the material if the fluence is above a specific ablation threshold, meaning that below a certain value, there will be no removal of material from the surface. From that point on, the fluence used affects mainly the size of the produced nanoparticles. Most results show that the higher the fluence above the threshold, the larger the nanoparticles will be

(DOLGAEV et al., 2002; KABASHIN; MEUNIER, 2003; KUMAR; THAREJA, 2013; SHAFEEV; STRATAKIS, 2012). This is most likely due to the excess energy being irradiated on the target, which increases the temperature of the system and the molten volume ejected from the surface. That molten volume tends to condensate into larger nanoparticles when compared to the fast ejection regime (HAMAD, 2016). In some cases, higher fluences may also induce an optical breakdown of the liquid, meaning that energy will be dissipated before it reaches the target (STREUBEL; BENDT; GÖKCE, 2016). Overall, it appears that for each specific case there is an optimum fluence to produce the desired nanoparticle size and size distribution.

The laser's characteristic wavelength also has its role to play in the ablation, mainly due to possible absorption peaks in the material. Lasers have a large range of possible wavelengths, from infrared to ultraviolet, depending on the material and active media (SINGH et al., 2012b), and each material to be used as a target during the ablation has a specific absorption spectrum, that indicates in which wavelength(s) they absorb more radiation. This means that depending on the combination of laser wavelength and material absorption spectrum there may be more or less radiation absorption by the target and by the nanoparticles generated in the dispersion. As an example, it is reported that during the ablation of silicon in the nanosecond regime, the use of a wavelength of 532 nm leads to higher yield when compared to a 1064 nm laser. This is due to the higher radiation absorption by silicon in the 500 nm range (CHEWCHINDA et al., 2013). When dealing with the ablation of metals, most wavelengths are appropriate due to the optical characteristics of metals (SHAFEEV; STRATAKIS, 2012). However, once the nanoparticles are formed and dispersed in the solution, there may be stronger interaction, especially with those that show surface plasmon resonance. As an example, we can take pulsed laser ablation of a silver target in liquid. Silver has a strong absorption around 500 nm, around the UV/Vis region. When irradiated by a laser with a wavelength in such a region, the dispersed nanoparticles absorb the energy from the laser beam, which in turn has two main effects: there may be further fragmentation of the particles and a reduction in the average particle size, and there is less energy being transferred to the main target (SCHWENKE et al., 2011), which may lower the ablation rate.

The post-irradiation effect aforementioned (Figure 8), while enhanced by the wavelength-specific absorption, is quite common in the laser ablation in liquids process. With the ejection of nanoparticles from the target into the solution, if the liquid is not stirred, there is a tendency for the particles to concentrate on top of the target, which shields the material from

the laser beams by either reflecting, absorbing or scattering the radiation. This obviously reduces the radiation that effectively reaches the surface of the target while increasing the energy of the dispersed nanoparticles, which may then fragment them further. This further fragmentation is more easily achieved in short and ultrashort lasers due to their higher energy density (SCHWENKE et al., 2011). Some experiments show that using this post-irradiation effect as a posterior treatment to nanoparticles produced by laser ablation in liquids can reduce the average size and size dispersion while stabilizing the particles even further, maintaining the dispersion without precipitation (BESNER; KABASHIN; MEUNIER, 2006; KUBILIUTE et al., 2013; TSUJI; WATANABE; TSUJI, 2003). This being said, the PLAL process can be setup so that there is no influence from the already ablated nanoparticles in the dispersion by quickly removing them from the laser's way, by a combination of scan speed and liquid flow, in liquid-chambers, for example. This ensures the highest possible ablation rate in the system, and the collected nanoparticles can then be processed even further if needed be (CHEN; ZHANG, 2012; KOHSAKOWSKI et al., 2017; SAJTI et al., 2010a; STREUBEL; BARCIKOWSKI; GÖKCE, 2016; STREUBEL; BENDT; GÖKCE, 2016).

Figure 8: Exemplification of different interactions happening during laser ablation in liquids, including the post-irradiation process.

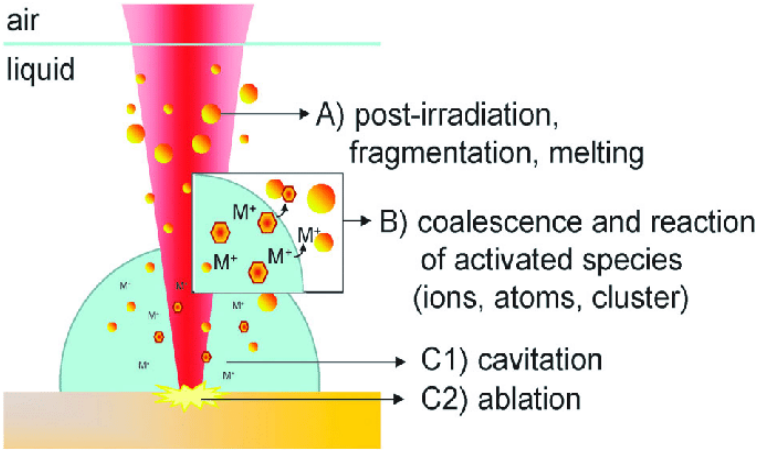

Source: (NEUMEISTER et al., 2014)

The last parameters to be discussed here are about the liquid layer above and around the target. By changing its composition and height, it is possible to fine-tune the produced nanoparticles as well as the ablation rate. Common liquids used in this ablation process are distilled water, ethanol and acetone, though several other organic liquids may be used depending on the desired effects (BAJAJ; SONI, 2009; DOLGAEV et al., 2002; KANITZ et al., 2016; MUSAEV et al., 2013; SCHWENKE et al., 2011). Plus, electrolytes, dispersants or

surfactants may be added to the dispersion to control some aspects of the generated nanoparticles (BAJAJ; SONI, 2009; FONG et al., 2013; KIM et al., 2015; ROSA et al., 2014; TAKEDA et al., 2002). For example, the ablation of tin under different liquids (ethanol, deionized water, or acetone) changes quite drastically the shape and size of the generated nanoparticles. In ethanol, they are thread-like structures; in water, slightly elongated non-spherical particles; and in acetone, interconnected spherical particles. As for their size, generation in water showed a size distribution of 37 ± 10 nm, while in acetone it was 2 ± 1 nm (BAJAJ; SONI, 2009). The same size-related behavior was found for copper and silver ablated in the same liquids (TILAKI; IRAJIZAD; MAHDAVI, 2006; TILAKI; ZAD; MAHDAVI, 2007). This difference is explained through the polarity of the liquid media and the dipole-dipole interactions between the nanoparticles and solvent during their generation. After the nucleation of the nanoparticle in the plasma phase, those nuclei can serve as growing centers for other nuclei, species in the plume, or even molten globules ejected from the surface. During this second stage of growth, highly polar solvents can help stabilize the nuclei and prevent the agglomeration by interacting with more strongly with the particle's surface electric double layer and increasing repulsion between new nuclei and species in the plasma plume. This can be evaluated from the dipole moments of ethanol (1.69 D), deionized water (1.85 D), and acetone (2.89 D) (BAJAJ; SONI, 2009; GE et al., 2003; LIAO et al., 2003).

Not only does the chosen solvent affect the size and aggregation of nanoparticles, but it may affect the composition as well. Depending on the medium, there may be higher or lower oxidation of the ablated material, as well as the presence of different groups attached to the surface. Particularly, in the plasma plume both solvent and solid target exist as ions and atoms, which facilitates the oxidation reactions. This takes into account not only surfactants or dispersants, purposely added to the mixture, but also OH groups coming from the solvent molecules. Tin ablated in a water medium generates polycrystalline particles of tin oxide (SnO_2), while the same ablation performed in ethanol generated single crystals of metallic tin coated with tin hydroxide ($Sn(OH)_2$) (MUSAEV et al., 2013). Silver, on the other hand, has been processed in different organic solvents, and quite different nanoparticles were obtained. When ablated in acetonitrile (AN) and N,N-dimethylformamide (DMF), free silver nanoparticles were generated, while when ablated in dimethyl sulfoxide (DMSO), the result was nanoparticles embedded in a carbon matrix. The last case, for silver ablated in tetrahydrofuran (THF) showed an intermediate structure, where a silver metal core was surrounded by a thin carbon layer (AMENDOLA; POLIZZI; MENEGHETTI, 2007).

Finally, the height of the liquid above the solid target also influences the ablation process. Besides lowering the thickness of liquid that the laser beam has to overcome in order to get to the target's surface (which may affect the laser focus and the energy that effectively gets to the material), a smaller liquid film can help improve the nanoparticle productivity. By analyzing the ablation rate during the ablation of silicon in water and germanium in water, the optimal liquid thickness is found to be around 1.1 mm and 1.2 mm, respectively. With liquid films thicker than that, the amount of water over the target is enough to interact with the laser so that the beam loses energy. Meanwhile, in regimes where the liquid film is thinner than that, the amount of water over the target is not enough to effectively confine the plasma plume, allowing some of it to escape and reducing the pressure and temperature inside it, having a negative effect on the productivity (JIANG et al., 2011; ZHU; LU; HONG, 2001). Besides, by carrying away the produced nanoparticles and clearing the beam path, the thinner liquid film helps with reducing energy losses to laser-nanoparticle interaction, considerably increasing the productivity, though, In some cases, this may lead to larger particle sizes due to the reduction of the post-irradiation effect (BÄRSCH, 2010; JIANG et al., 2011).

As can be seen from the previous paragraphs, the number of parameters that influence the PLAL process is quite large. Besides the aforementioned ones, which are essential for the description of the process, other parameters also have some effect on different aspects of the process, such as bath temperature (D'URSO et al., 2018; SHAJI et al., 2015), pH and target/laser inclination (AL-MAMUN; NAKAJIMA; ISHIGAKI, 2013) and the use of another laser for subsequent processing of the colloid solution for post-irradiation ablation of the nanoparticles (BATTIE et al., 2015; XIAO et al., 2017). Since many of the parameters for the process depend on the specifics of the laser machine, the materials chosen as substrates and the experimental setup available, our focus in this work is to experiment with the available laser system in order to better understand it and optimize main parameters such as fluence, pulse width, scan speed and ablation time so to characterize the nanoparticles being produced.

2.4 TITANIA

Titanium dioxide, usually known as titania, is an oxide material with the chemical formula TiO_2. Its physical, chemical and optical properties make it attractive to a considerable number of different applications such as pigments (GÁZQUEZ et al., 2014), sunscreens (NEWMAN; STOTLAND; ELLIS, 2009), photocatalysis (FUJISHIMA; ZHANG, 2006),

photovoltaics (BAI et al., 2014) and more. Due to this versatility, it is one of the most studied materials, both in the micro and in the nano scale.

There are three naturally occurring titania phases: rutile, anatase and brookite, which differ quite a lot in characteristics, as shown in Figure 9. While rutile and anatase (both with a tetragonal structure) are more commonly found both in nature and in artificial synthesis, brookite (orthorhombic) is rarer and its synthesis is more difficult in laboratories, hence more information is found about the first two phases (BELTRÁN; GRACIA; ANDRÉS, 2006; BICKLEY et al., 1991). As a bulk material, rutile is the most stable phase, and it is easily obtained by heat treatment of other titania phases such as anatase and brookite. In the usual titanium dioxide synthesis methods, one first produces an amorphous titania phase, which can then be heated to produce an amorphous-anatase transformation (at around 300-500°C) and then an anatase-rutile transformation (at around 600-700°C). The different phases also reflect in the bandgap energy of the materials. Anatase and rutile have a 3.2 eV and 3.0 eV bandgap, respectively (ALLEN et al., 2018; BAI et al., 2014; DA SILVA, 2016; GUPTA; TRIPATHI, 2011).

Figure 9: Different crystalline phases of titania. a) anatase (tetragonal); b) rutile (tetragonal); c) brookite (orthorhombic)

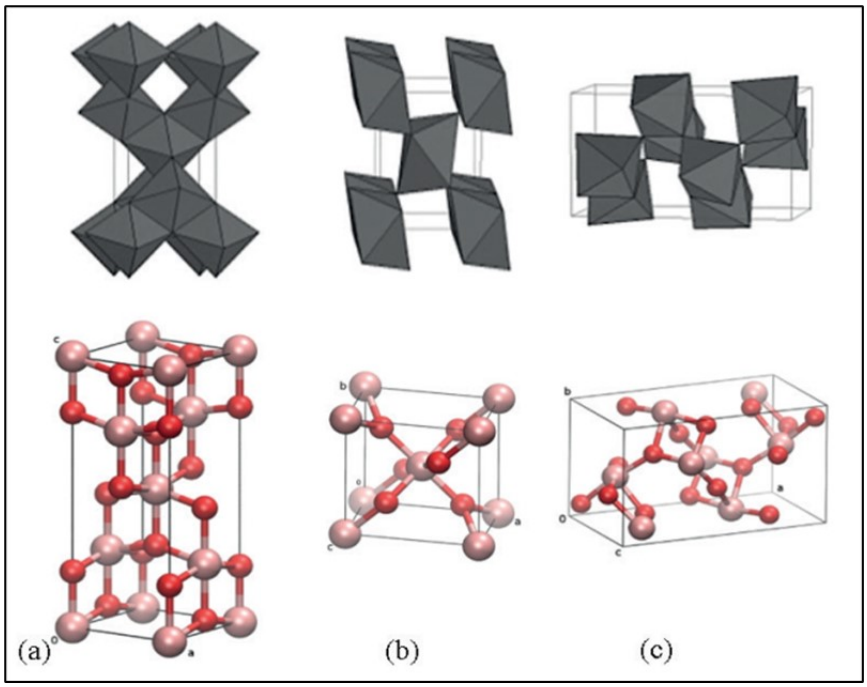

Source: (SCARPELLI et al., 2018)

For photocatalytic applications, anatase is the leading player. Rutile usually shows little to no photocatalytic activity on its own, while there is some research involving brookite

showing good results (ALLEN et al., 2018; GUPTA; TRIPATHI, 2011), anatase is by far more studied and understood. Factors such as a reduced particle/crystallite size, higher Fermi energy, higher mobility for charge carriers and smaller electron effective mass can contribute to anatase being a better catalyst when compared to rutile (ANDRONIC et al., 2011; GUPTA; TRIPATHI, 2011; LUTTRELL et al., 2015; MO; CHING, 1995). Finally, a synergistic effect of a mixture of titania phases was shown in several situations, where rutile-anatase and brookite-anatase mixtures performed better than pure-phase particles in photocatalysis experiments. Possibilities that might explain this behavior are mostly based on the phase to phase interface, where effects such as electron and hole exchanges, hindering of recombination, and even a higher surface area can be found (ALLEN et al., 2018; BOEHME; ENSINGER, 2011; LI et al., 2007; SCANLON et al., 2013; TZIKALOS; BELESSI; LAMBROPOULOU, 2013).

2.4.1 Nano titania

Lately, most of the research and development has been performed with TiO_2 nanomaterials, in order to enhance the activity of the particles and composites and have better control over their properties and characteristics. When going to the nanometer scale, a different regime is found where anatase appears as the most stable phase for certain nanoparticle sizes, as presented in Figure 10. Different calculations show different results for specific situations, with some authors pointing at a transition point below 15 nm for spherical particles and at higher values for particles with different shapes (CASTRO; WANG, 2011; DA SILVA; HOTZA; CASTRO, 2017; CHANG et al., 2012; GUPTA; TRIPATHI, 2011). This is yet another reason why more photocatalytic activity is found: besides increasing surface area, the phase composition of the particles tends to become more favorable to photocatalysis.

Figure 10: Phase stability of titania according to superficial area.

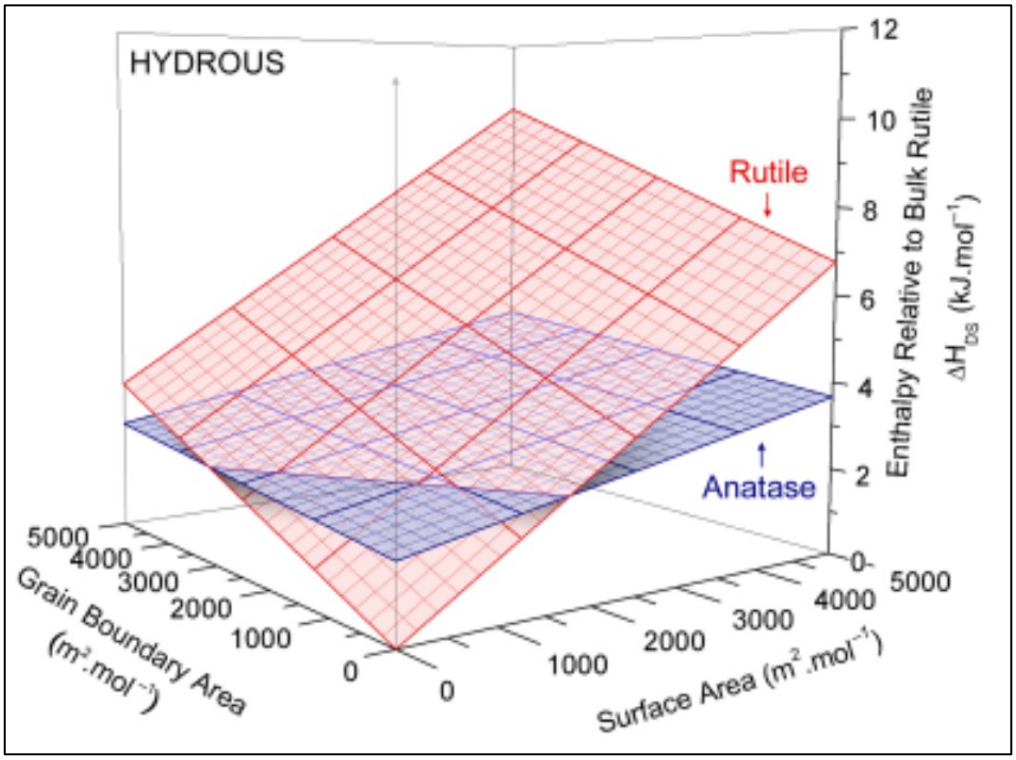

Source: (CASTRO; WANG, 2011)

Usually, titania nanoparticles are produced through chemical, bottom-up approaches mainly for scalability and cost reasons. Hydrothermal, solvothermal and sol-gel methods, assisted by surfactants, microwaving, sonochemical and even electrospinning approaches are commonly used both in laboratories and in higher volume, market applications (WANG et al., 2014).

Our interest, however, is to test and evaluate the production of these well-known titanium nanoparticles through the top-down method of pulsed laser ablation in liquids.

2.4.2 Blue titania

One of the main issues with titania as a photocatalyst is that, due to its high bandgap, UV light is required to generate the electron-hole pairs that will effectively act in the catalysis. Many efforts have been made in order to reduce the bandgap and hence extend the usability of the titanium dioxide to the visible range. Doping is one of the main methods studied to achieve that, with both metallic (Ag, W, Co, amongst others) and non-metallic (N, C) dopants for

example (BURDA et al., 2003; GUPTA; TRIPATHI, 2011; WANG et al., 2014; ZHANG et al., 2017).

Another method for extending the absorption range of titania is by inducing defects on the surface of the particles. For TiO_2 particles, several methods to induce those defects exist and have been studied, such as hydrogen thermal treatments, plasma treatment, chemical reduction, or oxidation (CHEN; LIU; HUANG, 2015; XIONG et al., 2012; YAN; LI; XIA, 2017). The exact nature of these defects is not yet fully understood, and different explanations have been proposed, including a disordered layer on the surface, creation/insertion of Ti^{3+} ions in place of the usual Ti^{4+} ions in the lattice, creation/insertion of oxygen vacancies and insertion of Ti-OH or Ti-H functional groups (CHEN; LIU; HUANG, 2015; GLEZAKOU; ROUSSEAU, 2018; YAN; LI; XIA, 2017). These defects change the absorption spectra of titania (considering the average charge of the titanium ion in these particles, they are usually referred to as TiO_{2-x}) towards the visible range and the usually white particles start showing color, from white to gray, blue and eventually black. Some processes will even yield yellow-colored titania particles (CHEN; LIU; HUANG, 2015).

Figure 11 a) shows images of hydrogenated titania as prepared (blue) and then annealed back to the original white color, process which removes hydrogen atoms from the particles. Figure 11 b) shows the diffuse reflectance spectra, which indicates how the hydrogenated titania absorbs much more of the visible and near infrared light when compared to the white titania, which induces photocatalytic activity in the visible range for processes such as dye degradation, hydrogen production and water splitting.

Figure 11: Characteristics of blue titania as produced (TiO_{2-x}:H) and annealing at 200, 300 e 400°C. a) photography; b) diffuse reflectance spectra; c) EPR (electron paramagnetic resonance); d) M-H measurement (magnetism)

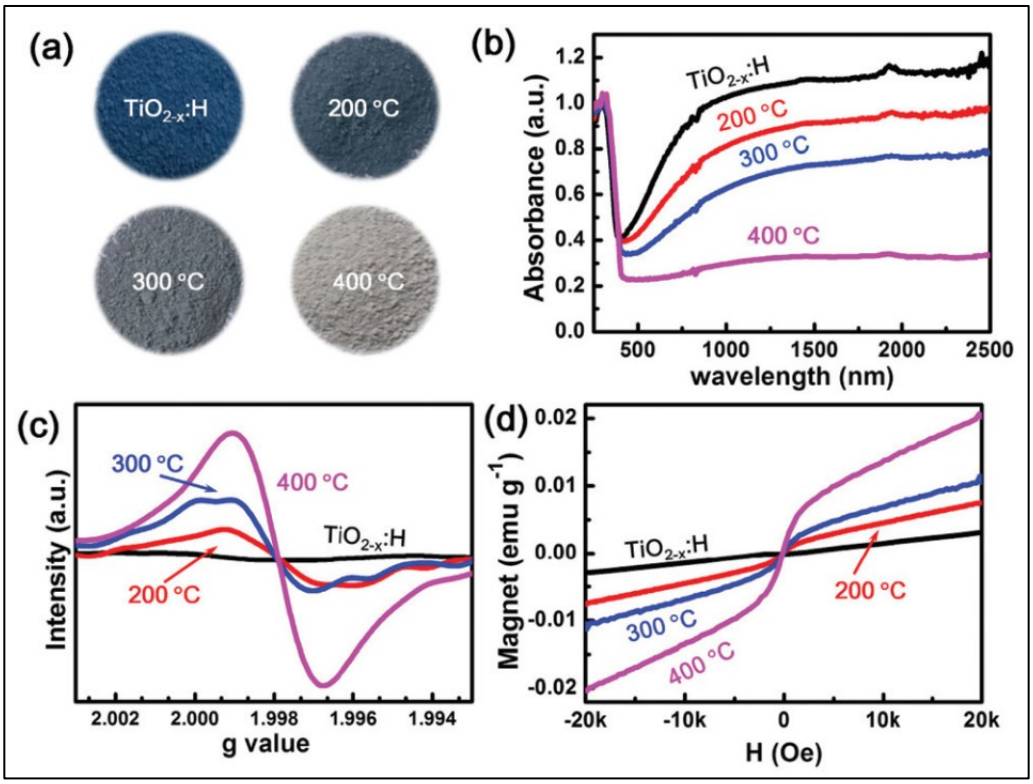

Source: (ZHU et al., 2016)

An exciting aspect of the PLAL process is that in most cases it produces blue titania in a single step, without the need for secondary treatments. Both from titanium targets, as presented in Table 2, or from TiO_2 powders, where the laser energy is used to further fragment the powder and to induce defects (CHANG et al., 2012; LE MERCIER et al., 1995). The first and more clear application of these materials is again in photocatalysis. Blue titania has been tested and shows promising results in CO_2 reduction, degradation of contaminants and even H_2 production (HAMDY; AMROLLAHI; MUL, 2012; SORCAR et al., 2017; YIN et al., 2018).

2.4.3 PLAL titania nanoparticles

Many groups have already produced and characterized nanoparticles through PLAL. Table 2 shows a list of references and some information on the laser system, the process parameters and the results obtained. When available, the data is related to process values for PLAL (ablation target material, liquid medium used, laser wavelength, pulse width and fluence) and main results such as particle diameter, identified crystalline phase and morphology.

The chosen references bring examples of different targets (solid targets, foils and powders), wavelengths (visible and infrared), pulse duration (ns, ps and fs) and fluences with different results. One example of an alternative medium (0.001 M SDS solution) is presented (SRIVASTAVA et al., 2016), and shows a difference in phase production, as well as in agglomeration patterns due to the stabilizer. Thus, variable phases, morphologies and particle sizes can be obtained according to the parameters and values applied.

Table 2: Comparison of different titania nanoparticles produced by PLAL.

Target	**Liquid**	**λ [nm]**	**τ [ns]**	**F [J/cm²]***	**d_p [nm]**	**Phase**	**Shape**	**Ref.**
99.99% Ti	Water	1064	800	-	30	Hybrid	Spherical	(TIAN et al., 2009)
Ti foil, 0.89 mm	Water	810	270E-6	38.7	25	Hybrid	Spherical	(KÖRSTGENS et al., 2015)
Rutile powder, <5 µm					150	Hybrid	Amorph	
99.99% Ti	DI Water	1064	500	34.6	8.1	Hybrid	Spherical	(SINGH et al., 2017)
99.6% Ti	DDI Water	1064	25E-3	2.21	5	Rutile or Anatase	Spherical	(GIORGETTI et al., 2015)
			25	7.81		Rutile		
99.5% rutile powder, 1 µm	DI Water	532	16	53.4	5	Amorphous, anatase, rutile, brookite	Spindle	(CHANG et al., 2012)
						Anatase		
99.99% Ti	DI Water	532	5	5	50	Anatase	Agglomerated	(SRIVASTAVA et al., 2016)
	0.001 M SDS					Rutile	Spherical	
99.99% Ti	DI Water	1064	10E-3	0.3717	37	-	Spherical	(HAMAD; LI; LIU, 2015)
		532	5	12.2	30			
99.99% Ti	DI Water	1064	6	20	5-30	Anatase	Spherical	(SIUZDAK et al., 2014)
99.99% Ti	DI Water	1064	10E-3	0.8	32	Rutile	-	(HAMAD; LI; LIU, 2016)
		532		5	34	Anatase, rutile		
99.99% Ti	DDI Water	1064	10	-	5**	Anatase	-	(SINGH; SWARNKAR; GOPAL, 2009)

* Underlined values were calculated by the author based on the specific reference.

** Value estimated from UV-Vis data

Source: Author (2020)

The variation among experiments can be attributed to the parameters mentioned in the previous sections such as the laser system, the setup built and even the chosen geometry of the laser beam scanning on the surface of the target. Since it is difficult to completely reproduce a specific setup (when compared to solution-based methods, for example), the variability between different groups is high. This also means that a group that is starting to work with PLAL will probably have to study and characterize their system on its own, and not entirely base their experiments on the literature.

Figure 12: TiO_2 nanoparticles produces by laser ablation in water. a) spherical and spindle-like particles; b) spherical particles

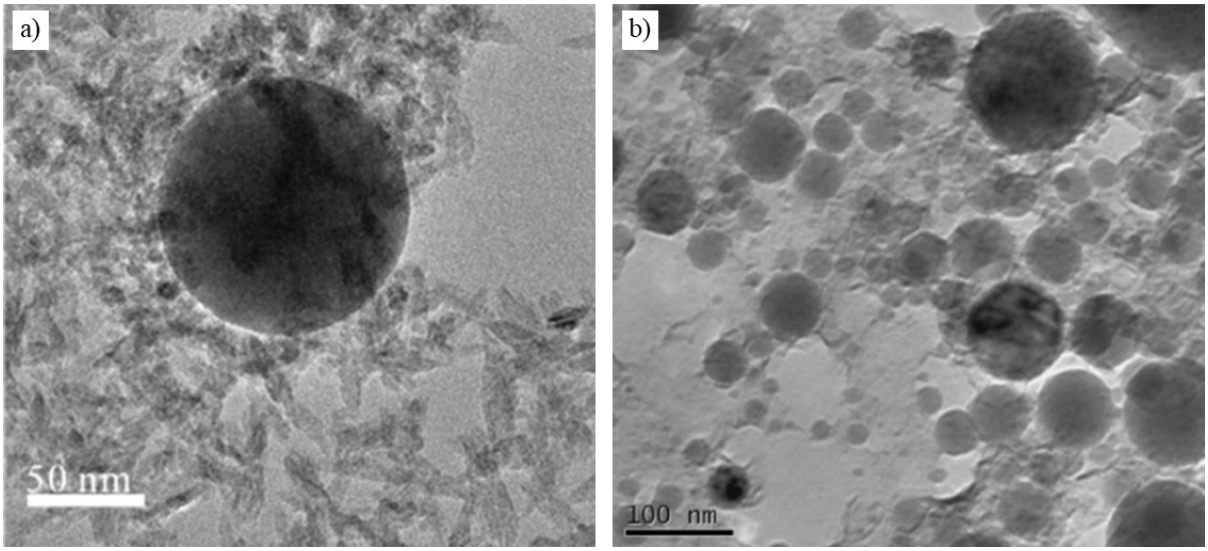

Source: a) (CHANG et al., 2012); b) (HAMAD; LI; LIU, 2016)

Figure 12 presents pictures obtained from two of the works in Table 2 in order to illustrate the appearance of the nanoparticles produced by PLAL. In the left, we see a majority of small spindle-like structures and one big spherical particle, which were produced from rutile powder irradiation in a work by Chang et al. (2012). In the right, Hamad et al. (2016) produced only spherical particles using a titanium 99.99% titanium target. Both nano titanias were synthesized using nanosecond lasers, as is the aim of this work.

There is yet another problem when reviewing the literature for PLAL synthesis of nanoparticles. Considering all the different parameters, it is common not to be able to compare experiments simply because not enough information is available on the respective papers. For example, it is very common for authors not to describe the geometry of the ablation, i.e., how the laser beam was “moved” on top of the target, whether as a rectangle, as parallel lines, circles or even if it was kept at the same place. The scan speed, pulse overlap, power/energy are other

parameters that are not always present. While it is possible to calculate some of them (in Table 2), the underlined values were calculated by the author, this is not always the case.

Still, this work is relevant and useful as an overview of how this process is being used in other groups, and to estimate expected particle size, energy and pulse width regime and even the resulting TiO_2 phases.

3 MATERIALS AND METHODS

> "The fact that we live at the bottom of a deep gravity well, on the surface of a gas covered planet going around a nuclear fireball 90 million miles away and think this to be normal is obviously some indication of how skewed our perspective tends to be."
>
> (ADAMS, Douglas)

Here, we report in details the main materials, structure, resources and methods used during this work, including where the funding and human resources came from.

3.1 MATERIALS

3.1.1 Laser machine

The laser machine used in this work (Figure 13) is a system produced and commercialized by the company Welle Laser, from Florianopolis and located in Palhoça, both in Santa Catarina. Welle is Nanogreen's partner in the development of laser ablation technology for the Brazilian market. Due to a disclosure agreement, the full specifications of the system such as the laser source and optical components exact details will not be shared, but the main parameters related to the ablation process are listed in Table 3.

Table 3: Laser parameters.

Nominal laser power (P)	20 W
Maximum pulse energy (E_p)	1 mJ
Maximum peak power (P_p)	14 kW
Pulse width range (τ)	3 – 500 ns
Central emission wavelength (λ)	1059 – 1065 nm
M^2	< 1.6
Frequency (f)	20 – 1000 kHz
Scan speed (v_s)	1 – 10000 mm/s
Focal length of lenses	100 mm
Nominal beam diameter (d_b)	27 μm

Source: Author (2020)

In this setup, the lenses used are non-telecentric, i.e., in the borders of the working area the laser beams might hit the target with a small angle due to divergence. This effect can be increased because of the galvo system used instead of an xyz-stage. This can affect works that are performed close to the edge of the working area, which is, in this case, 45 × 45 cm^2. Considering the size of our targets (25 × 25 mm^2) this is not relevant since all the ablation is performed right beneath the lenses.

Figure 13: LS2000 Marking Series Welle laser machine.

Source: Welle Laser (2020)

Thus, a low power, nanoseconds regime laser in the near-infrared region of the spectra was used. This setup can be considered a relatively “inexpensive” one, which goes along with the goal of trying to keep the overhead low. This machine is usually used for engraving of metals and other materials for decoration or quality control, for example. The system presents a fairly good M^2 value, which is the laser beam quality factor, for engraving processes, but recent laser machines for micro and nanofabrication usually work with lower values. In the

perfect, fundamental mode of a Gaussian beam, M^2 is 1, while for all practical applications M^2 is higher than 1. While most papers and works on nanoparticle production through laser ablation do not directly mention their M^2 values, some research on the laser systems reveals laser beam quality factors around 1.2 – 1.6, with a specific system presenting an average value of 1.05 (FITZSIMONS, 2012; FLORIAN BARON, 2016; SOLA; PEÑA, 2013; ŽEMAITIS et al., 2018). In our case, the Welle machine presents a beam with a 1.6 M^2 value, within the acceptable range for this kind of process, but still in the low end of laser systems for ablation in liquids.

This laser system operates in what is called "waveforms", which vary from 0 to 39. These waveforms will define the operation combination of frequency and pulse energy in order to guarantee a well-defined and known set of parameters such as pulse width and peak power. Examples of used waveforms are given in Table 4.

Table 4: Waveforms used in this work.

Waveform	**f (kHz)**	**E_p (mJ)**	**τ_{FWHM} (ns)**	**$\tau_{10\%}$ (ns)**	**P_p (kW)**
0	20	1.00	40	241	14
10	41	0.49	26	100	14
31	715	0.03	3	3	11

Source: Author (2020)

These waveforms were chosen initially in order to try the ablation method with the highest possible energy (waveform 0) as well as with the smallest possible pulse width (waveform 31). However, the fluence found in waveform 31 was not enough to cause ablation of the titanium target, and a new waveform had to be chosen. For the next tests, waveform 10 was used in order to have approximately half the fluence of the initial tests with waveform 0.

For this setup, the laser beam movement is controlled by a galvo system instead of having the machine's working area mounted on a xyz-axis as is common in many laser systems. The galvo is a set of two high-speed mirrors controlled by galvanometer drivers. This setup allows for high scan speeds and prevents the possibility of liquid spillage during the movement of the xyz-stage.

3.1.2 Titanium targets

Usually for laser ablation tests and experiments, very pure, laboratory-grade materials are used, as aforementioned in Table 2. These materials, however, while having purities of 99.99% or even more, are costly. For this work, we decided to produce titania nanoparticles from commercially available titanium alloys. The chosen material was Grade 2 Unalloyed Titanium and its composition is described in Table 5 (ASTM, 2020).

Table 5: Grade 2 titanium composition.

Titanium	**Carbon**	**Oxygen**	**Nitrogen**	**Hydrogen**	**Iron**
Balance	0.08	0.25	0.03	0.015	0.3

Source: Author, adapted from (ASTM, 2020)

Titanium alloys are graded according to their composition and physical properties. Grades 1 through 4 are considered unalloyed titanium, or commercially pure titanium, with a purity of 99%+ and no traces of other metallic elements other than iron (and titanium, of course). Grade 5 is the better-known Ti6Al4V with 6% aluminum and 4% vanadium, and from there on many different alloys are found.

Figure 14: Titanium CP2 targets

Source: Author (2020)

Nanogreen supplied the titanium targets, purchased from TiBrasil Titânio. Each of the targets has approximately 25×25 mm^2 of area and 5 mm height, and each one was hand polished with 400, 600 and then 1200 grit sandpaper in order to even the surfaces between different samples, as presented in Figure 14. They were then thoroughly washed with water and soap, rinsed with water and deionized water and put into a muffle oven to dry at 60-70º C for 30 min. Their mass was measured and noted as the “pre-ablation mass.”

3.1.3 Tungsten oxide-doped titania nanoparticles

For a simple photocatalysis test, 10 nm tungsten oxide-doped titanium dioxide nanoparticles (anatase phase) were obtained from Nanoamor and are shown in Figure 15. These small spherical shaped particles have approximately 94% TiO_2 and 6% WO_3, and are in theory highly photocatalytic, with extended activity extended into the visible range. This higher activity is usually attributed to the inhibition of electron-hole recombination and reduction of the band-gap energy by the substitution of Ti atoms in the crystal's lattice by W (MOMENI; GHAYEB; DAVARZADEH, 2015).

Figure 15: TiO_2/WO_3 nanoparticles

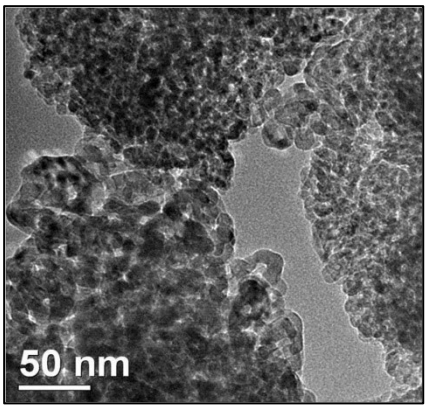

Source: (NANOAMOR, 2020)

3.1.4 Other materials

Besides titanium targets and titanium dioxide nanoparticles, other materials used were:

a) deionized water;
b) pipettes;
c) 15 mL storage vials;
d) Petry dishes and beakers;
e) magnetic stirrer and magnetic stirrer bars;
f) scale;
g) tweezers;
h) Reactive Red 141 (RR141) dye;
i) UV-B spectra lightbulb;
j) visible spectra lightbulb

3.2 PROCESSING AND CHARACTERIZATION METHODS

3.2.1 Pulsed Laser Ablation in Water

The experiment design for this work was based on the variation of 3 parameters in the laser ablation in liquids process: ablation time (the actual parameter set in the system is number of cycles, but the experiments were based on ablation time), scan speed and waveform number. As mentioned previously, the waveform number defines pulse width and peak power by setting the frequency and pulse energy. We wanted to evaluate the changes in nanoparticle productivity (here defined in mg/h) and nanoparticle characteristics (such as diameter, zeta potential, shape).

The constant laser parameters of the process were:

- Wavelength: 1064 nm
- Nominal Power: 100%
- Focal length: 100 mm
- Nominal beam diameter: 27 μm

The liquid medium parameters were also kept constant and as follows:

- Liquid medium: Deionized water
- Liquid height above the target surface: 4 mm
- Liquid volume: 30 mL
- Agitation: 500 rpm

For the variables, the following parameters were used:

- Waveform 0 ($f = 20$ kHz; $E_p = 1.00$ mJ; $\tau = 40$ ns) and 10 ($f = 41$ kHz; $E_p = 0.49$ mJ; $\tau = 26$ ns).
- Waveform 31 ($f = 715$ kHz; $E_p = 0.03$ mJ; $\tau = 3$ ns) was used for a single test
- Scan speed (S_s): 270 mm/s and 1350 mm/s;
- Ablation time (t): 5 min, 15 min and 30 min.

By changing the waveform, we expected to identify the influence of changing the energy and pulse width on the nanoparticles. Unfortunately, in this setup we could not "disconnect" these variables, both being tied to the waveform. However, it was still interesting to evaluate whether this relatively small difference in energy and pulse width (~1 order of magnitude) would have any relevant effect on the final product.

Considering a same ablation time, scan speed directly affects how many times the laser beam will hit the same place in the target (for the same time and a higher speed, longer distance

will be covered, and since the distance is fixed, more passes will be performed to fill that time). In theory, increasing the number of passes should implicate in more substantial material removal, but competing effects might be found such as the concentration of particles on the liquid, for example. Another factor that the scan speed directly affects is what we called “pulse overlap” (PO), which represents how much the laser beam has moved horizontally in relation to the last pulse’s position. While this relation can be expressed by Equation (2) below, Figure 16 shows what this factor means in a more illustrative manner, where v_s is the scan speed, f is the frequency and S_s is the spot size.

$$PO\ (\%) = [S_s - (v_s / f)] / S_s * 100 \qquad (2)$$

Figure 16: Pulse overlap examples. a) 100%; b) 50%; c) 0% and d) -50%.

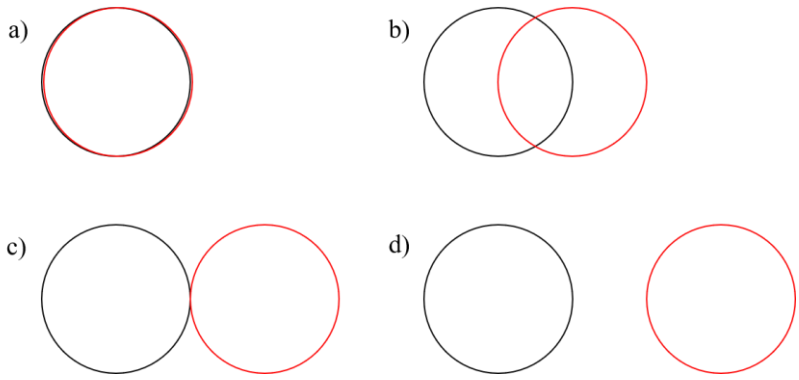

Source: Author (2020)

Finally, ablation time is bound to show an increase in the total mass produced for obvious reasons, but this does not mean that it will have a better per hour productivity due to factors such as the increase in the concentration of particles on the liquid for example. This irradiation not only causes less energy to reach the target surface, but also can affect the particles already ablated, by changing its morphology or size. While this work will study these possible differences, flow setups for example can help remove such particles, prevent the loss of energy, and enhance size distribution, morphology and productivity. For each of the desired ablation times (5, 15 and 30 min), the duration of a single pass over the ablation design (showed below) was measured without the target and then the number of passes necessary to reach the mentioned ablation time was calculated.

The ablation design on each sample was the same, as presented in Figure 17 (not to scale). Black arrows represent the path of the laser beam when it is turned on. The red arrows show the path the laser performs with the beam off, meaning that there is no ablation on the transition between lines. This way, the length ablated by each pass is the same for all experiments, and by increasing ablation time or scan speed we are increasing the total ablated length.

Figure 17: Ablation design on the titanium targets

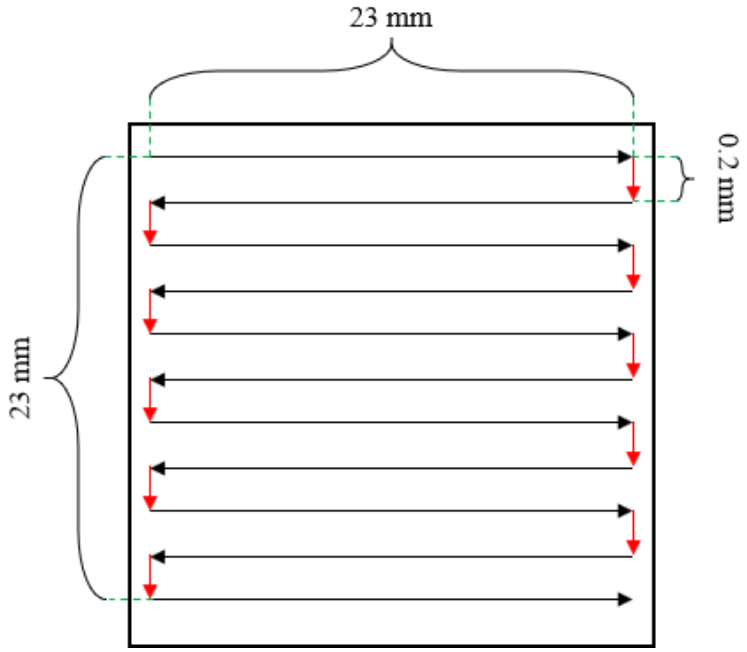

Source: Author (2020)

For the practical setup, the grade 2 titanium target was placed in a 250 mL glass beaker and then covered with 30 mL deionized water. A magnetic stirrer bar was placed beside the target. This beaker was then placed on top a magnetic stirrer equipment mounted on the working area of the LS2000 laser machine. The laser machine was focused directly on the surface of the titanium target to maximize fluence on that spot. A schematic of the whole system is shown in Figure 18.

During the longer experiments such as 15 min and 30 min, an increase in the water temperature was noticed. For 5 min that increase was negligible, but it was quite considerable at 15 min. For the 30 min experiments, the beaker was placed inside a larger plastic recipient filled with a 50:50 mixture of water and ethanol in order to reduce the excessive temperature rise. This simple change in the setup allowed the 30 min tests' temperature rise to be comparable to that of the 15 min. Unfortunately, we were not able to measure the temperature increase during the experiments.

Figure 18: Laser ablation in liquids setup schematic.

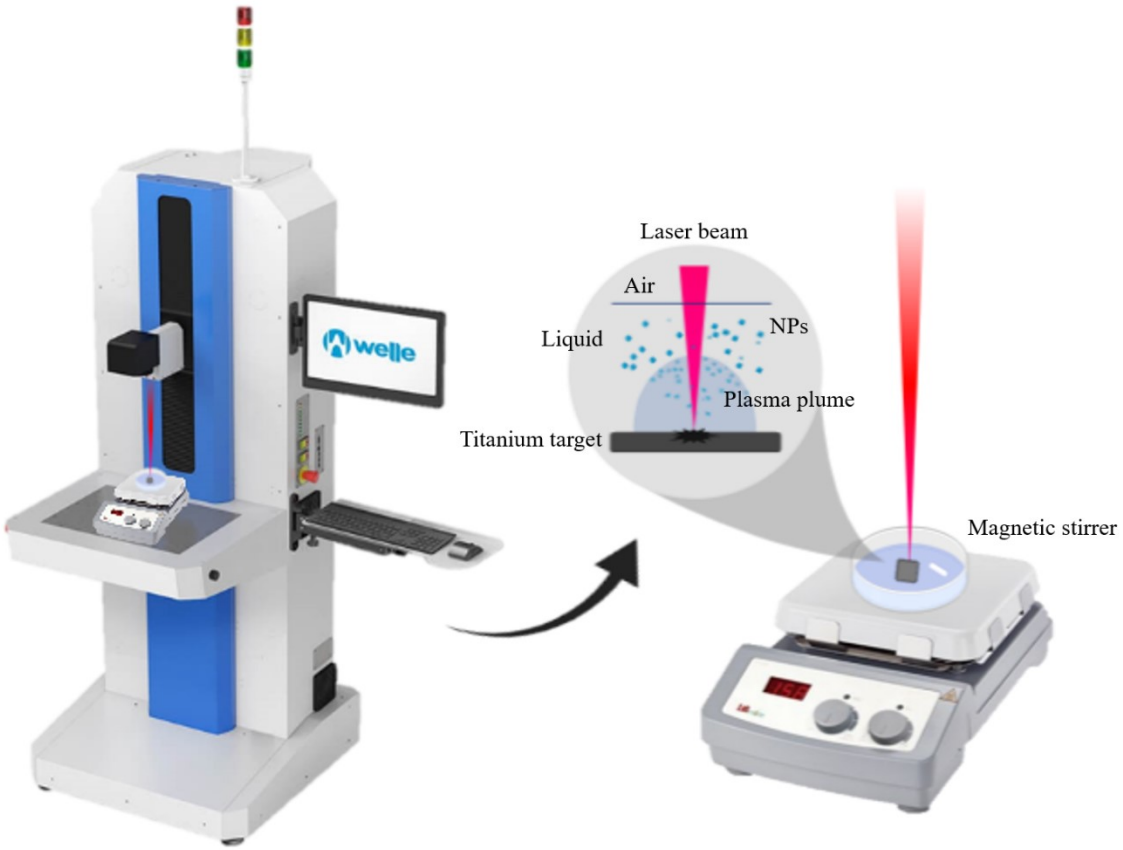

Source: Letícia Silva de Bortoli, unpublished (2020)

The experimental setup is shown in Figure 19, where the optical system is visible, as well as the magnetic stirrer, stirrer bar and an example target. A video of the process is also available through the QR code in Figure 20 for those with the printed version and/or through the link in the description of said Figure for the ones reading it on the computer. This illustrates the operation of the system and might help with the understanding of the experiments.

Figure 19: Welle laboratory experimental setup.

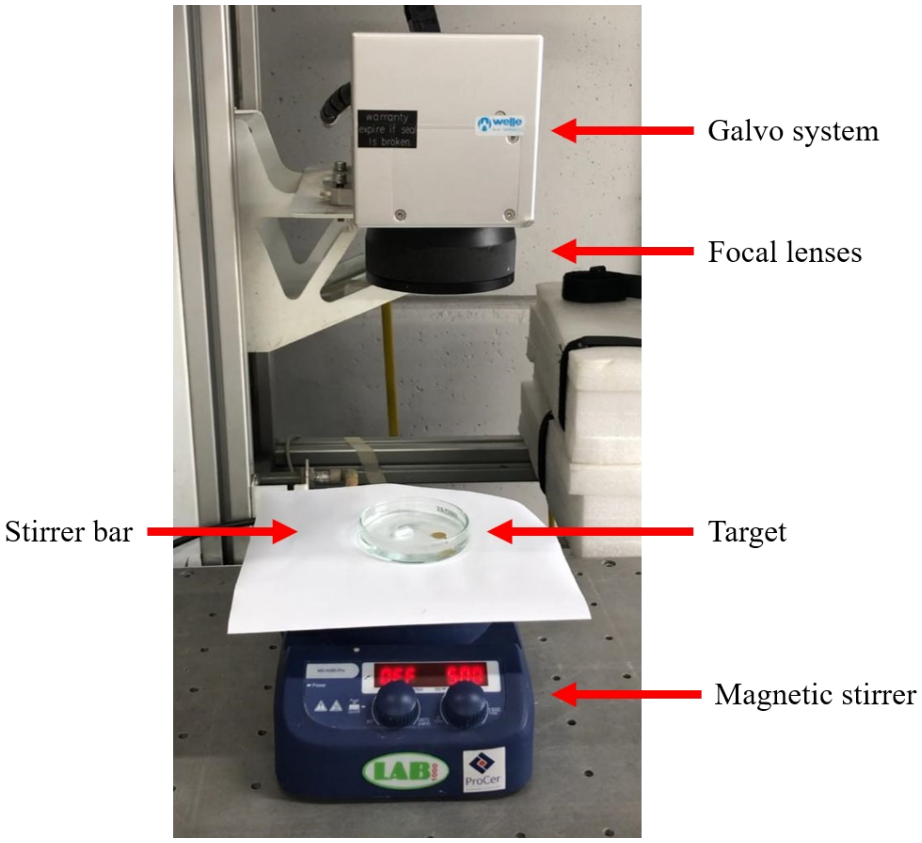

Source: Author (2020)

Figure 20: QR code to the laser ablation process experimental setup, Link to the video: https://1drv.ms/v/s!Ar9ILkt5W35ygqorqzz6RtqwkL-QLQ

Source: Author (2020)

The experimental planning was made varying the waveform, scan speed (v_s) and ablation time (t) as previously mentioned. Table 6 presents the parameters of each of the tests, with the values in blue being calculated by the author. Pulse Overlap (PO) is calculated based on the scan speed, theoretical spot size and frequency, as explained previously. The number of

cycles presented is the amount of times the pattern shown in Figure 17 is irradiated on the surface of the target. Depending on the chosen scan speed, this number of cycles varies between samples in order to keep a constant ablation time. This choice of keeping time constant and not the number of cycles (which means that higher speeds will in general mean a higher mass removal because of more overall irradiation) is related to the objective of evaluating the produced nanoparticles as well as the productivity. After all, while it is expected to see a higher productivity related to time with higher speeds, the influence of that increase in scan speed in the particles themselves must be considered.

Table 6: Experimental planning.

Sample	**Waveform**	**f [kHz]**	**E_p [mJ]**	**τ_{FWHM} [ns]**	**$\tau_{10\%}$ [ns]**	**P_p [kW]**	**Lens [mm]**	**d_b [µm]**	**v_s [mm/s]**	**PO**	**t [min]**	**# cycles**
w1v1t1	0	20	1.00	40	241	14	100	27	270	91.0%	5	30
w1v1t2	0	20	1.00	40	241	14	100	27	270	91.0%	15	91
w1v1t3	0	20	1.00	40	241	14	100	27	270	91.0%	30	181
w1v2t1	0	20	1.00	40	241	14	100	27	1350	55.0%	5	141
w1v2t2	0	20	1.00	40	241	14	100	27	1350	55.0%	15	424
w1v2t3	0	20	1.00	40	241	14	100	27	1350	55.0%	30	848
w2v1t1	10	41	0.49	26	100	14	100	27	270	95.6%	5	30
w2v1t2	10	41	0.49	26	100	14	100	27	270	95.6%	15	91
w2v1t3	10	41	0.49	26	100	14	100	27	270	95.6%	30	181
w2v2t1	10	41	0.49	26	100	14	100	27	1350	78.0%	5	139
w2v2t2	10	41	0.49	26	100	14	100	27	1350	78.0%	15	418
w2v2t3	10	41	0.49	26	100	14	100	27	1350	78.0%	30	836
w3v1t1*	31	715	0.03	3	3	11	100	27	270	99.7%	5	30

* This combination of parameters did not lead to effective ablation, and it was disregarded.

Source: Author (2020)

The numbering of the successful tests was done according to the waveform, scan speed and then ablation time, respectively. This means the first number (w1, w2 or w3) will indicate whether it is the waveform 0, 10 or 31; the second number (v1 or v2), whether the scan speed used was 270 or 1350 mm/s; and the third number (t1, t2 or t3), whether that sample was treated for 5, 15 or 30 min. This nomenclature will be used during the rest of this work.

During the 30-min experiments, the setup was slightly changed as mentioned before. The outer recipient used was filled with an ethanol-water mixture to help with heat dissipation in order to prevent excessive temperature rise in the ablation liquid and target. This was helpful up to a certain point (temperature rise was around the same as on the 15-min experiments), but

it added a complication, which was to prevent the movement of the target inside the ablation container. Mainly during the experiments w1v1t3 and w1v2t3, we noticed a slight movement on the target, that resulted in a shift in the ablated area of the target. The result of this movement can be seen in Figure 27, which will be presented and explained in the next session.

Finally, after the ablation process, the liquid with dispersed nanoparticles was pipetted into glass vials for storage and transportation. All produced samples were stored in the dark when not being used, so to ensure no influence from sunlight or artificial light on particle agglomeration and morphology, as happens to silver nanoparticles, for example. The titanium targets were removed, gently rinsed with water and set aside for weighting and imaging.

3.2.2 Characterization techniques

Characterization techniques were performed in different laboratories in the Federal University of Santa Catarina and focused on specific properties of the nanoparticles. Prior to any characterization, the samples were put in an ultrasound bath (Ultronique Q1.8L) for 5 min and then for another minute in a Unique USC-800 ultrasound homogenizer in order to minimize aggregation problems.

3.2.2.1 Microstructural analysis

Microstructural analysis was performed in order to understand the interactions between laser and target and also the morphology of the produced nanoparticles.

3.2.2.1.1 Optical Microscopy (OM)

In order to evaluate the laser effect on the titanium targets, an optical microscope (Leica DM4000) operated at 50x by software (LAS 4.9) was used to take pictures of the surface before and after each experiment. The Fiji distribution of the Image J software was used to measure and estimate spot size.

3.2.2.1.2 Transmission Electron Microscopy (TEM)

Images of the produced nanoparticles were obtained with a transmission electron microscope (TEM, JEM-1011 Jeol) operated at 100 kV in order to evaluate the size and morphology of the particles. Again, Fiji was used for image processing, size measurement and count, with a third-party macro for drawing and estimating an ellipse´s minor and major axis from a polygon drawn on the image.

3.2.2.2 Composition

3.2.2.2.1 X-Ray Diffraction

X-Ray Diffraction (XRD, Rigaku MiniFlex600) spectra were obtained through a slightly modified method. Because of the small amount of produced material dispersed in water, the regular protocol of filling the XRD's sample holder would not be feasible. After initial testing, the chosen protocol was: after sample centrifugation at 4500 rpm for 5 min, the supernatant was separated back to the storing vial, and the concentrated dispersion was dripped onto the sample holder using a micropipette. The sample was then dried in the oven for 1 h at 80°C. After that, with the help of a plastic spatula, the dried sample was scrapped towards the center of the sample holder in order to create a region with more concentration of nanoparticles. During the scraping procedure, sometimes tiny amounts of water were added to the sample holder to help moving the mass to the center. This concentrated sample was then read in the equipment (2θ from 5º to 90º, step size 0.05º, scan speed 10º/min) and we subtracted the signal of the empty sample holder so to get a better look at the XRD spectra.

3.2.2.2.2 UV-Vis spectrometry

A UV-Vis spectrophotometer (Hitachi U-1900 NIR) was used to obtain the absorption spectra of the produced dispersions. Readings were taken from 190 nm to 800 nm with 10 nm step. Some of the samples were diluted in order not to extrapolate the equipment's absorbance limit. This spectrum allows for a view on how each sample behaves in regard to light absorption, and can help explain the bluish hue and allow for an estimation of the bandgap energy, which is an essential parameter for the photocatalytic properties of materials.

3.2.2.2.3 Raman spectrometry

A Raman spectroscope (Renishaw inVia micro-Raman with an argon laser at 514 nm) was used. This equipment is usually used for solid samples such as powders, thus, the dispersions produced in this work needed to be dried before being analyzed. Three accumulations and acquisition time of 10 s were used, within a spectrum range from 100 to 1000 cm^{-1}. In this case, drip drying small amounts of centrifuged samples on a regular glass slide and on aluminum foil-covered slides (both surfaces of the aluminum foil) were tested. A reading was also performed without letting the dispersion dry (this means trying to read the liquid drop on the substrates). Again, after some tests, the best results were obtained by dripping the sample onto glass slides covered with aluminum foil with the shiny surface faced outward. The substrate was then dried at room temperature and read in the equipment.

3.2.2.3 Particles size and stability

A measure of nanoparticles size and size distribution and polydispersity was made by Dynamic Light Scattering (Malvern Zetasizer Nano ZS). Besides reading the particles' sizes, this equipment also calculates the zeta potential (ζ) of said particles. This measurement reveals the electrokinetic potential near the particle's surface and is a good indicator of whether the dispersion is stable or not. Dispersions with a high ζ value (in modulus) are considered stable, while values closer to 0 are unstable and tend to agglomerate quickly. Usually values around ±30 mV are considered moderately stable, and one usually looks for the highest possible value (again, in modulus) for this factor (LOWRY et al., 2016).

3.2.3 Photocatalysis

For a possible application of the produced nanoparticles, a simple dye degradation test was performed, both in the UV and in the Visible range. A 15 mL dispersion of 400 ppm nanoparticles was used to degrade Reactive Red (RR141) dye solution at 10 ppm. Here, we used both the PLAL nanoparticles and commercial TiO_2-WO_3 nanoparticles (Nanoamor) for comparison.

The absorbance of the dispersions was measured at 544 nm (absorption peak for the RR141) at specific intervals in a UV-Vis spectrometer (Molecular Devices SpectraMax

Plus384). The system was first left in the dark under 500 rpm agitation for 15 min to ensure any possible adsorption to occur before turning on the lamp for the catalysis. After the adsorption phase, the lamps were turned on and the absorbance measured to assess the degradation of the dye. These experiments were performed both with UV and Visible lamps, first without any nanoparticles added to the dye solution, in order to verify if any photolysis (degradation without any catalyst) would take place, and then with each type of nanoparticle available so to compare the results. Figure 21 shows a schematic image of the photocatalysis setup developed for this work.

Figure 21: Photocatalysis setup schematic. The interior of the box and the front lid (not shown) are covered in aluminum foil so to contain and optimize radiation reflection.

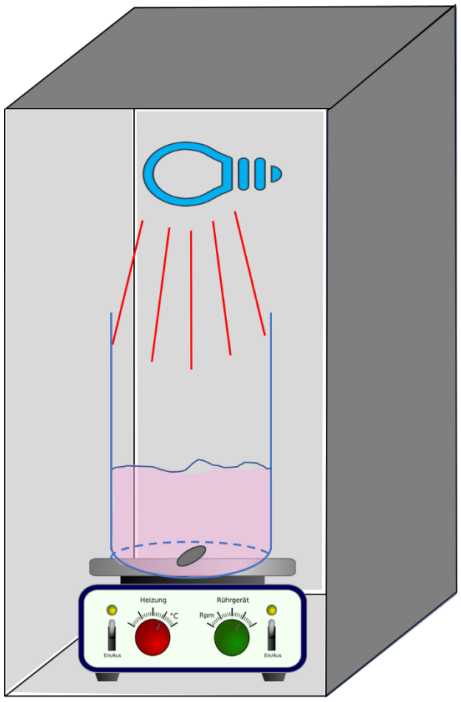

Source: Author (2020)

3.3 INFRASTRUCTURE AND RESOURCES

This session briefly describes the infrastructure used during this work and where the resources came from in order to enable this project.

3.3.1 UFSC

The infrastructure used in this work was based on the Federal University of Santa Catarina. All laboratories belong to the Interdisciplinary Laboratory for the Development of Nanostructures (LINDEN) network, and contributed with analysis, equipment and help in the operation of those.

Table 7: Laboratories used in this work and their contribution.

Laboratory	Activity
PROCER	Photocatalysis, sample preparation, workspace
LINDEN-metro	DLS, XRD
LABMAT	Optical Microscopy
LCME	TEM
LCM	Raman

Source: Author (2020)

3.3.2 Nanogreen

Nanogreen is a nanotechnology startup from Joinville – SC that works with the laser ablation in liquids method. Nanogreen is able to quickly prototype and tests customized nanoparticles, testing and adapting the particles to the client's demands.

During the last few years Nanogreen has developed projects with private companies and grants from public organizations. Companies such as Marisol, Thermo Off and Cor.Sync have worked with Nanogreen to test nanoparticles in textiles, paints, coatings and biosensors. The main focus of the company now is working with materials with a higher value, the lower overall volume and applied to medical, health and diagnosis markets.

The work here presented was funded by the Sinapse da Inovação program by FAPESC, which grants the startup money, courses and mentorship to validate and test a business idea. The grant involves money for material, services and one scholarship which was granted to the author.

3.3.3 Welle Laser

Welle develops cutting-edge laser marking, cleaning and cutting equipment. Its solutions adapt to the most varied markets, mainly to the large-scale industry. The equipment

can be easily integrated into their exclusive SMART system for online predictive monitoring, which reduces costs and waste.

With headquarters in Brazil and presence in several countries, Welle collaborates with the world's main centers of laser technology, such as the Fraunhofer Institute, in Germany. Important industries around the world have already shown significant advantages in reducing costs and increasing production using laser technology, such as GE, Whirlpool, Bosch, Borgwarner, Mahle, Siemens, Black & Decker, among others.

In this project, Welle Laser collaborated by renting periods of one of their laser machines and giving us access to their research laboratory and staff, which helped us throughout the work. The partnership between Nanogreen and Welle was not for this project only, and other lines of work are already under way since the laser company has an interest in developing this new application for their machines.

3.3.4 FAPESC

FAPESC is the Foundation for the Support of Research and Innovation of the State of Santa Catarina and their primary mission is to promote the Santa Catarina ecosystem of science, technology and innovation by promoting and integrating its agents, aiming at advancing all areas of knowledge, regional balance, sustainable economic development and improving the quality of life.

Along with the CERTI Foundation, they are the ones responsible for the Sinapse da Inovação program, both in the financial and management aspects. This program has been going on for around 6 years and is a model for other states and Support Foundations around Brazil. Recently, a nationwide program called Centelha was developed and is launching its first batch, and the whole structure was built on the Sinapse da Inovação basis.

4 RESULTS AND DISCUSSION

"For a moment, nothing happened.
Then, after a second or so, nothing continued to happen."
(ADAMS, Douglas)

Here we present the results followed by some discussion on different aspects of the work, from the setup and visual aspects of the process to the microscopic, structural and physicochemical characteristics of the produced nanoparticles. After going through each of the characterization methods, we discuss the influence of the varied parameters on productivity, particle size and stability.

4.1 PULSED LASER ABLATION IN WATER

Pictures were taken of each experiment in order to illustrate and compare the color and appearance of the produced dispersions. These are presented in Figure 22. The codes on the vials represent the sample numbers from Table 6. In a few words, each image represents one combination of waveform and scan speed (v_s), while each of the vials in each image represents ablation times of 5, 15 and 30 min, respectively. In all the images, one can notice the darker shade of blue from the increased ablation time. This change in color is mainly because of the concentration increase of nanoparticles, but some of it may be due to different sizes and shapes of particles, as we will see in the next sections.

From these images, taken just after production, one can also see how well dispersed the particles are, considering the homogeneity of the dispersion, with no visible agglomeration in a short time period after the production. The transparent and clear suspensions are also indicative of a low concentration of nanoparticles.

Figure 22: Pictures of different samples of the produced nano titania dispersions: a) w1v1 (waveform 0, v_s = 270 mm/s); b) w1v2 (waveform 0, v_s = 1350 mm/s); c) w2v1 (waveform 10, v_s = 270 mm/s); d) w2v2 (waveform 10, v_s = 1350 mm/s). Inside each image, the vials from left to right show ablation times of 5, 15 and 30 min (t1, t2 and t3).

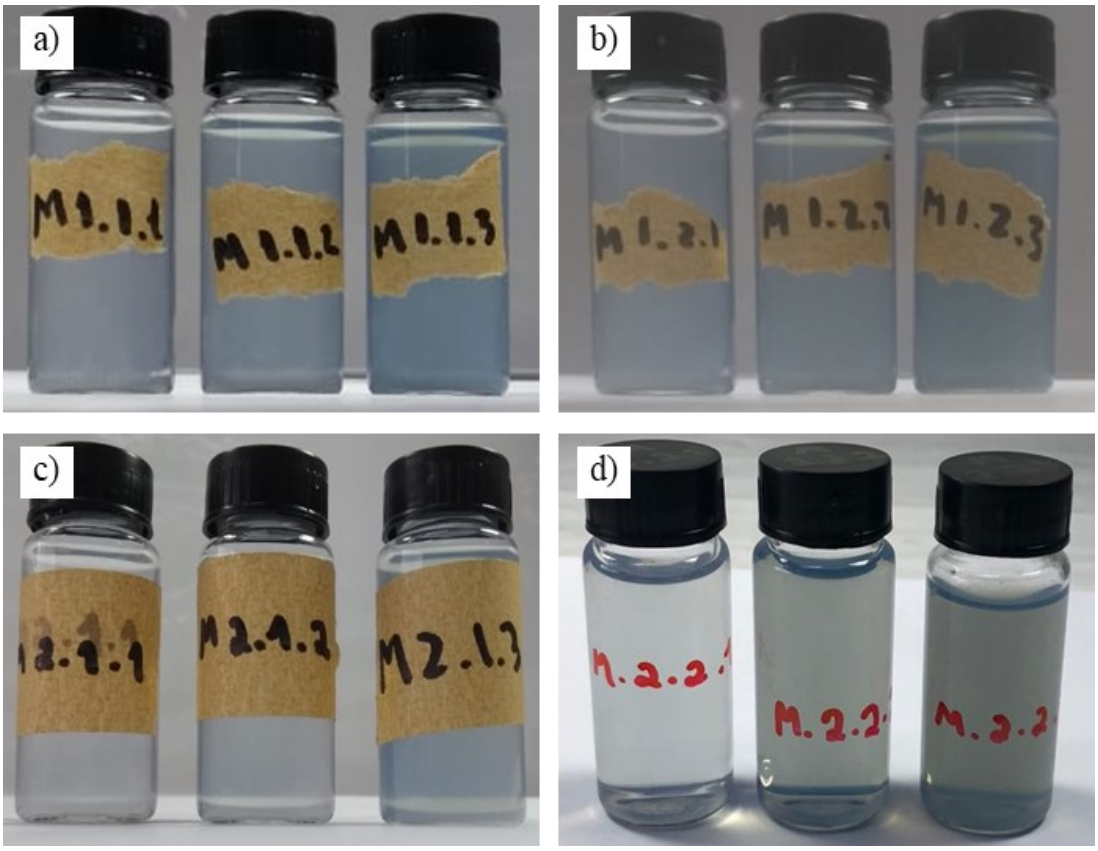

Source: Author (2020)

Figure 23a, however, shows a sample after 3 h, with a certain amount of aggregation, compared to a sample recently agitated. Figure b shows the situation of a sample after 2 days. As we will see later, the zeta potential values of these particles are in a range corresponding to a stable dispersion. However, zeta potential measures the electrostatic repulsive forces in action on the system, and the most accepted colloid stability theory of DLVO (Derjaguin, Landau, Verwy, and Overbeek) understands that the overall stability will be a sum of the attractive van de Waals and the repulsive electrostatic forces (BHATTACHARJEE, 2016). That way, we can conclude that the contribution of the Van der Waals (VdW) term in our case trumps the electric double layer created by the surface charges of the particles and induces aggregation and clarification. In this case, the redispersion of the particles is considerably easy, which may itself be a result of the high value of the zeta potential.

Increased stability can be achieved by altering the Hamaker constant, which is based on the relative refractive index and dielectric constants between particles and medium. In order to reduce the VdW factor, adding steric stabilization with the use of surfactants or stabilizers is an option (steric stabilization is a method to keep the particles separated by adding polymers, for example, preventing a physical approximation which may induce aggregation), but this adds another source of impurities and foreign molecules to the system (LEITE et al., 2012; TREFALT; BORKOVEC, 2014).

Figure 23: Nano titania suspensions: a) initial agglomeration of nanoparticles; b) further agglomeration at longer periods of time up to a sedimentation point.

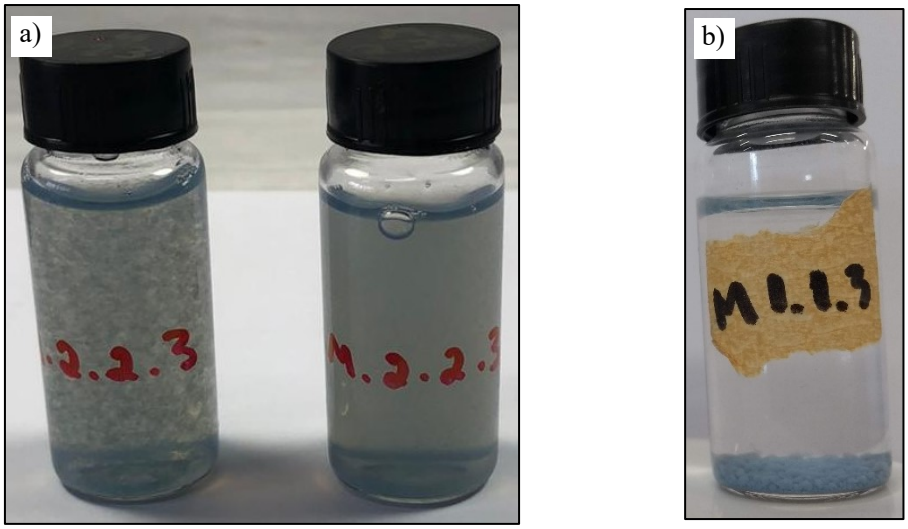

Source: Author (2020)

4.2 CHARACTERIZATION OF TARGETS AND NANOPARTICLES

Here, different characterization techniques are used in order to evaluate laser impact on the targets and visualize the produced nanoparticles.

4.2.1 Titanium targets surface

Pictures of the surface of the targets help us understand the interaction between the laser and the materials. Figure 24 shows the surface of the polished titanium target. This is how all the initial samples look like.

Figure 24: Surface of the untreated, polished titanium target.

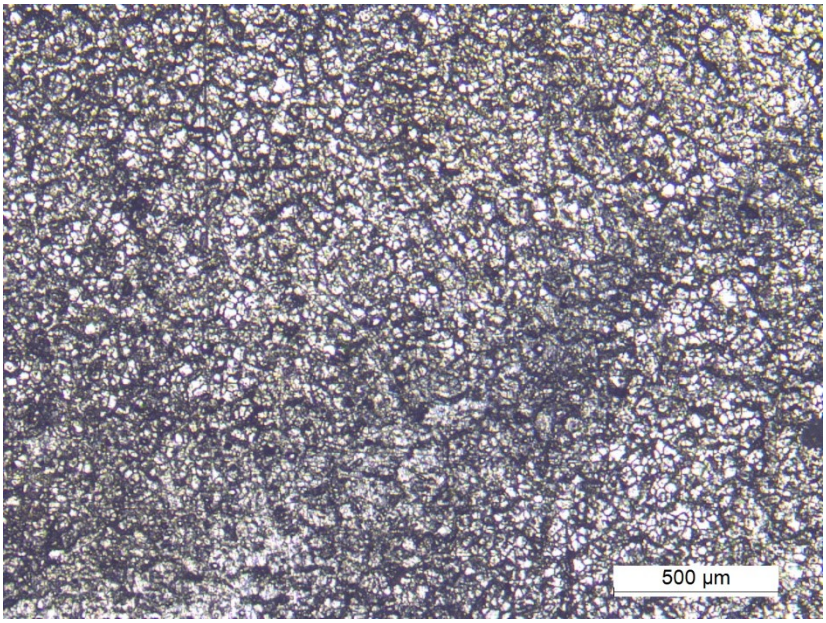

Source: Author (2020)

In the experiment labeled as w3v1t1 in Table 6 (using waveform 31), as shown in Figure 25, the energy used was not enough to effectively ablate and remove material from the titanium target, not generating (or generating too little) nanoparticles to consider it for the next steps of this work. By observing the picture and optical microscopy images of the surface of the titanium target during the ablation, we can see that the generated bubbles remain attached to it, and this results in colorful areas in the magnified image. The low energy regime of this experiment (E_p = 0.03 mJ/pulse) is not enough to actively ablate the titanium surface and heats the area until bubbles are produced. These bubbles then act as diffraction centers for the laser, spreading the energy and resulting in even lower fluence levels on the surface. Due to this effect, it was not possible to estimate the effective spot size in this experiment, and the exact fluence could not be determined. "Guesstimating" the spot size to be around 150 µm (based on calculations that will be shown a little further ahead), we would obtain a fluence of around 0.170 J/cm^2, which is indeed pretty low compared to numbers found in the literature. Vladoiu et al found an estimated ablation threshold value for titanium alloys of 4.5 J/cm^2 for ablation with a 1064 nm laser in air (VLĂDOIU et al., 2008). As mentioned in the literature review, it has been shown that ablation in liquids tend to reduce the threshold, but 0.17 J/cm^2 is still very low.

Figure 25: Surface of the titanium target irradiated in test w3v1t1: a) bubbles on the surface of the sample even with the laser on (highlighted with the red arrow); b), c) and d) different parts of the target imaged with optical microscopy. The colored areas (image not artificially colored), are thought to be resulting from persisting bubbles' diffraction patterns, while the gray areas are treated by the laser at a too low fluence.

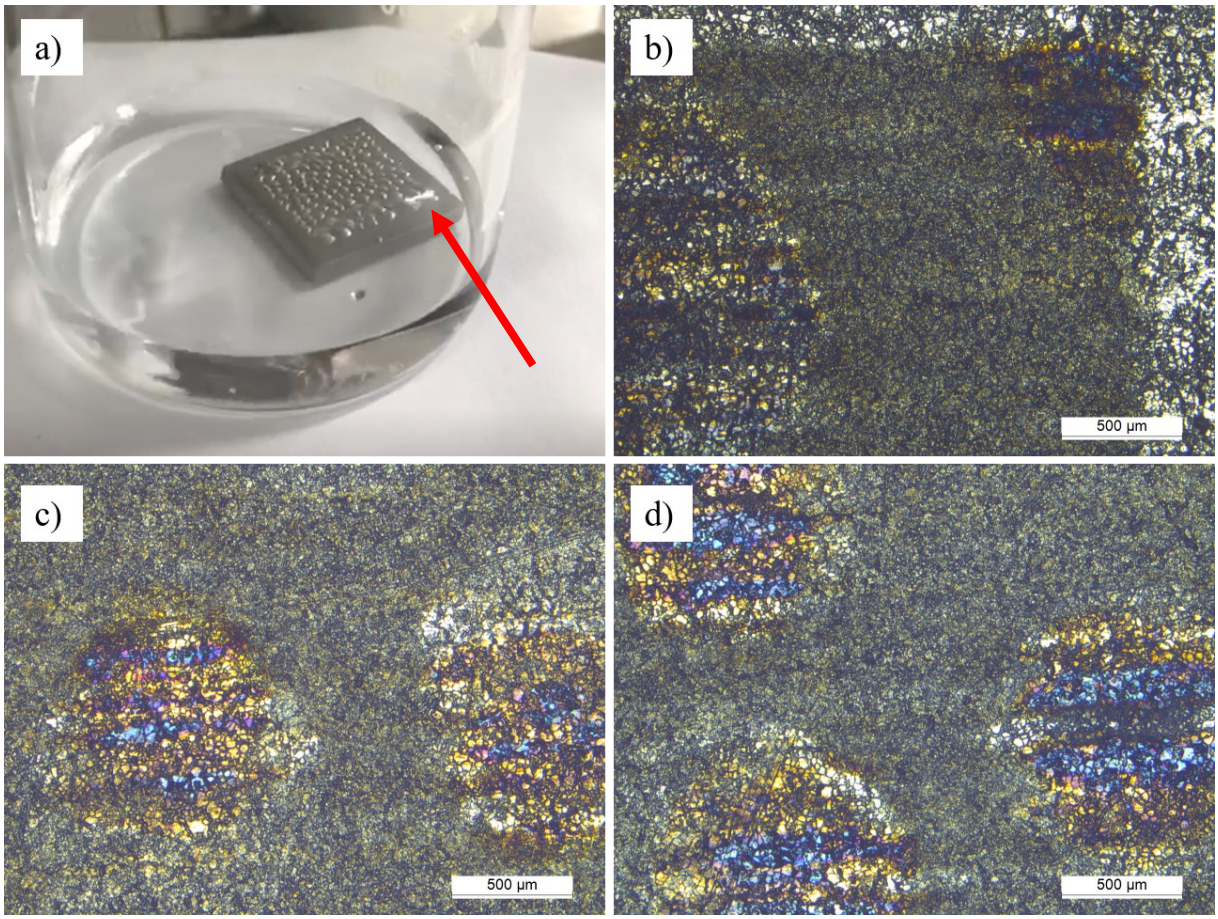

Source: Author (2020)

Figure 26 has a QR Code and link to a video showing this process. If compared to the video in Figure 20, one can notice that the ablation does not even have the same sound, which is an indication of the cavitation bubbles being generated in a successful ablation process. With this in mind, while the results for this test were interesting and even pretty in the images, the regime was not considered for further studies and we selected a new waveform (10) that was used for the next steps.

Figure 26: QR code to the ablation process at low fluence video. Link: https://1drv.ms/v/s!Ar9ILkt5W35ygqosg0ej7m7CKNtl9A

Source: Author (2020)

Images were put in a grid organized in Figure 27, according to the parameters of each test. The first clear takeaway here is that the effect of these two regimes (waveform 0 and 10) on the material is quite larger than the one seen in Figure 25, with actual material removal from the grooves created by the laser. The surfaces in the first column, of 5 min ablation time, show these grooves more clearly and allow the effective spot size (S_s) to be estimated. By measuring the width of these grooves, we can calculate the diameter of the circle that created them, and this value was used to calculate the fluence for each set of parameters.

For images a), d), g) and j) in Figure 27, the measured width was 143.9, 138.0, 149.4, and 152.6 µm, respectively. These values are then used to calculate the fluences for each waveform and scan speed, as presented in Table 8.

Table 8: Spot size and fluence calculated for each waveform-scan speed combination.

Waveform	**Scan speed [mm/s]**	**Pulse energy [mJ]**	**Effective spot size [µm]**	**Fluence [J/cm^2]**
0	270	1.00	143.9	6.149
0	1350	1.00	138.0	6.689
10	270	0.49	149.4	2.794
10	1350	0.49	152.6	2.680

Source: Author (2020)

Figure 27: Effect of laser ablation on the surface of the titanium targets.

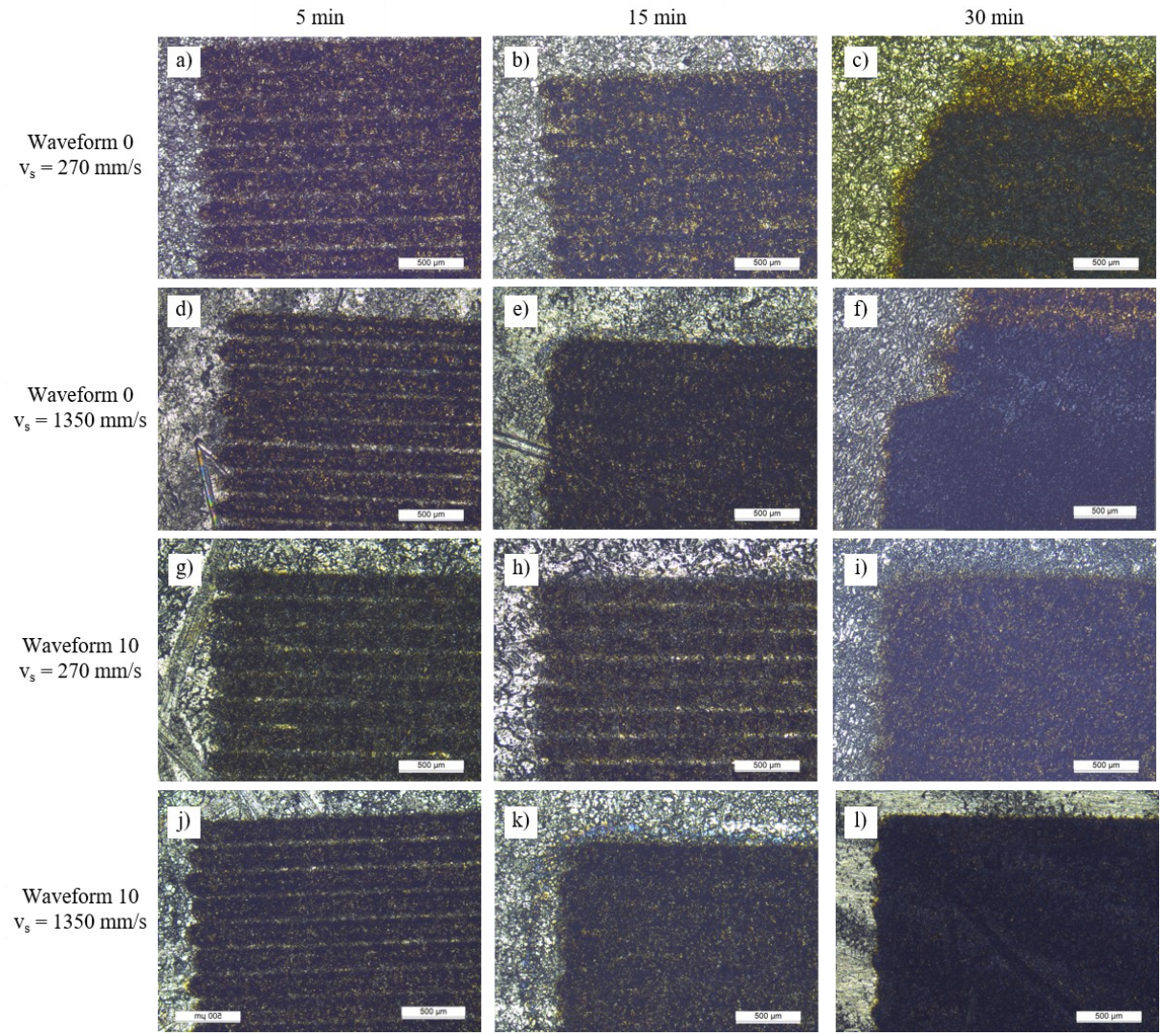

Source: Author (2020)

Moving on to the columns 15 and 30 min, we no longer see the clearly defined grooves, and it seems that the whole surface was treated by the laser. Besides the heat effect generated by the constant incidence of the laser beam over the same places (images f) and l) refer to samples that were irradiated almost 850 times, for example), the effect of the concentration of nanoparticles in the liquid above the target must also be taken into account. The presence of said particles increases the absorption of the liquid media and help with diffracting the laser, creating a larger affected area, and smaller fluence on the target.

When comparing row 2 to row 1 and row 4 to row 3 we are looking at the effect of increasing scan speed while maintaining the ablation time. This means we increase the number

of times the laser goes over the designed path, as can be seen by the depth and even by the color of the ablated area.

Images c) and f) show some irregular marks due to movement of the beaker. The 30-min experiments were performed inside another reservoir, and the movement of the water in the outer container slightly moved the target in front of the laser, causing that second set of grooves we see in the images.

4.2.2 Ablation rate

In this work, we defined the ablation rate as "productivity," that is, how much mass is removed from the titanium target (in mg/h). In order to calculate this, each sample was weighed before and after the ablation, and the difference was divided by the ablation time in order to obtain the productivity value. Table 9 presents the average productivity of all experiments.

Table 9: Productivity [mg/h] according to the laser ablation parameters.

Experiment	**Ablation time [min]**	**Productivity [mg/h]**
w1v1 (waveform 0, v_s = 270 mm/s)	5	9.20
	15	10.27
	30	11.87
w1v2 (waveform 0, v_s = 1350 mm/s)	5	14.00
	15	14.40
	30	14.53
w2v1 (waveform 10, v_s = 270 mm/s)	5	3.60
	15	6.27
	30	8.87
w2v2 (waveform 10, v_s = 1350 mm/s)	5	20.80
	15	18.67
	30	15.27

Source: Author (2020)

While it is known that the productivity of laser ablation in liquids is considerably small, with experiments and simulations reaching rates of few milligrams per hour, we did not expect values this low. Considering the highest obtained productivity, for waveform 10, v_s =

270 mm/s and ablation time of 5 min (20.80 mg/h), this still means that it would take around 48 h of continuous laser processing to obtain one gram of our particles.

4.2.3 Particle size and stability

Two methods were used for particle size determination: Dynamic Light Scattering (DLS) and Transmission Electron Microscopy (TEM). For a better comparison with the TEM results, all DLS results shown will refer to the "number measurement" and not intensity or volume options. Moreover, an indicative of the dispersion's stability, zeta potential, was also measured.

Figure 28: DLS size distribution and average particle diameter (d_p) according to waveform, scan speed and ablation time

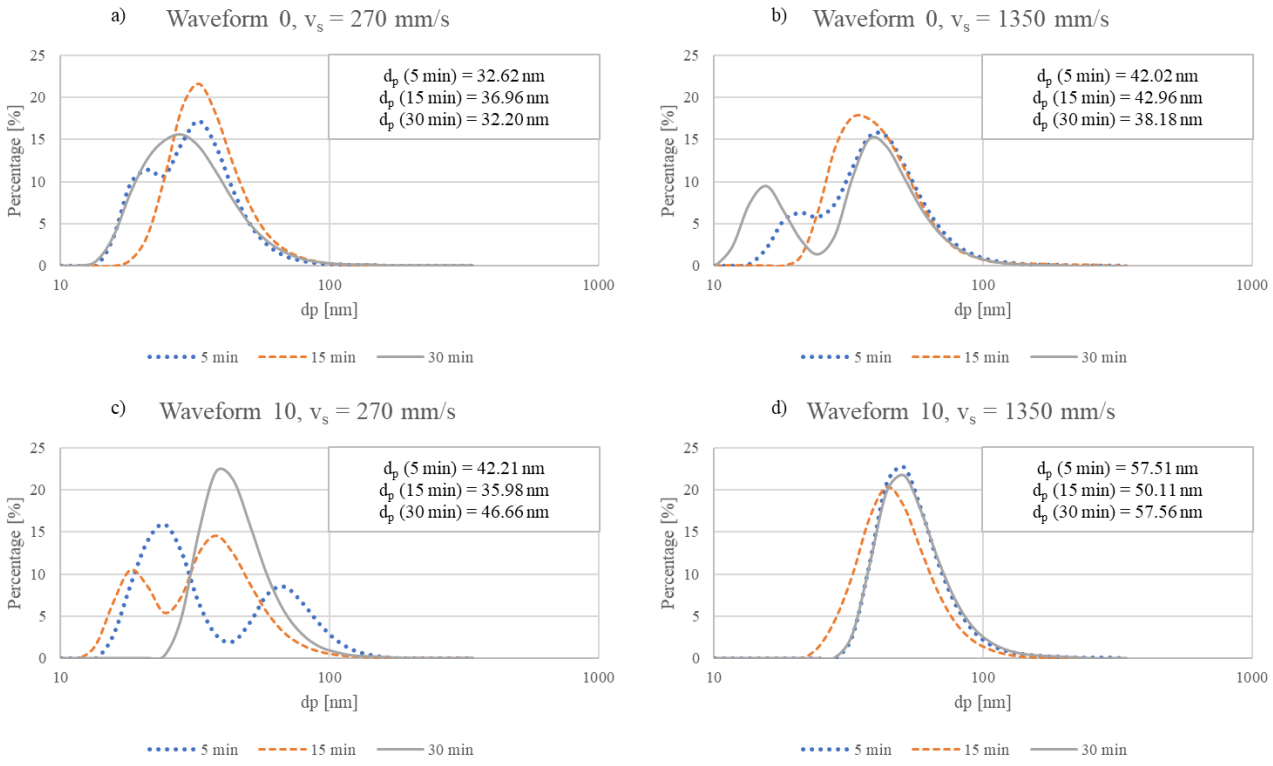

Source: Author (2020)

Figure 28 presents the DLS results. As can initially be seen, the average particle diameters (d_p) are not as small as expected. Other works in the literature (such as the ones presented in Table 2) obtained particles with a diameter smaller than 10 nm some cases (CHANG et al., 2012; GIORGETTI et al., 2015; SINGH et al., 2017; SIUZDAK et al., 2014). Besides this observation, except for image d), produced with waveform 10 and a scan speed of 1350 mm/s, all the other setups showed at least one case of bimodal peak and distribution from

~10 to ~100 nm. At first, one may believe sample in letter d) presents the most controlled process, with a smaller size distribution and sharper peaks. However, considering some of the assumptions and requirements used by the DLS equipment to convert information from intensity to number distributions, as presented further in this discussion, this behavior may be an indication that this method is not the best option for the sizing of our particles.

In order to better understand the morphology of the particles, TEM images were taken and analyzed, as presented in Figure 29. One can see spindle-like particles in addition to the spherical ones. This presence of morphologies other than spherical already rule out the possibility of using the DLS technique for size determination, since the basis of its measurement is defining the hydrodynamic diameter of a sphere that has the mobility (based on the translational diffusion coefficient, as described by the Stokes-Einstein equation) of whatever particle the equipment is measuring. With particles with odd shapes and aspect ratios different than 1, such as the ones we see, this hydrodynamic diameter does not accurately reflect the actual particle size, since even the orientation of the particles in the liquid will result in different mobility and hence a different size.

Table 10: Zeta potential of nano titania in aqueous suspension.

Sample	**Zeta potential [mV]**
w1v1t1	-47,467
w1v1t2	-46,433
w1v1t3	-43,967
w1v2t1	-38,967
w1v2t2	-47,033
w1v2t3	-45,067
w2v1t1	-36,867
w2v1t2	-34,900
w2v1t3	-39,333
w2v2t1	-51,500
w2v2t2	-42,733
w2v2t3	-43,833

Source: Author (2020)

Besides the morphology of the spindle-like particles, we have the presence of spherical particles. When analyzing these particles, we can also see a broad size distribution for the

spherical particles. This is also another probable cause for the unreliable DLS results. While intensity measurements are obtained straight from the measured particles, volume and number measurements (such as the ones we are using) depend on a mathematical conversion based on the Mie Scattering Theory, which has some assumptions such as: data quality is acceptable (repeatability of measurement, for example), optical properties of the particles are well known (e.g., real and imaginary terms of the refractive index of the particles), all particles are spherical, and all particles are homogeneous (MALVERN PANALYTICAL LTD., 2018). This presents problems for our set of samples because not only are they not spherical, but we also do not know them well enough to be sure of optical properties and homogeneity (different titania phases and compositions are not defined).

Zeta potential measured values are presented in Table 10. Considering all of them are below -30 mV, as per literature standards, the nanoparticles dispersion should be stable, at least from an electrostatic point of view (MALVERN PANALYTICAL LTD., 2009). As seen in Figure 23, this does not translate to the actual dispersions, which turn out to aggregate and sediment within 2 days. The high zeta potential value may, however, explain the easy redispersion of the particles by simple agitation.

Figure 29: TEM images of PLAL produced nanoparticles. The inset shows a zoomed in view of the highlighted region.

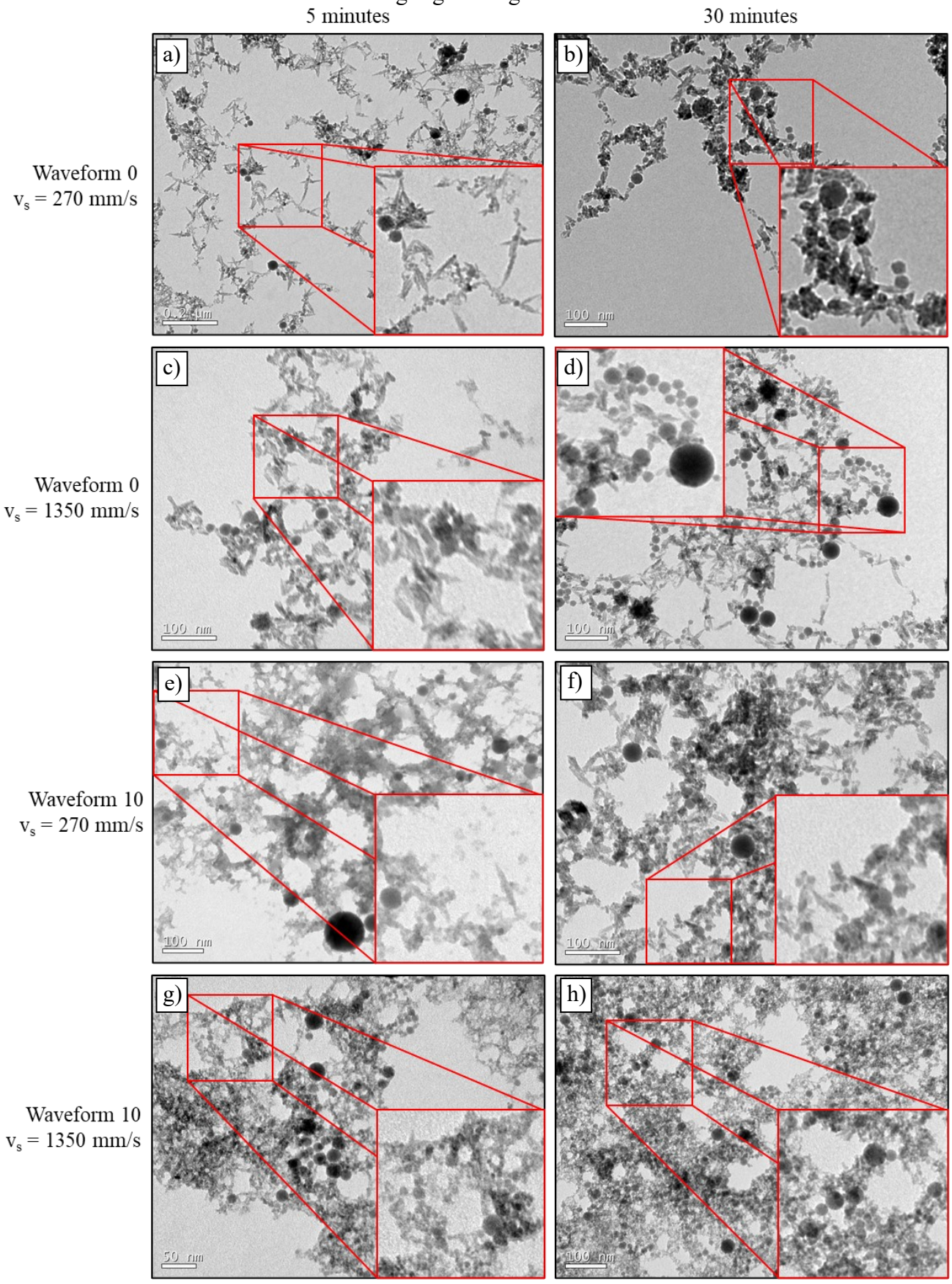

Source: Author (2020)

The TEM images were analyzed for the size distribution. Both spheres and spindles were measured by hand, and the histograms are presented in Figure 30 and Figure 31. The number of particles measured in each case is shown in the inset, as well as the average diameter in the case of spheres and the length of the long axis of the spindles, both with their respective standard deviations. Considering the quality of the images, not all particles were accounted for, mainly because of the agglomeration of particles visible in most pictures. Those regions became too densely packed, and individual shapes are not distinguishable. The last sample, w2v2t3 (waveform 10, scan speed of 270 mm/s and ablation time of 30 min), did not present any spindle-like particles.

Table 11 presents a comparison of the average number diameter obtained from DLS measurement, with calculated uncertainties (GOLDSCHMIDT et al., 2020) and the average measured diameter of spheres and spindles long axis from the TEM images. From this, we can see the apparent discrepancy of the data, and from here on the DLS measures will not be taken into account for the measurement of diameter.

Table 11: Comparison of DLS diameter and TEM sphere diameter and spindle long axis.

Sample	DLS diameter (nm ± uncertainty)	TEM spheres diameter (nm ± standard deviation)	TEM spindles long axis (nm ± standard deviation)
w1v1t1	32.6 ± 0.2	9 ± 5	30 ± 9
w1v2t1	42.0 ± 0.2	10 ± 8	24 ± 8
w2v1t1	42.2 ± 0.2	8 ± 7	31 ± 12
w2v2t1	57.5 ± 0.3	8 ± 5	18 ± 6
w1v1t3	32.2 ± 0.2	11 ± 7	23 ± 6
w1v2t3	38.2 ± 0.2	13 ± 7	36 ± 10
w2v1t3	42.7 ± 0.2	10 ± 7	34 ± 17
w2v2t3	57.6 ± 0.3	8 ± 5	-

Source: Author (2020)

Figure 30: TEM size distribution, average diameter, standard deviation and particle count for spherical and spindle-like nanoparticles produced for a 5-min ablation time.

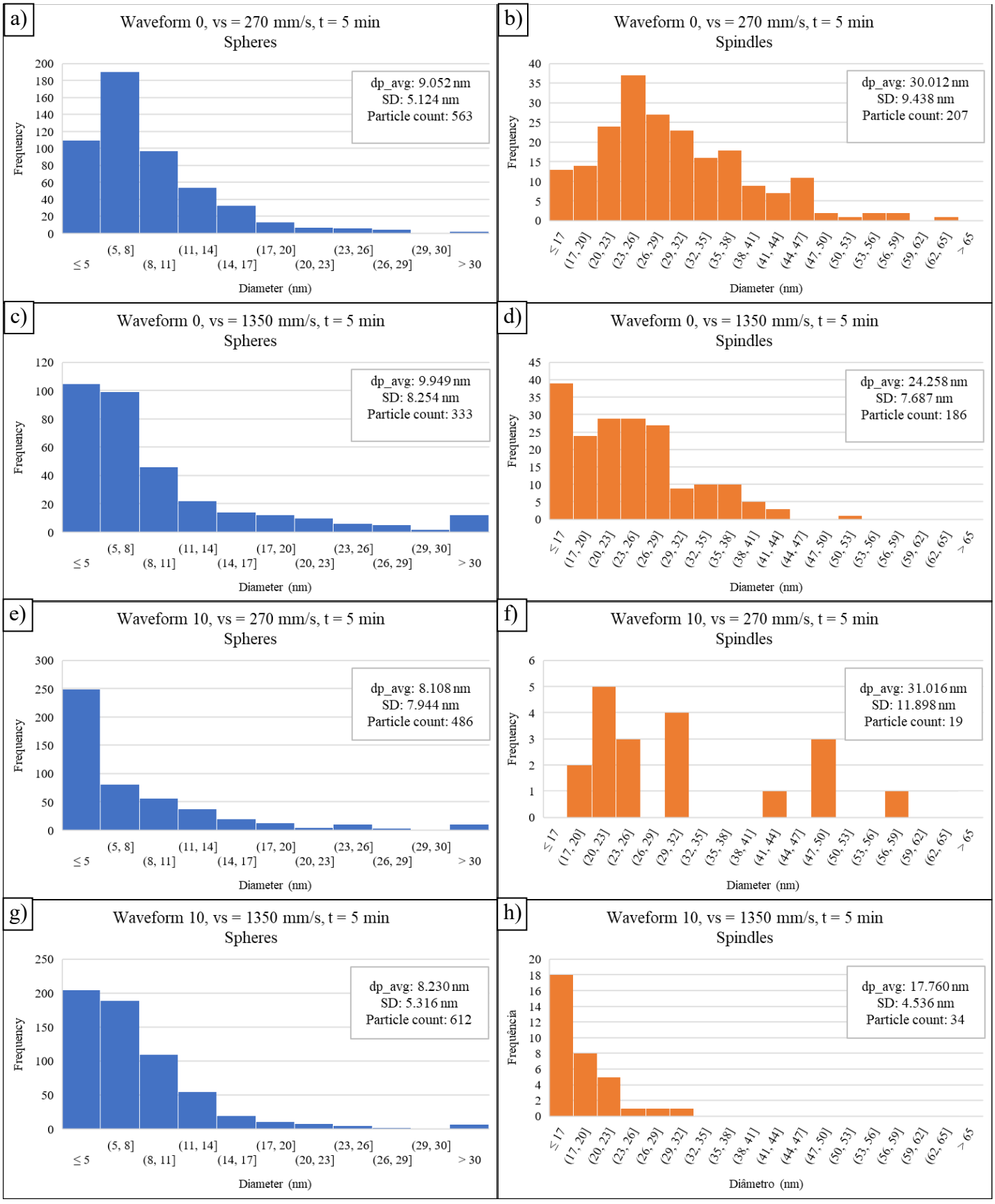

Source: Author (2020)

Figure 31: TEM size distribution, average diameter, standard deviation and particle count for spherical and spindle-like nanoparticles produced for a 30-min ablation time.

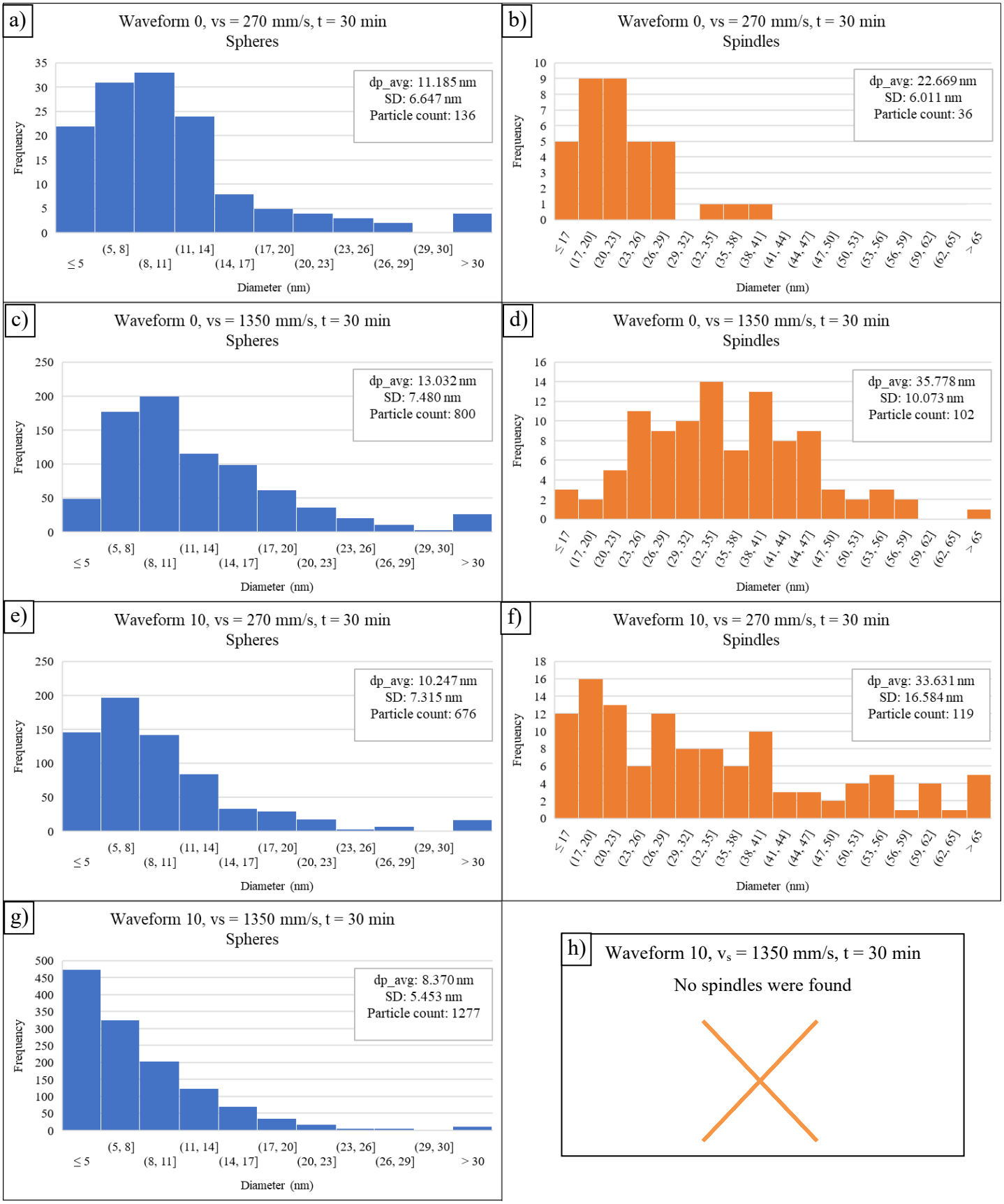

Source: Author (2020)

As previously mentioned, the measured particle sizes presented in Figure 30 and Figure 31 are restricted to the visible and distinguishable particles, which is a downside of our TEM analysis. This can be improved for further experiments by diluting the samples before the TEM grid preparation in order to reduce the number of particles agglomerations and allow for better distribution. The way they are agglomerated in the images indicates that this is probably due to concentration problems in the drying step of sample preparing, and not an agglomeration in the dispersion itself.

By optimizing this procedure, a better statistical significance can be achieved, mainly by increasing the particle count. Some of the analysis counted less than 50 particles in the case of spindles, which makes it difficult for any statistical affirmation. This lack of statistical relevance of some of the results can be also noticed by the non-normal distribution of particle size found mainly for sample w2v1t1 (Figure 30, f), which is also another example of a low number of counted particles.

Figure 32 also shows the presence of particles smaller than 5 nm. The equipment resolution was not enough to clearly distinguish these particles, and their contribution to the measured size distribution is hardly accounted for since actively measuring their diameter by hand when processing the TEM images is very difficult.

All images in Figure 32 have a scale bar of 20 nm, which is around the maximum resolution for the TEM equipment used. Below that size, features of the structures become indistinguishable. That way, while it is possible to identify really small particles, exemplified in the highlighted areas of the images, measuring and even resolving their shape and morphology is not possible or would be prone to a considerable error.

Image c) in Figure 32 is perhaps the best one to analyze considering that the particles are better distributed on the grid. Overall, particles in the whole image have diameters around 3.4 nm. However, in the highlighted area, we can see some even smaller particles, too small to be considered for the calculations.

Figure 32: TEM images of particles and structures under 5 nm.

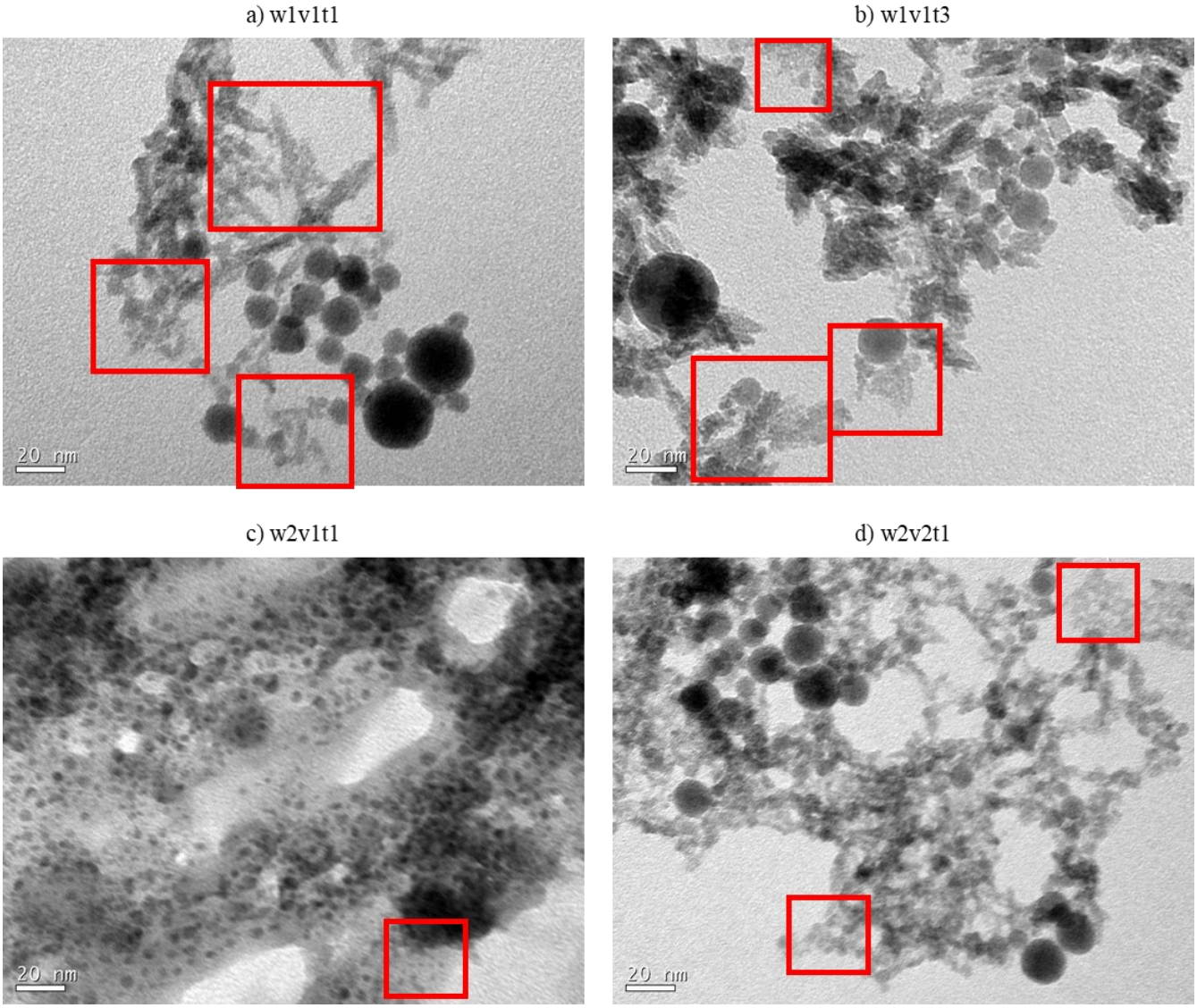

Source: Author (2020)

Finally, considering all samples and measured particles, the distribution of particle size was very large. This can be readily seen from the standard deviation value of all the measured size distributions. This was expected considering the images obtained, where we can see small spherical particles with diameters close to 1 nanometer to large ones getting to around 60 nm. When analyzing the spindles, the minimum long axis length obtained was around 9 nm, while the largest one was over 100 nm. The average coefficient of variation (CV, also known as relative standard variation, obtained by dividing the SD by the average value) was 69% for spheres and 33% for the spindles, as presented in Table 12. While this is within numbers found in the literature (SCARAMUZZA; ZERBETTO; AMENDOLA, 2016; SEMALTIANOS et al., 2010; SINGH; GOPAL, 2007; TILAKI; ZAD; MAHDAVI, 2007b), it must be optimized in

order to get this kind of product to market. While for some applications of micro- and submicrometric particles the required size distribution is not that strict, for most nanoparticle applications having a single particle size is very important.

Table 12: Coefficient of Variation (CV) of the spheres and spindles of the analyzed samples.

Sample	**CV - Spheres**	**CV - Spindles**
w1v1t1	57%	31%
w1v1t3	59%	27%
w1v2t1	83%	32%
w1v2t3	57%	28%
w2v1t1	98%	38%
w2v1t3	71%	49%
w2v2t1	65%	26%
w2v2t3	65%	-
Average	**69%**	**33%**

Source: Author (2020)

The experimental setup used in this work is one of the sources of these results. For being one of the most straightforward possible setups there is this for this process, it is prone to several factors that decrease the control and reproducibility of the pulsed laser ablation. The main factor considered relevant to this wide range of particle sizes is the fact that the system works in a batch mode, with no flow of any sort.

This means that particles produced at time t = 0, the beginning of the process and the first laser shots, will still be in suspension by the time the last particles are being produced at the end of the process, and during the time of ablation, those first particles may have been hit by the laser beam multiple times. As mentioned in the literature review, this post-irradiation, besides reducing the laser energy that actively reaches the target surface and hence affecting productivity and particle generation, also transfers energy to the particles in its path and can lead to different effects, including fragmentation and melting of the outer layer of the particles (CHEN; ZHANG, 2012).

While this may be an interesting effect in some cases, looking at the size distribution of the particles it adds some degree of uncertainty, both due to not being able to predict how many times each particle will be hit by the laser and to the fact that the early nanoparticles will be more irradiated than the ones produced close to the end of the process. Hence, their size will deviate even more than the regular expected distribution. Adding stirring to the setup may help

with homogenizing the post-irradiation over all of the volume of the batch, but does not help with the temporal differences. The best way to treat this is to add flow to the process, in a way that particles are dragged away from the laser pulses and taken to another container, preventing any further interaction with the laser energy. Better reproducibility and size control are expected from this method (BARCIKOWSKI; CHICHKOV; RAČIUKAITIS, 2007; CHEN; ZHANG, 2012; KOHSAKOWSKI et al., 2017; MESSINA et al., 2013; STREUBEL; BARCIKOWSKI; GÖKCE, 2016).

4.2.4 Particle shape

As seen in the last section, the laser ablation process yielded two populations of particles: spheres and spindles. A complete investigation of this phenomena is quite a complex subject, requiring equipment such as HRTEM (High Resolution Transmission Electron Microscopy) with EDS (Energy Dispersive X-ray Spectroscopy) and SAED (Selected Area Electron Diffraction) probes and involving quantum effects, phase transition, and crystalline planes, for example, but there are studies on the reason why some nanoparticles in PLAL systems solidify as spindles.

Some studies using cationic surfactants such as CTAB (cetyltrimethylammonium bromide) and ammonia (NH_4^+) to stabilize the produced nanoparticle dispersion of zinc oxide (ZnO) and copper oxide (CuO) yielded spindle-like structures. These particles were analyzed as being crystalline, and susceptible to having their growth rate in specific crystallographic directions hindered, for example, by the adsorption of molecules of the solvent or surfactant on specific planes, enabling anisotropic growth (HE et al., 2008; PRZYBYLSKI, 2011). External force, such as an electric field, was also used to force GeO_2 particles into growth in a specific crystallographic direction (XIAO et al., 2017). In another study, YVO_4:Eu^{3+} nanoparticles produced by laser ablation were found to aggregate through “orientated attachment” of crystalline planes and develop ovoid and spindle-like structures (WANG; ODAWARA; WADA, 2016).

Titanium dioxide spindles through laser ablation have been reported as well, with different routes such as using ammonia as a stabilizer during laser ablation (PRZYBYLSKI, 2011), using a platinum-doped titanium dioxide target (SASAKI et al., 2004) and through irradiation treatment of rutile powders (CHANG et al., 2012). The common factor between those works is that the spindles are determined to be anatase-phase titania. This crystalline

phase is known to be less dense than its counterpart rutile and elongated along the c-axis, which is the preferred direction of growth according to reports (JENSEN et al., 2010; PAN et al., 2014).

Interestingly, this work's process did not use any of the mentioned routes to synthesize the spindles, with their production happening naturally from the selected raw material, along with the spherical particles. A noticeable fact is that an increase in ablation time and scan speed seems to yield a higher ratio of spheres to spindles, as illustrated in Figure 33. Analyzing the images, mainly from image a) to image d), the reduction of the number of spindles particles, and the increase in the number of spherical particles. While it is hard to assess this trend in the current work quantitatively, it is possible to correlate this behavior to the discussed large size dispersion measured and the batch setup used.

Figure 33: Comparison of sphere and spindles production according to scan speed (v_s) and ablation time.

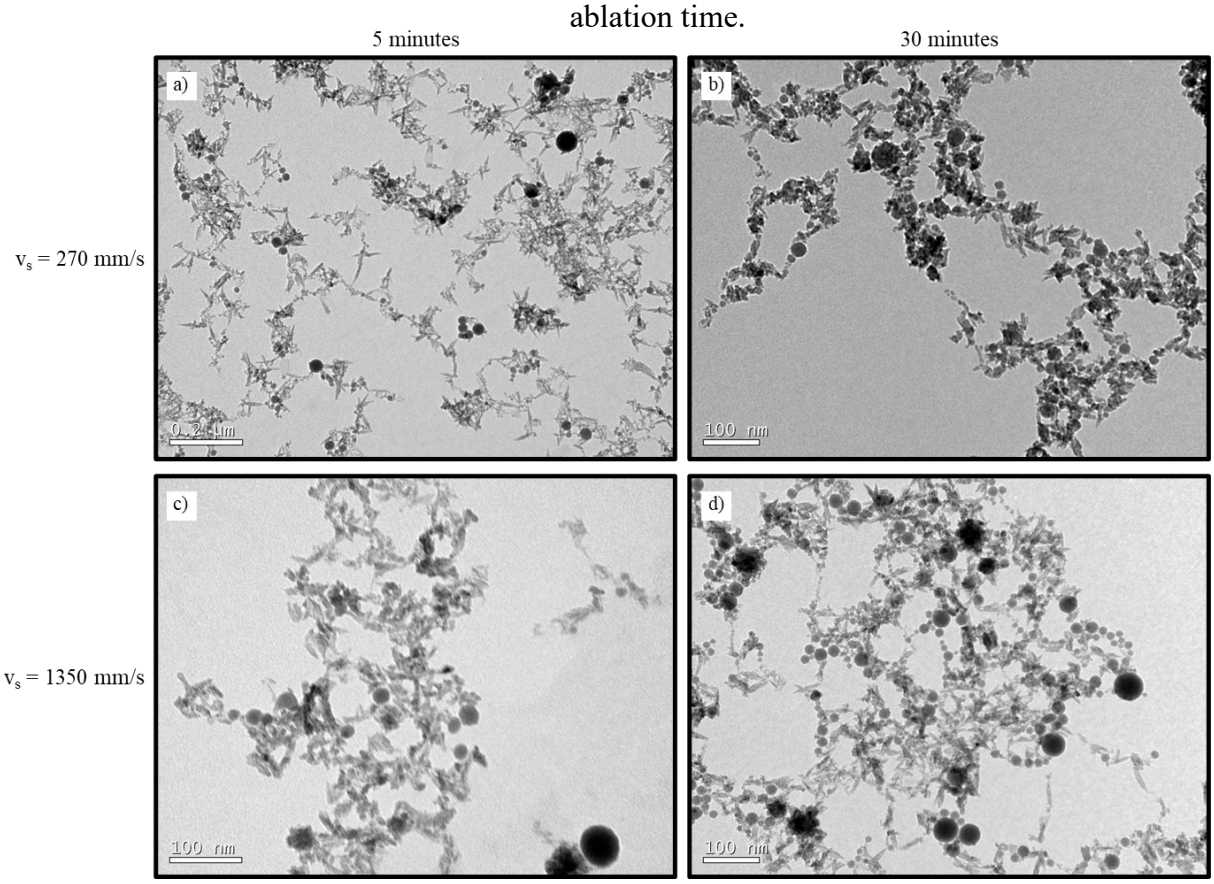

Source: Author (2020)

The author hypothesizes is that at first, during laser ablation, plasma formation, and nanoparticle generation, the high pressure and temperatures allow for the formation of ultra-small anatase particles (based on the identified anatase stability below 15 nm), which during

the cavitation bubble generation and collapse are released into the liquid as either spheres or coalesced into the spindles. During the rest of the process, due to the (possible) interaction with the laser beam still ablating the target, some of these spheres and spindles receive energy enough to trigger anatase-rutile transformation (ART), which comes with a density increase. This would force the spindles to assume a more stable spherical morphology with phase change. Besides, for the particles that are less affected by subsequent laser pulses, the amount of energy/heat tends to facilitate the coalescence into larger spherical particles, such as the ones we can see on most of the TEM images. The increase in scan speed in the experiments would also have a positive effect in this hypothesis since with the laser beam moving faster over the target, more total area is covered in the same amount of time, meaning there is more chance of the particles to be hit with a laser shot again. Finally, when changing the waveform of the experiment, we see fewer spindles for the waveform 10 (waveform 10, v_s = 1350 mm/s and t = 30 min, for example, did not show any spindles in the images). This is also something that goes according to the hypothesis since when moving from waveform 0 to waveform 10 we're reducing the pulse energy (1.0 mJ to 0.49 mJ) but increasing the frequency (20 kHz to 41 kHz). At a higher frequency, more lasers pulses are performed by unit time, meaning the chances of the particles being hit again increase. This is a theory, and a few different tests and experiments must be performed in order to confirm it, but it finds a theoretical basis on articles and previous experiments by other authors presented in the literature review.

4.2.5 Particle composition

At first, tests were performed in order to evaluate the best way to analyze the titania particles produced using the least amount of material possible, considering the reduced mass of ablated nanoparticles and their dispersion in water. At first, we tried reading the sonicated sample from the vial itself. This did not result in any relevant result and for now was not pursued.

Then, the samples were centrifuged and the concentrated liquid was dripped on different glass slides, covered or not with aluminum foil, with the reflective side facing inward or outward. For these validation tests, commercial pure titania in the anatase phase (Nanoamor) was used as a reference. Figure 34 shows the comparison of Raman readings of the reference material in both regular glass slides and the best result for aluminum covered glass slide, with the reflective surface facing outward.

Figure 34: Commercial anatase Raman spectroscopy: aluminum foil and glass slide comparison at 10% laser power.

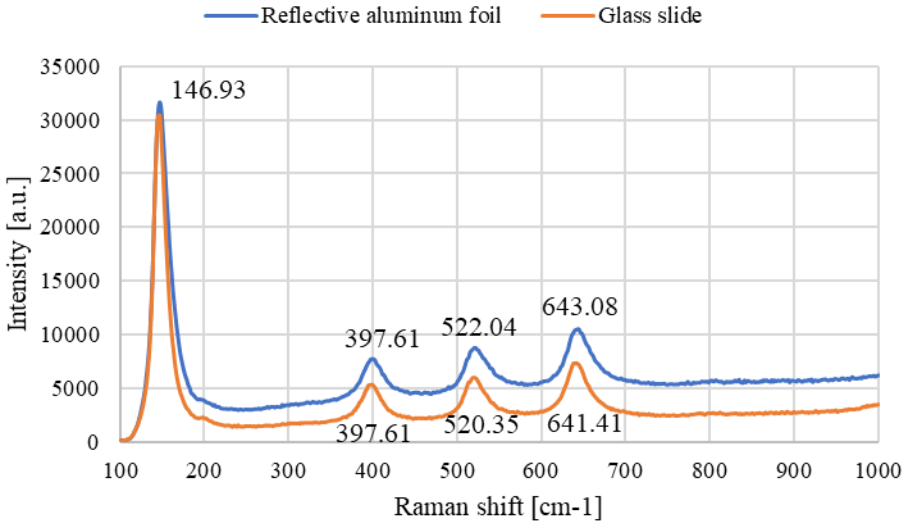

Source: Author (2020)

The initial validity of the method is established by comparison to anatase common Raman shift value found in the literature. Though values differ among different reports, the usual anatase bands are found at 143, 391, 511 and 633 cm^{-1} and rutile bands are at 243, 443 and 605 cm^{-1} (ALLEN et al., 2018; CHANG et al., 2012; GIORGETTI et al., 2015; HAMDY; AMROLLAHI; MUL, 2012; HANAOR; SORRELL, 2011). Because of the relatively good agreement of the obtained values of the experimental setup and the literature, and higher intensity than plain glass slide, drip drying on a glass slide covered with aluminum foil was chosen for the tests with PLAL particles.

Figure 35: PLAL titania Raman spectroscopy: samples w1v1t3 and w2v1t3 at 100% laser power.

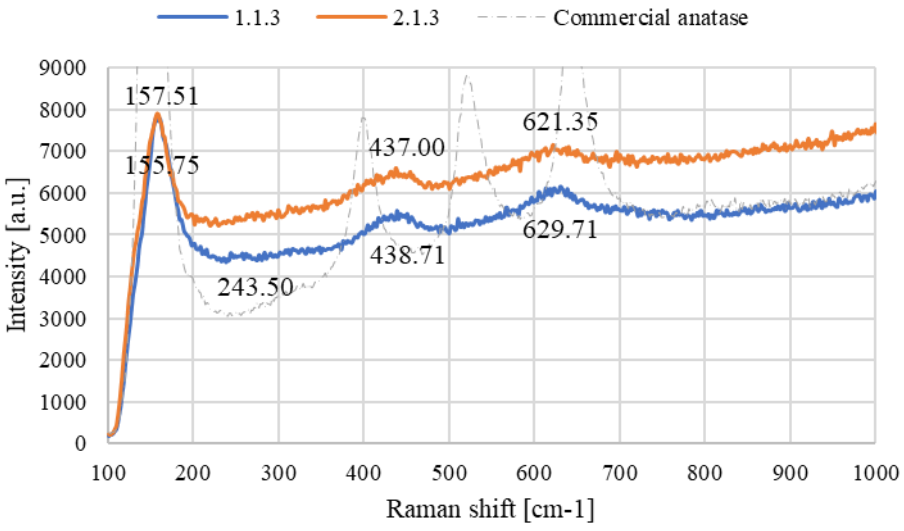

Source: Author (2020)

Figure 35 presents the results of two test samples according to the described procedure. Before starting the phase composition analysis, the intensity of the signal obtained is considerably smaller than the commercial reference, even with an increase in the laser power. This is probably due to the small concentration in dispersion, which translates into minimal amounts of material deposited on the substrate. Besides causing a smaller intensity signal, this small amount of particles also induces a higher noise, explaining the smoother lines in Figure 34, even taking into account the scale. A shadow of the commercial anatase spectra is plotted as a reference.

Analyzing the phases present on the samples, the first result is the noticeably high baseline and width of the peaks. This is an indication of a significant contribution of an amorphous phase, which is not noticed on the previous tests with commercial titania. This phase can be composed of amorphous titania, which is not uncommon in nanoparticle synthesis. A comparison with the gray dashed line helps visualize this baseline and peak width difference. As for the identified peak positions, what can be seen is a mixture of rutile and anatase characteristics. The peaks of both samples at around 155 cm^{-1} are attributed to the anatase phase, while the peaks at 437 cm^{-1} are usually for the rutile phase. However, the peaks at 621 and 629 cm^{-1} are at a more shifted position, possibly from the anatase phase's peak at 633 cm^{-1}. Finally, a small peak located at 243.50 cm^{-1} for sample w1v1t3 is indicative of a rutile phase, though that peak disappears for sample w2v1t3.

Overall, from Raman spectroscopy, it is expected that our sample consists of amorphous, anatase, and rutile phase of titania. A complication of this analysis is the fact that as seen in previous sections, the sample is composed of different populations of particles such as spindles and spheres. As the Raman analysis is performed on the sample as a whole, it is impossible from this test to define the phases of individual populations of particles.

As with the Raman spectroscopy, some sample preparation and adaptation were required in order to obtain relevant results in the XRD analysis. In some equipment, the amount of sample required is small, in the milligram range, by using a unique sample holder composed of monocrystalline silicon and a small sample cavity. Even with such an accessory, our sample volume is still quite small, and care must be taken with the quantity used. However, that kind of sample holder was not available, and a regular glass sample holder with a considerably large sample cavity was used. Adaptations such as using a glass slide or cover glass as a substrate for drip drying the sample and then mounting the substrate on the glass sample holder were tried, but the signal obtained was not usable.

The best procedure in terms of signal quality and intensity was to drip dry the sample on the regular glass sample holder's cavity and perform some cycles of scraping the dried material towards the center of the sample holder with a plastic tool and minute amounts of deionized water (basically just wetting the tip of the plastic tool and removing excess with tissue paper). Figure 36a shows the appearance of the sample holder after the first dry step, and Figure 36 c) shows the final look of the sample. The final substrate was then mounted on the XRD equipment and measured.

Figure 36: XRD sample preparation and final substrate.

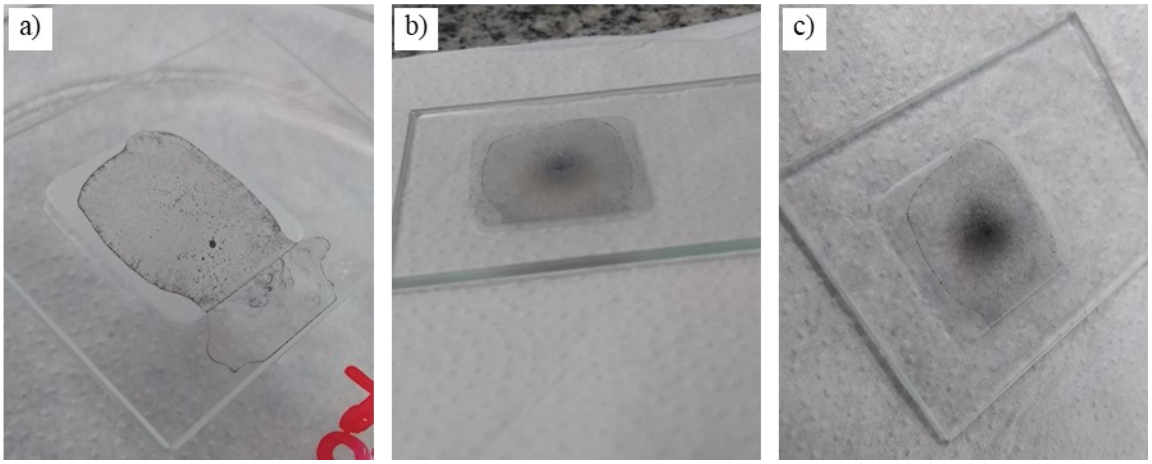

Source: Author (2020)

The obtained spectrum for sample w1v1t3 is found in Figure 37, and compared to ICSD's structure files 9852 for anatase and 9161 for rutile. Treatment had to be performed in the spectrum in order to remove the sample holder's background (which was considerably large in the sued setup) and reduce some of the noise by smoothing the fitted curve. After the fitting and treatment, the remaining signal is relatively low, as occurred with the Raman analysis. This can be confirmed by analyzing the scale on the left of the figure (relative to the obtained data), where the identified peaks do not even reach 1000 a.u. of intensity, and even with a smoothing process, one can still clearly see the noise of the baseline.

Figure 37: XRD spectra of PLAL nanoparticles, sample w1v1t3.

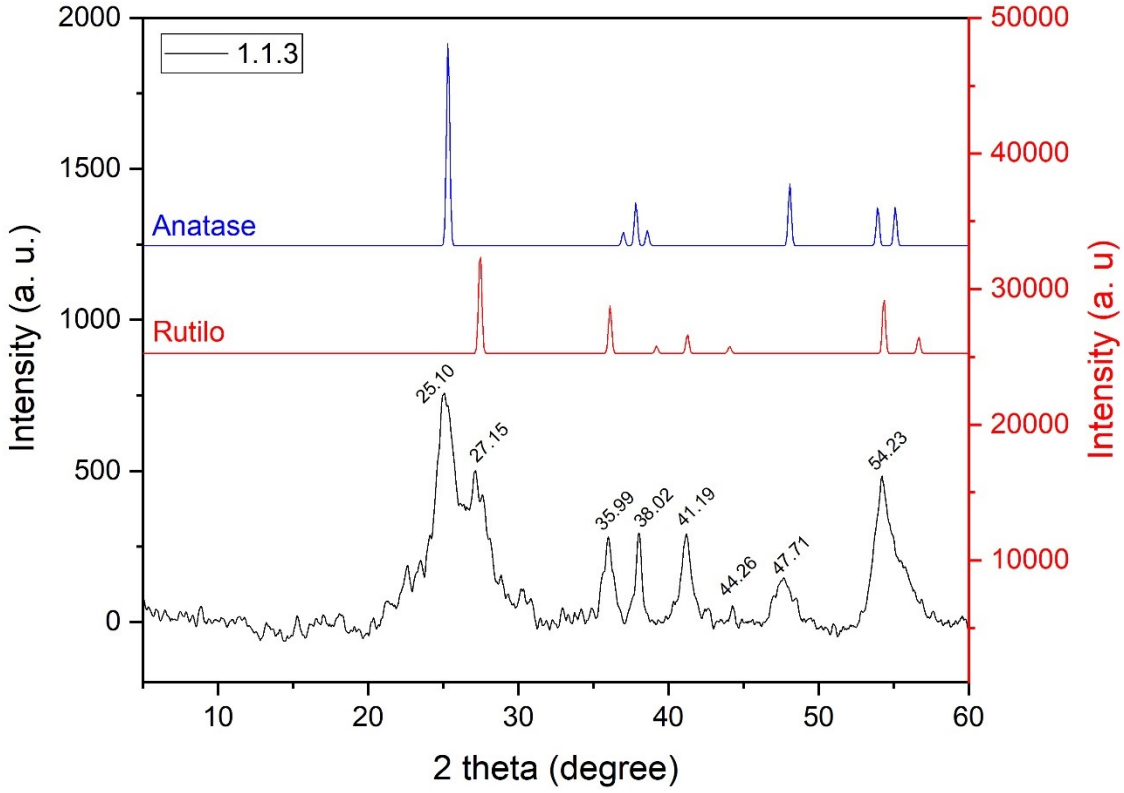

Source: Author (2020)

When analyzing the phases identified in the sample, the conclusion reinforces the findings obtained in the Raman spectroscopy. The broad peaks indicate a considerable amount of amorphous material, while the present peaks can be attributed to both anatase and rutile phases. The sample can then be considered a mixture of those three structures.

Further refining was not performed for two reasons: the low intensity and high noise from the unoptimized procedure and the sample composition. Since the quality of the data is not optimal, any refining might carry on errors from our procedure and yield results that are not reliable. The sample composition aspect is again the same as with the Raman analysis. Since the different phases are not a feature of each particle, meaning we cannot affirm as of right now whether anatase, rutile and amorphous titania exist in a single particle, any refinement would represent an average composition of the mixture of spindles and spheres, which does not bring enough information on itself to be useful.

Overall, while the presence of three phases of titanium dioxide is clearly defined from the characterizations, these methods were not able to completely identify and characterize the individual particles to be able to affirm that spindles are anatase and spheres can be both anatase

and/or rutile. In order to reach that kind of certainty, some routes are possible. Particle-specific characterization techniques such as HRTEM and SAED are able to select a specific part of a single particle during microscopy and identify the crystallographic planes and from that resolve the phase. Another option would be to try to isolate the different particles in order to obtain a dispersion of a specific population. That is problematic because of the difficulty of such a procedure. While methods exist to separate particles by size including in the nanometer range (Field-Flow Fractionation, FFF, for example), there is no guaranteed way to separate them by shape.

4.3 APPLICATION

As an initial test to evaluate a possible application of the blue titania produced through laser ablation in liquids, a photocatalysis degradation of RR141 dye experiment was performed. The surface defects on the particles, as reviewed in Section 2, usually enhance the photocatalytic activity of the material by reducing the band-gap and extending the absorption range to the visible range.

Following the procedure described in Section 3, Figure 38 presents the relative absorbance during the time of the experiment. For a better visualization, t = 0 is considered to be when the UV or Vis light was placed atop the dye and catalyst system, and the negative time presented represents the adsorption phase of the process, with the setup in the dark. This first step is essential to make sure that the drop in absorbance to be measured is not due to interactions happening in the dispersion. Photolysis experiments were performed with both UV and Vis lights for comparison and validation of the catalysis activity.

Figure 38: RR141 photocatalysis degradation experiment with UV and Visible lights

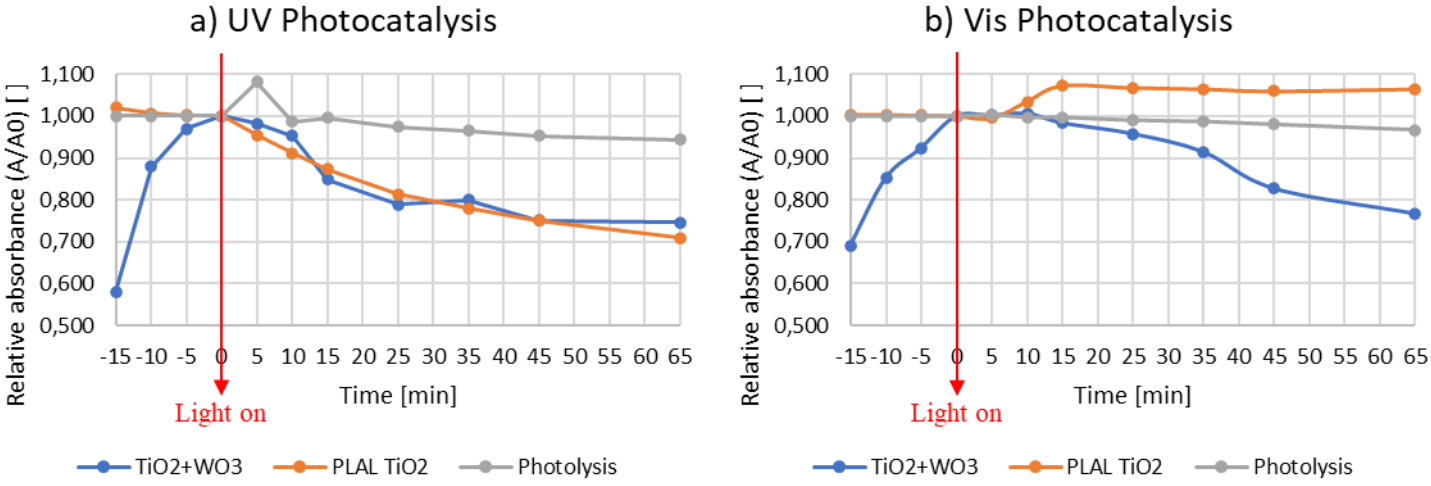

Source: Author (2020)

While the results in the UV range were well within the expected, with the PLAL nanoparticles showing an efficiency comparable to the commercial TiO_2+WO_3 particles, the experiment in the visible range showed no activity for the PLAL nanoparticles, but a good activity for the doped ones. This goes against the hypothesis about the colored suspension we obtained during the laser ablation process.

Figure 39: a) UV-Vis spectrum and b) indirect bandgap calculated by Tauc's plot.

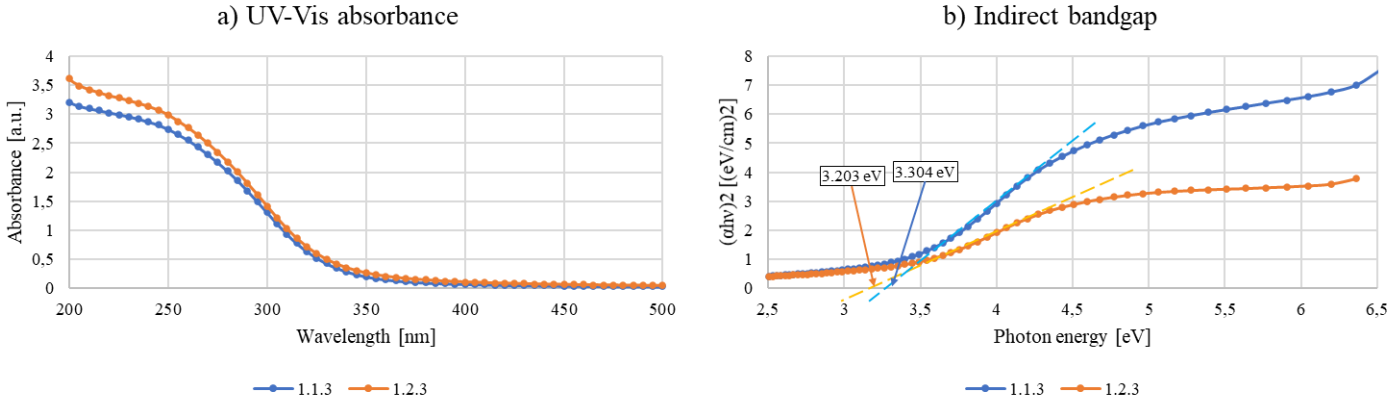

Source: Author (2020)

To investigate this, UV-Vis spectroscopy was performed over the range of 190-800 nm on the PLAL particles. Figure 39 a) shreds evidences that there was no real extension of the absorption band to the visible range, with a peak absorbance and absorbance plateau at around 250 nm. In order to estimate the indirect bandgap of the samples, Tauc's plot was used, as is presented in image b), and values of 3.203 eV and 3.304 eV were found for the analyzed samples, which are closer to the anatase phase of titanium dioxide. Once again, the effect of the

presence of different phases and particle populations is difficult to quantify with this method, and some sort of separation process would be needed in order to calculate bandgap for individual populations.

5 CONCLUSIONS AND PERSPECTIVES

"I may not have gone where I intended to go,
but I think I have ended up where I needed to be."
(ADAMS, Douglas)

5.1 CONCLUDING REMARKS

The proposed nanoparticles were successfully obtained by pulsed laser ablation in water. Some characterization techniques were applied to better understand what the products of the process were. Overall, DLS analyses resulted in particles with sizes between 30 nm and 60 nm, while TEM showed spherical particles ranging from 8 nm to 13 nm and spindle-like particles ranging from 17 nm to 35 nm. This difference is mainly because of assumptions used by the DLS method to measure hydrodynamic diameter, which fall short considering the different geometries of particles present. Hence, for this work, TEM is a better option in measuring particle size.

The most remarkable aspect of the results was the two populations of produced nanoparticles, spheres and spindle-like particles. This result complicated the analysis and interpretation of some of the characterizations that measure properties and characteristics of the whole sample, such as XRD and Raman and UV-vis spectroscopy. Still, anatase, rutile and amorphous phases were identified through those characterizations. Further studies are needed in order to evaluate the composition of individual particles, such as SAED HRTEM.

Because of these different populations and difficulty in analyzing phase and constitution of the particles, the study of the influence of different laser parameters was not fully completed. Initial results showed that higher ablation times, scan speeds and waveforms (and consequently, frequency) yielded less spindle particles and more spherical ones, possibly due to the increased number of pulses to which the solid target and solution were submitted in those cases. However, the influence of these parameters in phase formation, for example, were hard to quantify in the developed work.

Another exciting aspect of the produced samples was the bluish color, which tends to indicate nanoparticles with surface defects that extend the light absorption into the visible range. However, UV-vis spectroscopy of the produced samples did not show any absorption in that range, so the color might be from the presence of impurities in the crystal (from the commercially pure titanium alloy used for the synthesis, for example). A TEM with EDS could be used to identify these possible impurities. Besides the absorption spectra, UV-vis data was

also used to calculate the indirect bandgap of our titania samples to verify whether the process had lowered the bandgap in any way. The results found were around 3.25 eV, putting the sample close to the anatase phase of titania, hence not showing any reduction in bandgap value, which was also confirmed by a photocatalysis experiment, where the PLAL samples showed photocatalytic activity in the UV range but not in the visible range.

During the period of this work, this method, in partnership with Nanogreen, was presented in different events and programs such as InovAtiva Brasil, Startup Summit, LinkLab, and the PANNANO conference. The technology and possible applications attracted the interest of companies such as Marisol, WEG, and Brinox, for example, and Marisol even developed a proof of concept with Nanogreen for the application of some nanoparticles in their fabrics. With these demands, other materials were tested as targets for laser ablation, such as silver, gold, niobia, ceria and even cinnamon sticks. Besides events and projects with companies, Nanogreen has also submitted several grants, having approved in partnership with the LINDEN laboratory a project for the Inovação para a Indústria grant by SENAI, focusing on the production of nanoparticles for application in paints and coatings, aiming for better reflectance and photocatalytic activity.

5.2 CURRENT AND FUTURE WORK

Considering the abovementioned interest in the PLAL technology, different projects and works have stemmed from this original work and research. The Inovação para a Indústria grant is still an active project finalizing research in the paints and coatings market, but new applications are being targeted.

The production and optimization of gold nanoparticles is being studied by Letícia Silva de Bortoli here in PGMAT. This material opens a vast market in the medical and health-related areas, with applications in sensors, biosensors, diagnostics and even imaging, and has already gotten the interest of different companies and research groups.

Finally, the development of customized bare or functionalized nanoparticle prototypes is another field of work where Nanogreen and this technology are being applied, uniting the ever-growing interest in green nanotechnology and the possibility to quickly produce an enormous variety of materials using laser ablation.

Much work still needs to be done in order to fully characterize the production of titania nanoparticles through the defined PLAL setup. The number of chosen parameters to change in

this work, while still just a fraction of all the possible ones, was already a lot considering that the most essential aspects of the setup and method were not experimentally tested yet. At first, before varying laser parameters, a good strategy would be to better characterize the process itself. A suggestion of next steps might be:

a) *Figuring out how to produce a single population of nanoparticles, either spherical or spindle-like:* in order to achieve this, the PLAL setup must possibly change. Adding a flow of the liquid media that drags the nanoparticles to another compartment might be a good way to prevent the post-irradiation effect, meaning that the particles are more likely to remain in a morphology closer to what they are immediately after they are released from the cavitation bubble. Another option might be removing the solid target from the setup and focusing the laser in the liquid media itself for a certain amount of time, so to guarantee that all particles are treated with post-irradiation and that no new particles are being generated, which may evade the treatment. Notice that none of these methods present a sure way to either increase or decrease particle size, and that is not the main goal, but may help to obtain a homogeneous dispersion at least morphology-wise.
b) *Characterizing individual particles for phase composition:* By obtaining a single nanoparticle morphology, it becomes easier to correctly and definitely define the phase or phases present in the particles, and, from there, the resulting bandgap. This information can help direct a specific application of the dispersion produced.
c) *Parameters study:* With that basic setup in hand, optimizing laser parameters for better particle size, size distribution, zeta potential, or other characteristics becomes easier and may yield better results. This step can also be used to customize the functionalization of the particles with a change in the liquid media, for example, or to optimize productivity. These last options, however, might require a change in the physical setup or on the fundamental morphology of the particles and are hence more complex.

However, by the end of this project and with an enormously broader knowledge not only of the process itself, but also its advantages, shortcomings, and even possible markets of application, a conclusion is reached that the production of titania nanoparticles through PLAL is not the best strategy. Factors such as productivity and overall cost of the process make it very difficult for it to compete with the conventional, chemical-based methods especially in a market

such as the titanium dioxide one, very established and with a product that can almost be considered a commodity, applied in considerable quantities in volume-intensive markets such as polymers, fabrics, paints, and others. Besides, most of the current applications do not require the highly pure and customized nanoparticles produced through PLAL.

With that in mind, the more recent option of working with the production and customization of gold nanoparticles seems like a much more attractive option, considering the volume x price factor. This means that overall, gold nanoparticles are applied in more “noble” markets, where a lot less volume is used, with a much higher aggregated value. Applications in medical devices, sensors, biosensors and diagnostics require minute quantities of gold and benefit from the pureness obtained through laser ablation in liquids.

Hence, Nanogreen is currently pivoting and plans on focusing on the abovementioned markets, having already secured partnerships with laboratories, startups and established companies to develop and test products such as diagnostic kits and biosensors.

REFERENCES

"Human beings, who are almost unique in having the ability to learn from the experience of others, are also remarkable for their apparent disinclination to do so."

(ADAMS, Douglas)

ALLEN, N. S.; MAHDJOUB, N.; VISHNYAKOV, V.; KELLY, P. J.; KRIEK, R. J. The effect of crystalline phase (anatase, brookite and rutile) and size on the photocatalytic activity of calcined polymorphic titanium dioxide (TiO2). **Polymer Degradation and Stability**, v. 150, n. February, p. 31–36, 2018.

AL-MAMUN, S. A.; NAKAJIMA, R.; ISHIGAKI, T. Tuning the size of aluminum oxide nanoparticles synthesized by laser ablation in water using physical and chemical approaches. **Journal of Colloid and Interface Science**, v. 392, n. 1, p. 172–182, 2013.

AMENDOLA, V.; POLIZZI, S.; MENEGHETTI, M. Free silver nanoparticles synthesized by laser ablation in organic solvents and their easy functionalization. **Langmuir**, v. 23, n. 12, p. 6766–6770, 2007.

ANDRONIC, L.; ANDRASI, D.; ENESCA, A.; VISA, M.; DUTA, A. The influence of titanium dioxide phase composition on dyes photocatalysis. **Journal of Sol-Gel Science and Technology**, v. 58, n. 1, p. 201–208, 2011.

ANU MARY EALIA, S.; SARAVANAKUMAR, M. P. A review on the classification, characterisation, synthesis of nanoparticles and their application. **IOP Conference Series: Materials Science and Engineering**, v. 263, p. 032019, 2017.

ASTM. Standard Terminology Relating to Nanotechnology. **ASTM International**, n. E2456-06, 2006.

ASTM. Standard Specification for Titanium and Titanium Alloy Strip, Sheet, and Plate. **Annual Book of ASTM Standards**, n. B265 − 20a, p. 1–9, 2020.

BAI, Y.; MORA-SERÓ, I.; DE ANGELIS, F.; BISQUERT, J.; WANG, P. Titanium dioxide nanomaterials for photovoltaic applications. **Chemical Reviews**, v. 114, n. 19, p. 10095–10130, 2014.

BAJAJ, G.; SONI, R. K. Effect of liquid medium on size and shape of nanoparticles prepared by pulsed laser ablation of tin. **Applied Physics A: Materials Science and Processing**, v. 97, n. 2, p. 481–487, 2009.

BARCIKOWSKI, S.; HAHN, A.; KABASHIN, A. V.; CHICHKOV, B. N. Properties of nanoparticles generated during femtosecond laser machining in air and water. **Applied Physics A: Materials Science and Processing**, v. 87, n. 1, p. 47–55, 2007.

BARCIKOWSKI, S.; CHICHKOV, B.; RAČIUKAITIS, G. Production of nanoparticles with high repetition rate Picosecond laser. **Journal of Laser Micro/Nanoengineering**, v. 2, n. 3, p. 230–233, 2007.

BÄRSCH, N. Improving Laser Ablation of Zirconia by Liquid Films: Multiple Influence of Liquids on Surface Machining and Nanoparticle Generation. **Journal of Laser Micro/Nanoengineering**, v. 4, n. 1, p. 66–70, 2010.

BEHARI, J. Principles of nanoscience: An overview. **Indian Journal of Experimental Biology**, v. 48, n. 10, p. 1008–1019, 2010.

BELTRÁN, A.; GRACIA, L.; ANDRÉS, J. Density functional theory study of the brookite surfaces and phase transitions between natural titania polymorphs. **Journal of Physical Chemistry B**, v. 110, n. 46, p. 23417–23423, 2006.

BERTHE, L.; FABBRO, R.; PEYRE, P.; TOLLIER, L.; BARTNICKI, E. Shock waves from a water-confined laser-generated plasma. **Journal of Applied Physics**, v. 82, n. 6, p. 2826–2832, 1997.

BESNER, S.; KABASHIN, A. V.; MEUNIER, M. Fragmentation of colloidal nanoparticles by femtosecond laser-induced supercontinuum generation. **Applied Physics Letters**, v. 89, n. 23, p. 1–4, 2006.

BHATTACHARJEE, S. DLS and zeta potential - What they are and what they are not? **Journal of Controlled Release**, v. 235, p. 337–351, 2016.

BICKLEY, R. I.; GONZALEZ-CARRENO, T.; LEES, J. S.; PALMISANO, L.; TILLEY, R. J. D. A structural investigation of titanium dioxide photocatalysts. **Journal of Solid State Chemistry**, v. 92, n. 1, p. 178–190, 1991.

BOEHME, M.; ENSINGER, W. Mixed Phase Anatase/rutile Titanium Dioxide Nanotubes for Enhanced Photocatalytic Degradation of Methylene-blue. **Nano-Micro Letters**, v. 3, n. 4, p. 236–241, 2011.

BOHOLM, M.; ARVIDSSON, R. A Definition Framework for the Terms Nanomaterial and Nanoparticle. **NanoEthics**, v. 10, n. 1, p. 25–40, 2016.

BURDA, C.; LOU, Y.; CHEN, X.; SAMIA, A. C. S.; STOUT, J.; GOLE, J. L. Enhanced nitrogen doping in TiO2 nanoparticles. **Nano Letters**, v. 3, n. 8, p. 1049–1051, 2003.

CASTRO, R. H. R.; WANG, B. The hidden effect of interface energies in the polymorphic stability of nanocrystalline titanium dioxide. **Journal of the American Ceramic Society**, v. 94, n. 3, p. 918–924, 2011.

CHANG, E. C.; LIN, B. C.; SHEN, P.; CHEN, S. Y. Size, composition and structural changes of TiO2 rutile nanoparticles by pulsed laser ablation in water. **Journal of Nanoscience and Nanotechnology**, v. 12, n. 11, p. 8337–8348, 2012.

CHEN, Q. H.; ZHANG, W. G. Laser ablation in flowing liquid. In: YANG, G. (Ed.). **Laser Ablation in Liquids: Principles and Applications in the Preparation of Nanomaterials**. 1. ed. [s.l.] Pan Stanford Publishing Pte. Ltd., 2012. p. 549–572.

CHEN, X.; LIU, L.; HUANG, F. Black titanium dioxide (TiO2) nanomaterials. **Chemical Society Reviews**, v. 44, n. 7, p. 1861–1885, 2015.

CHEWCHINDA, P.; TSUGE, T.; FUNAKUBO, H.; ODAWARA, O.; WADA, H. Laser wavelength effect on size and morphology of silicon nanoparticles prepared by laser ablation in liquid. **Japanese Journal of Applied Physics**, v. 52, n. 2, 2013.

DA SILVA, A. L.; HOTZA, D.; CASTRO, R. H. R. Surface energy effects on the stability of anatase and rutile nanocrystals: A predictive diagram for Nb 2 O 5 -doped-TiO 2. **Applied Surface Science**, v. 393, p. 103–109, 2017.

DE GIACOMO, A.; DELL'AGLIO, M.; SANTAGATA, A.; GAUDIUSO, R.; DE PASCALE, O.; WAGENER, P.; MESSINA, G. C.; COMPAGNINI, G.; BARCIKOWSKI, S. Cavitation dynamics of laser ablation of bulk and wire-shaped metals in water during nanoparticles production. **Physical Chemistry Chemical Physics**, v. 15, n. 9, p. 3083–3092, 2013.

DELL'AGLIO, M.; GAUDIUSO, R.; DE PASCALE, O.; DE GIACOMO, A. Mechanisms and processes of pulsed laser ablation in liquids during nanoparticle production. **Applied Surface Science**, v. 348, p. 4–9, 2015.

DEVAUX, D.; VIRMONT, J.; FOURNIER, J.; BALLARD, P.; FABBRO, R.; FOURNIER, J.; BALLARD, P.; DEVAUX, D.; VIRMONT, J. Physical study of laser-produced plasma in confined geometry. **Journal of Applied Physics**, v. 68, n. 2, p. 775–784, 2002.

DOLGAEV, S. I.; SIMAKIN, A. V.; VORONOV, V. V.; KIRICHENKO, N. A.; SHAFEEV, G. A. Nanoparticles produced by laser ablation of solids in liquid environment. **Applied Surface Science**, v. 186, p. 546–551, 2002.

D'URSO, L.; SPADARO, S.; BONSIGNORE, M.; SANTANGELO, S.; COMPAGNINI, G.; NERI, F.; FAZIO, E. Zinc oxide nanocolloids prepared by picosecond pulsed laser ablation in water at different temperatures. **EPJ Web of Conferences**, v. 167, p. 1–5, 2018.

FANG, V.; KENNEDY, J.; FUTTER, J.; MANNING, J. A review of near infrared reflectance properties of metal oxide nanostructures. **GNS science report**, v. 39, n. July, p. 23, 2013.

FITZSIMONS, P. Selective ablation of thin films with ultra short pulses. PhD Thesis. University of Liverpool, UK, p. 203, 2012.

FLORIAN BARON, C. Laser direct-writing for microfabrication. University of Barcelona, Spain. PhD Thesis. p. 213, 2016.

FONG, Y.-Y.; GASCOOKE, J. R.; VISSER, B. R.; HARRIS, H. H.; COWIE, B. C. C.; THOMSEN, L.; METHA, G. F.; BUNTINE, M. A. Influence of Cationic Surfactants on the Formation and Surface Oxidation States of Gold Nanoparticles Produced via Laser Ablation. **Langmuir**, v. 29, n. 40, p. 12452–12462, 2013.

FUJISHIMA, A.; ZHANG, X. Titanium dioxide photocatalysis: present situation and future approaches. **Comptes Rendus Chimie**, v. 9, n. 5–6, p. 750–760, 2006.

GÁZQUEZ, M. J.; BOLÍVAR, J. P.; GARCIA-TENORIO, R.; VACA, F. A Review of the Production Cycle of Titanium Dioxide Pigment. **Materials Sciences and Applications**, v. 05, n. 07, p. 441–458, 2014.

GE, C.; YU, W.; GU, N.; ZHANG, Y.; LIU, J.; XU, L.; LIAO, J. Linear aggregation of gold nanoparticles in ethanol. **Colloids and Surfaces A: Physicochemical and Engineering Aspects**, v. 223, n. 1–3, p. 177–183, 2003.

GIORGETTI, E.; MUNIZ MIRANDA, M.; CAPORALI, S.; CANTON, P.; MARSILI, P.; VERGARI, C.; GIAMMANCO, F. TiO2 nanoparticles obtained by laser ablation in water: Influence of pulse energy and duration on the crystalline phase. **Journal of Alloys and Compounds**, v. 643, n. S1, p. S75–S79, 2015.

GLEZAKOU, V. A.; ROUSSEAU, R. Shedding light on black titania. **Nature Materials**, v. 17, n. 10, p. 856–857, 2018.

GOLDSCHMIDT, G.; HOTZA, D.; PLENTZ, F.; CAMARANO, D.; LIRA, I. Evaluation of the uncertainty in the measurement of nanoparticle size by dynamic light scattering. **Measurement Science and Technology**, v. 31, n. 7, p. 075005, 2020.

GUO-WEI, Y.; JIN-BIN, W.; QUI-XIANG, L. Preparation of nano-crystalline diamonds using pulsed laser induced reactive quenching. **Journal of Physics: Condensed Matter**, v. 10, n. 35, p. 7923, 1998.

GUPTA, S. M.; TRIPATHI, M. A review of TiO2 nanoparticles. **Chinese Science Bulletin**, v. 56, n. 16, p. 1639–1657, 2011.

HAMAD, A. H. Effects of Different Laser Pulse Regimes (Nanosecond, Picosecond and Femtosecond) on the Ablation of Materials for Production of Nanoparticles in Liquid Solution. In: VISKUP, R. (Ed.). **High Energy and Short Pulse Lasers**. [s.l.] IntechOpen, 2016. p. 305–325.

HAMAD, A. H.; KHASHAN, K. S.; HADI, A. A. Laser Ablation in Different Environments and Generation of Nanoparticles. In: **Applications of Laser Ablation - Thin Film Deposition, Nanomaterial Synthesis and Surface Modification References**. 1. ed. [s.l.] IntechOpen, 2016. v. 1p. 177–196.

HAMAD, A.; LI, L.; LIU, Z. A comparison of the characteristics of nanosecond, picosecond and femtosecond lasers generated Ag, TiO2 and Au nanoparticles in deionised water. **Applied Physics A: Materials Science and Processing**, v. 120, n. 4, p. 1247–1260, 2015.

HAMAD, A.; LI, L.; LIU, Z. Comparison of characteristics of selected metallic and metal oxide nanoparticles produced by picosecond laser ablation at 532 and 1064 nm wavelengths. **Applied Physics A: Materials Science and Processing**, v. 122, n. 10, p. 1–15, 2016.

HAMDY, M. S.; AMROLLAHI, R.; MUL, G. Surface Ti3+-containing (blue) titania: A unique photocatalyst with high activity and selectivity in visible light-stimulated selective oxidation. **ACS Catalysis**, v. 2, n. 12, p. 2641–2647, 2012.

HANAOR, D. A. H.; SORRELL, C. C. Review of the anatase to rutile phase transformation. **Journal of Materials Science**, v. 46, n. 4, p. 855–874, 2011.

HE, C.; SASAKI, T.; SHIMIZU, Y.; KOSHIZAKI, N. Synthesis of ZnO nanoparticles using nanosecond pulsed laser ablation in aqueous media and their self-assembly towards spindle-like ZnO aggregates. **Applied Surface Science**, v. 254, n. 7, p. 2196–2202, 2008.

JENSEN, G. V.; BREMHOLM, M.; LOCK, N.; DEEN, G. R.; JENSEN, T. R.; IVERSEN, B. B.; NIEDERBERGER, M.; PEDERSEN, J. S.; BIRKEDAL, H. Anisotropic crystal growth kinetics of anatase Tio2 nanoparticles synthesized in a nonaqueous medium. **Chemistry of Materials**, v. 22, n. 22, p. 6044–6055, 2010.

JIANG, Y.; LIU, P.; LIANG, Y.; LI, H. B.; YANG, G. W. Promoting the yield of nanoparticles from laser ablation in liquid. **Applied Physics A: Materials Science and Processing**, v. 105, n. 4, p. 903–907, 2011.

JIMENEZ, R.; FITZ-GERALD, J. M.; O'MALLEY, S. M.; STEINER, M.; BUBB, D. M.; NADDEO, J. J.; TOMKO, J.; TAN, Y. Size and polydispersity trends found in gold nanoparticles synthesized by laser ablation in liquids. **Physical Chemistry Chemical Physics**, v. 17, n. 25, p. 16327–16333, 2015.

KABASHIN, A. V.; DELAPORTE, P.; PEREIRA, A.; GROJO, D.; TORRES, R.; SARNET, T.; SENTIS, M. Nanofabrication with pulsed lasers. **Nanoscale Research Letters**, v. 5, n. 3, p. 454–463, 2010.

KABASHIN, A. V.; MEUNIER, M. Synthesis of colloidal nanoparticles during femtosecond laser ablation of gold in water. **Journal of Applied Physics**, v. 94, n. 12, p. 7941–7943, 2003.

KANITZ, A.; HOPPIUS, J. S.; GUREVICH, E. L.; OSTENDORF, A. Influence of the liquid on femtosecond laser ablation of iron. **Physics Procedia**, v. 83, p. 114–122, 2016.

KHAN, I.; SAEED, K.; KHAN, I. Nanoparticles: Properties, applications and toxicities. **Arabian Journal of Chemistry**, 2017.

KIM, D.; LEE, H. Enhanced ablation and photoacoustic excitation in near-threshold laser ablation of liquid-coated surfaces. **Journal of Applied Physics**, v. 89, n. 10, p. 5703–5706, 2001.

KIM, K. K.; ROY, M.; KWON, H.; SONG, J. K.; PARK, S. M. Laser ablation dynamics in liquid phase: The effects of magnetic field and electrolyte. **Journal of Applied Physics**, v. 117, n. 7, 2015.

KIM, M.; OSONE, S.; KIM, T.; HIGASHI, H.; SETO, T. Synthesis of nanoparticles by laser ablation: A review. **KONA Powder and Particle Journal**, v. 2017, n. 34, p. 80–90, 2017.

KOHSAKOWSKI, S.; SANTAGATA, A.; DELL'AGLIO, M.; DE GIACOMO, A.; BARCIKOWSKI, S.; WAGENER, P.; GÖKCE, B. High productive and continuous nanoparticle fabrication by laser ablation of a wire-target in a liquid jet. **Applied Surface Science**, v. 403, p. 487–499, 2017.

KÖRSTGENS, V.; PRÖLLER, S.; BUCHMANN, T.; MOSEGUÍ GONZÁLEZ, D.; SONG, L.; YAO, Y.; WANG, W.; WERHAHN, J.; SANTORO, G.; ROTH, S. V.; et al. Laser-ablated titania nanoparticles for aqueous processed hybrid solar cells. **Nanoscale**, v. 7, n. 7, p. 2900–2904, 2015.

KUBILIUTE, R.; MAXIMOVA, K. A.; LAJEVARDIPOUR, A.; YONG, J.; HARTLEY, J. S.; MOHSIN, A. S. M.; BLANDIN, P.; CHON, J. W. M.; SENTIS, M.; STODDART, P. R.; et al. Ultra-pure, water-dispersed Au nanoparticles produced by femtosecond laser ablation and fragmentation. **International Journal of Nanomedicine**, v. 8, p. 2601–2611, 2013.

KUMAR, B.; THAREJA, R. K. Laser ablated copper plasmas in liquid and gas ambient. **Physics of Plasmas**, v. 20, n. 5, 2013.

LE MERCIER, T.; MARIOT, J. M.; PARENT, P.; FONTAINE, M. F.; HAGUE, C. F.; QUARTON, M. Formation of Ti3+ ions at the surface of laser-irradiated rutile. **Applied Surface Science**, v. 86, n. 1–4, p. 382–386, 1995.

LEITE, F. L.; BUENO, C. C.; DA RÓZ, A. L.; ZIEMATH, E. C.; OLIVEIRA, O. N. Theoretical models for surface forces and adhesion and their measurement using atomic force microscopy. **International Journal of Molecular Sciences**, v. 13, n. 10, p. 12773–12856, 2012.

LEWIS, L. J.; PEREZ, D. Computer models of laser ablation in liquids. In: YANG, G. (Ed.). **Laser Ablation in Liquids: Principles and Applications in the Preparation of Nanomaterials**. 1. ed. [s.l.] Pan Stanford Publishing Pte. Ltd., 2012. p. 111–155.

LI, G.; CHEN, L.; GRAHAM, M. E.; GRAY, K. A. A comparison of mixed phase titania photocatalysts prepared by physical and chemical methods: The importance of the solid-solid interface. **Journal of Molecular Catalysis A: Chemical**, v. 275, n. 1–2, p. 30–35, 2007.

LIAO, J. H.; CHEN, K. J.; XU, L. N.; GE, C. W.; WANG, J.; HUANG, L.; GU, N. Self-assembly of length-tunable gold nanoparticle chains in organic solvents. **Applied Physics A: Materials Science and Processing**, v. 76, n. 4, p. 541–543, 2003.

LIU, P.; LIN, X. Z.; YU, J. M.; YANG, G. W. From nanocrystal synthesis to nanomanufacturing: Laser ablation in liquid. In: YANG, G. (Ed.). **Laser Ablation in Liquids: Principles and Applications in the Preparation of Nanomaterials**. [s.l.] Pan Stanford Publishing Pte. Ltd., 2012. p. 855–946.

LOWRY, G. V.; HILL, R. J.; HARPER, S.; RAWLE, A. F.; HENDREN, C. O.; KLAESSIG, F.; NOBBMANN, U.; SAYRE, P.; RUMBLE, J. Guidance to improve the scientific value of zeta-potential measurements in nanoEHS. **Environmental Science: Nano**, v. 3, n. 5, p. 953–965, 2016.

LUTTRELL, T.; HALPEGAMAGE, S.; TAO, J.; KRAMER, A.; SUTTER, E.; BATZILL, M. Why is anatase a better photocatalyst than rutile? - Model studies on epitaxial TiO2 films. **Scientific Reports**, v. 4, p. 1–8, 2015.

MAKAROV, V. V.; LOVE, A. J.; SINITSYNA, O. V.; MAKAROVA, S. S.; YAMINSKY, I. V.; TALIANSKY, M. E.; KALININA, N. O. **"Green" Nanotechnologies: Synthesis of Metal Nanoparticles Using PlantsACTA NATURAE**, 2014.

MALVERN PANALYTICAL LTD. **Zetasizer Nano user manualMan0317-5.0**. [s.l: s.n.]. Disponível em: <www.malvern.com>.

MALVERN PANALYTICAL LTD. **Dynamic light scattering: An introduction in 30 min. Tecnical note (MRK656-01)**. [s.l: s.n.]. Disponível em: <https://www.malvernpanalytical.com/en/learn/knowledge-center/technical-notes/TN101104DynamicLightScatteringIntroduction>.

MESSINA, G. C.; WAGENER, P.; STREUBEL, R.; DE GIACOMO, A.; SANTAGATA, A.; COMPAGNINI, G.; BARCIKOWSKI, S. Pulsed laser ablation of a continuously-fed wire in liquid flow for high-yield production of silver nanoparticles. **Physical Chemistry Chemical Physics**, v. 15, n. 9, p. 3093–3098, 2013.

MO, S. DI; CHING, W. Y. Electronic and optical properties of three phases of titanium dioxide: Rutile, anatase, and brookite. **Physical Review B**, v. 51, n. 19, p. 13023–13032, 1995.

MOMENI, M. M.; GHAYEB, Y.; DAVARZADEH, M. Electrochemical construction of different titania–tungsten trioxide nanotubular composite and their photocatalytic activity for pollutant degradation: a recyclable photocatalysts. **Journal of Materials Science: Materials in Electronics**, v. 26, n. 3, p. 1560–1567, 2015.

MUSAEV, O. R.; DRIVER, M. S.; SUTTER, E. A.; CARUSO, A. N.; WROBEL, J. M.; KRUGER, M. B. Influence of the liquid environment on the products formed from the laser ablation of tin. **Applied Physics A: Materials Science and Processing**, v. 113, n. 2, p. 355–359, 2013.

NANOAMOR. Titanium Oxide Nanopowder (tungsten oxide doped, TiO_2/WO_3, anatase, 10 nm). Nanostructured & Amorphous Materials, Inc. Available: https://www.nanoamor.com/inc/sdetail/45711. Accessed on 15 June 2020.

NEUMEISTER, A.; JAKOBI, J.; REHBOCK, C.; MOYSIG, J.; BARCIKOWSKI, S. Monophasic ligand-free alloy nanoparticle synthesis determinants during pulsed laser ablation of bulk alloy and consolidated microparticles in water. **Physical Chemistry Chemical Physics**, v. 16, n. 43, p. 23671–23678, 2014.

NEWMAN, M. D.; STOTLAND, M.; ELLIS, J. I. The safety of nanosized particles in titanium dioxide- and zinc oxide-based sunscreens. **Journal of the American Academy of Dermatology**, v. 61, n. 4, p. 685–692, 2009.

NIU, Y.; WANG, Y.; LIU, X.; ZHANG, C.; ZHU, S. Laser beam quality factor M 2 and its measurement. **Laser Processing of Materials and Industrial Applications II**, v. 3550, n. August 1998, p. 378, 1998.

NNI. What's So Special about the Nanoscale. National Nanotechnology Initiative. Available: https://www.nano.gov/nanotech-101/special. Accessed on 15 June 2020.

PAN, D.; HUANG, H.; WANG, X.; WANG, L.; LIAO, H.; LI, Z.; WU, M. C-axis preferentially oriented and fully activated TiO2 nanotube arrays for lithium ion batteries and supercapacitors. **Journal of Materials Chemistry A**, v. 2, n. 29, p. 11454–11464, 2014.

PAREEK, V.; JAIN, N.; PANWAR, J.; BHARGAVA, A.; GUPTA, R. Synthesis and Applications of Noble Metal Nanoparticles: A Review. **Advanced Science, Engineering and Medicine**, v. 9, n. 7, p. 527–544, 2017.

PATEL, D. N.; SINGH, R. P.; THAREJA, R. K. Craters and nanostructures with laser ablation of metal/metal alloy in air and liquid. **Applied Surface Science**, v. 288, p. 550–557, 2014.

PELLARIN, M.; KOCIAK, M.; WEISSKER, H.-C.; HILLENKAMP, M.; TROC, N.; CAMPOS, A.; COTTANCIN, E.; LERMÉ, J.; TROC, N.; COTTANCIN, E.; et al. Plasmonic quantum size effects in silver nanoparticles are dominated by interfaces and local environments. **Nature Physics**, 2018.

PILLAI, S.; CATCHPOLE, K. R.; TRUPKE, T.; GREEN, M. A. Surface plasmon enhanced silicon solar cells. **Journal of Applied Physics**, v. 101, n. 9, 2007.

PRZYBYLSKI, A. Synthesis of Uniform Spindle-Type Titania Particles by the Gel–Sol Method. **Kardiologia Polska**, v. 69, n. 11, p. 1212, 2011.

RESANO-GARCIA, A.; BATTIE, Y.; KOCH, A.; EN NACIRI, A.; CHAOUI, N. Influence of the laser light absorption by the colloid on the properties of silver nanoparticles produced by laser ablation in stirred and stationary liquid. **Journal of Applied Physics**, v. 117, n. 11, p. 117, 2015.

ROSA, R. G. T.; DE ARAUJO DUARTE, C.; SCHREINER, W. H.; FILHO, N. P. M.; BEZERRA, A. G.; BARISON, A.; OCAMPOS, F. M. M.; BEZERRA, A. G.; ROSA, R. G. T.; SCHREINER, W. H.; et al. Structural, morphological and optical properties of Bi NPs obtained by laser ablation and their selective detection of L-cysteine. **Colloids and Surfaces A: Physicochemical and Engineering Aspects**, v. 457, n. 1, p. 368–373, 2014.

SAHEHCO. **Lasis**. Disponível em: <https://commons.wikimedia.org/wiki/File:Lasis.jpg>. Acesso em: 31 maio. 2020.

SAJTI, C. L.; SATTARI, R.; CHICHKOV, B. N.; BARCIKOWSKI, S. Gram scale synthesis of pure ceramic nanoparticles by laser ablation in liquid. **Journal of Physical Chemistry C**, v. 114, n. 6, p. 2421–2427, 2010.

SASAKI, K. Dynamics of Liquid-Phase Laser Ablation. In: YANG, G. (Ed.). **Laser Ablation in Liquids: Principles and Applications in the Preparation of Nanomaterials**. 1. ed. [s.l.] Pan Stanford Publishing Pte. Ltd., 2012. p. 269–297.

SASAKI, T.; LIANG, C.; NICHOLS, W. T.; SHIMIZU, Y.; KOSHIZAKI, N. Fabrication of oxide base nanostructures using pulsed laser ablation in aqueous solutions. **Applied Physics A: Materials Science and Processing**, v. 79, n. 4–6, p. 1489–1492, 2004.

SAVASTENKO, N.; VOLPP, H. R.; GERLACH, O.; STREHLAU, W. Synthesis of nanostructured lean-NO x catalysts by direct laser deposition of monometallic Pt-, Rh- and bimetallic PtRh-nanoparticles on SiO2 support. **Journal of Nanoparticle Research**, v. 10, n. 2, p. 277–287, 2008.

SCANLON, D. O.; DUNNILL, C. W.; BUCKERIDGE, J.; SHEVLIN, S. A.; LOGSDAIL, A. J.; WOODLEY, S. M.; CATLOW, C. R. A.; POWELL, M. J.; PALGRAVE, R. G.; PARKIN, I. P.; et al. Band alignment of rutile and anatase TiO2. **Nature Materials**, v. 12, n. 9, p. 798–801, 2013.

SCARAMUZZA, S.; ZERBETTO, M.; AMENDOLA, V. Synthesis of gold nanoparticles in liquid environment by laser ablation with geometrically confined configurations: Insights to improve size control and productivity. **Journal of Physical Chemistry C**, v. 120, n. 17, p. 9453–9463, 2016.

SCARPELLI, F.; MASTROPIETRO, T. F.; POERIO, T.; GODBERT, N. Mesoporous TiO2 Thin Films: State of the Art. **Titanium Dioxide - Material for a Sustainable Environment**, n. June, 2018.

SCHWENKE, A.; WAGENER, P.; NOLTE, S.; BARCIKOWSKI, S.; LI-YUN, C.; CHUAN-BO, Z.; JIAN-FENG, H.; SCHWENKE, A.; WAGENER, P.; NOLTE, S.; et al. Influence of processing time on nanoparticle generation during picosecond-pulsed fundamental and second harmonic laser ablation of metals in tetrahydrofuran. **Applied Physics A: Materials Science and Processing**, v. 104, n. 1, p. 77–82, 2011.

SEMALTIANOS, N. G.; LOGOTHETIDIS, S.; FRANGIS, N.; TSIAOUSSIS, I.; PERRIE, W.; DEARDEN, G.; WATKINS, K. G. Laser ablation in water: A route to synthesize nanoparticles of titanium monoxide. **Chemical Physics Letters**, v. 496, n. 1–3, p. 113–116, 2010.

SEMALTIANOS, N. G. Nanoparticles by laser ablation. **Critical Reviews in Solid State and Materials Sciences**, v. 35, n. 2, p. 105–124, 2010.

SHAFEEV, G. A.; STRATAKIS, E. Nanostructures' formation under laser ablation of solids in liquids. In: YANG, G. (Ed.). **Laser Ablation in Liquids: Principles and Applications in the Preparation of Nanomaterials**. 1. ed. [s.l.] Pan Stanford Publishing Pte. Ltd., 2012. p. 815–853.

SHAJI, S.; ROY, T. K. D. K. D.; CASTILLO, G. A. A.; KRISHNAN, B.; GUILLÉN, G. G.; PALMA, M. I. I. M. M. I. M.; AVELLANEDA, D.; KRISHNAN, B.; AVELLANEDA, D.; CASTILLO, G. A. A.; et al. Structure and morphologies of ZnO nanoparticles synthesized by pulsed laser ablation in liquid: Effects of temperature and energy fluence. **Materials Chemistry and Physics**, v. 162, p. 561–570, 2015.

SILVA, A. L. DA. **Anatase-Rutile Phase Stability and Photocatalytic Activity of Nb2O5-doped TiO2**. [s.l: s.n.].

SINGH, A.; VIHINEN, J.; FRANKBERG, E.; HYVÄRINEN, L.; HONKANEN, M.; LEVÄNEN, E. Effect of laser power on yield of TiO2nanoparticles synthesized by pulsed laser ablation in water. **Journal of Ceramic Science and Technology**, v. 8, n. 1, p. 39–44, 2017.

SINGH, S. C.; ZENG, H.; YANG, S.; CAI, W.; HONG, M.; CHEN, G.; CHONG, T. C. Nanomaterials: Laser-Based Processing in Liquid Media. In: **Nanomaterials**. [s.l: s.n.]. p. 317–494.

SINGH, S. C.; ZENG, H.; GUO, C.; CAI, W. Lasers: Fundamentals, Types, and Operations. In: **Nanomaterials: Processing and Characterization with Lasers**. [s.l: s.n.]. p. 1–34.

SINGH, S. C.; GOPAL, R. Zinc nanoparticles in solution by laser ablation technique. **Bulletin of Materials Science**, v. 30, n. 3, p. 291–293, 2007.

SINGH, S. C.; SWARNKAR, R. K.; GOPAL, R. Synthesis of titanium dioxide Nanomaterial by pulsed laser ablation in water. **Journal of Nanoscience and Nanotechnology**, v. 9, n. 9, p. 5367–5371, 2009.

SIUZDAK, K.; SAWCZAK, M.; KLEIN, M.; NOWACZYK, G.; JURGA, S.; CENIAN, A. Preparation of platinum modified titanium dioxide nanoparticles with the use of laser ablation in water. **Physical Chemistry Chemical Physics**, v. 16, n. 29, p. 15199–15206, 2014.

SOLA, D.; PEÑA, J. I. Study of the wavelength dependence in laser ablation of advanced ceramics and glass-ceramic materials in the nanosecond range. **Materials**, v. 6, n. 11, p. 5302–5313, 2013.

SORCAR, S.; HWANG, Y.; GRIMES, C. A.; IN, S. IL. Highly enhanced and stable activity of defect-induced titania nanoparticles for solar light-driven CO2 reduction into CH4. **Materials Today**, v. 20, n. 9, p. 507–515, 2017.

SRIVASTAVA, A. K.; SINHA, A. K.; JOSHI, M. P.; CHATURVEDI, A.; MONDAL, P. Growth of anatase and rutile phase TiO 2 nanoparticles using pulsed laser ablation in liquid: Influence of surfactant addition and ablation time variation. **Applied Surface Science**, v. 396, p. 303–309, 2016.

STAUSS, S.; URABE, K.; MUNEOKA, H.; TERASHIMA, K. Pulsed Laser Ablation in High-Pressure Gases, Pressurized Liquids and Supercritical Fluids: Generation, Fundamental Characteristics and Applications. In: **Applications of Laser Ablation - Thin Film Deposition, Nanomaterial Synthesis and Surface Modification fabrication**. [s.l: s.n.]. p. 221–244.

STREUBEL, R.; BARCIKOWSKI, S.; GÖKCE, B. Continuous multigram nanoparticle synthesis by high-power, high-repetition-rate ultrafast laser ablation in liquids. **Optics Letters**, v. 41, n. 7, p. 1486, 2016.

STREUBEL, R.; BENDT, G.; GÖKCE, B. Pilot-scale synthesis of metal nanoparticles by high-speed pulsed laser ablation in liquids. **Nanotechnology**, v. 27, n. 20, 2016.

TAKEDA, Y.; KONDOW, T.; KOHNO, J.; SAWABE, H.; MAFUNÉ, F. Formation and Size Control of Silver Nanoparticles by Laser Ablation in Aqueous Solution. **The Journal of Physical Chemistry B**, v. 104, n. 39, p. 9111–9117, 2002.

TIAN, F.; SUN, J.; YANG, J.; WU, P.; WANG, H. L.; DU, X. W. Preparation and photocatalytic properties of mixed-phase titania nanospheres by laser ablation. **Materials Letters**, v. 63, n. 27, p. 2384–2386, 2009.

TILAKI, R. M.; IRAJIZAD, A.; MAHDAVI, S. M. Stability, size and optical properties of silver nanoparticles prepared by laser ablation in different carrier media. **Applied Physics A: Materials Science and Processing**, v. 84, n. 1–2, p. 215–219, 2006.

TILAKI, R. M.; ZAD, A. I.; MAHDAVI, S. M. Size, composition and optical properties of copper nanoparticles prepared by laser ablation in liquids. **Applied Physics A: Materials Science and Processing**, v. 88, n. 2, p. 415–419, 2007.

TOMKO, J.; O'MALLEY, S. M.; TROUT, C.; NADDEO, J. J.; JIMENEZ, R.; GRIEPENBURG, J. C.; SOLIMAN, W.; BUBB, D. M. Cavitation bubble dynamics and nanoparticle size distributions in laser ablation in liquids. **Colloids and Surfaces A: Physicochemical and Engineering Aspects**, v. 522, p. 368–372, 2017.

TREFALT, G.; BORKOVEC, M. Overview of DLVO Theory. **Laboratory of Colloid and Surface Chemistry, University of Geneva**, p. 1–10, 2014.

TSUJI, T. Preparation of nanoparticles using laser ablation in liquids: Fundamental aspects and efficient utilization. In: **Laser Ablation in Liquids: Principles and Applications in the Preparation of Nanomaterials**. [s.l: s.n.]. p. 207–268.

TSUJI, T.; WATANABE, N.; TSUJI, M. Laser induced morphology change of silver colloids: Formation of nano-size wires. **Applied Surface Science**, v. 211, n. 1–4, p. 189–193, 2003.

TZIKALOS, N.; BELESSI, V.; LAMBROPOULOU, D. Photocatalytic degradation of Reactive Red 195 using anatase/brookite TiO2 mesoporous nanoparticles: Optimization using response surface methodology (RSM) and kinetics studies. **Environmental Science and Pollution Research**, v. 20, n. 4, p. 2305–2320, 2013.

VLĂDOIU, I.; STAFE, M.; NEGUŢU, C.; POPESCU, I. M. The dependence of the ablation rate of metals on nanosecond laser fluence and wavelength. **JOURNAL OF OPTOELECTRONICS AND ADVANCED MATERIALS**, v. 10, n. 12, p. 3177–3181, 2008.

WANG, H.; ODAWARA, O.; WADA, H. Facile and Chemically Pure Preparation of YVO4:Eu3+Colloid with Novel Nanostructure via Laser Ablation in Water. **Scientific Reports**, v. 6, n. January, p. 4–11, 2016.

WANG, J. B.; YANG, G. W. Phase transformation between diamond and graphite in preparation of diamonds by pulsed-laser induced liquid-solid interface reaction. **Journal of Physics Condensed Matter**, v. 11, n. 37, p. 7089–7094, 1999.

WANG, X.; SHEPHARD, J. D.; DEAR, F. C.; HAND, D. P. Optimized nanosecond pulsed laser micromachining of Y-TZP ceramics. **Journal of the American Ceramic Society**, v. 91, n. 2, p. 391–397, 2008.

WANG, X.; LI, Z.; SHI, J.; YU, Y. One-dimensional titanium dioxide nanomaterials: Nanowires, nanorods, and nanobelts. **Chemical Reviews**, v. 114, n. 19, p. 9346–9384, 2014.

XIAO, J.; LIU, P.; WANG, C. X.; YANG, G. W. External field-assisted laser ablation in liquid: An efficient strategy for nanocrystal synthesis and nanostructure assembly. **Progress in Materials Science**, v. 87, p. 140–220, 2017.

XIONG, L. BIN; LI, J. L.; YANG, B.; YU, Y. Ti 3+ in the surface of titanium dioxide: Generation, properties and photocatalytic application. **Journal of Nanomaterials**, v. 2012, 2012.

YAN, X.; LI, Y.; XIA, T. Black Titanium Dioxide Nanomaterials in Photocatalysis. **International Journal of Photoenergy**, v. 2017, 2017.

YIN, G.; HUANG, X.; CHEN, T.; ZHAO, W.; BI, Q.; XU, J.; HAN, Y.; HUANG, F. Hydrogenated Blue Titania for Efficient Solar to Chemical Conversions: Preparation, Characterization, and Reaction Mechanism of CO2 Reduction. **ACS Catalysis**, v. 8, n. 2, p. 1009–1017, 2018.

ŽEMAITIS, A.; GAIDYS, M.; BRIKAS, M.; GEČYS, P.; RAČIUKAITIS, G.; GEDVILAS, M. Advanced laser scanning for highly-efficient ablation and ultrafast surface structuring: experiment and model. **Scientific Reports,** v. 8, n. 1, p. 1–14, 2018.

ZHANG, D.; LIU, J.; LI, P.; TIAN, Z.; LIANG, C. Recent Advances in Surfactant-Free, Surface-Charged, and Defect-Rich Catalysts Developed by Laser Ablation and Processing in Liquids. **ChemNanoMat**, v. 3, n. 8, p. 512–533, 2017.

ZHU, S.; LU, Y. F.; HONG, M. H.; CHEN, X. Y. Laser ablation of solid substrates in water and ambient air. **Journal of Applied Physics**, v. 89, n. 4, p. 2400–2403, 2001.

ZHU, S.; LU, Y. F.; HONG, M. H. Laser ablation of solid substrates in a water-confined environment. **Applied Physics Letters**, v. 79, n. 9, p. 1396–1398, 2001.

ZHU, G.; SHAN, Y.; LIN, T.; ZHAO, W.; XU, J.; TIAN, Z.; ZHANG, H.; ZHENG, C.; HUANG, F. Hydrogenated blue titania with high solar absorption and greatly improved photocatalysis. **Nanoscale**, v. 8, n. 8, p. 4705–4712, 2016.